SINGULARITIES AND PHASE TRANSITIONS IN ELASTIC SOLIDS: NUMERICAL STUDIES AND STABILITY ANALYSIS

Thesis by

Stewart Andrew Silling

In Partial Fulfillment of the Requirements

for the Degree of

Doctor of Philosophy

California Institute of Technology

Pasadena, California

1986

(Submitted May 21, 1986)

ACKNOWLEDGMENTS

I gratefully acknowledge the assistance and guidance of Professor James K. Knowles, who supervised this work. I am also indebted to my other teachers at Caltech, especially to Professor Eli Sternberg, whose course in elasticity theory caused me to start thinking about mechanics in an entirely new way.

ABSTRACT

Numerical studies of the deformation near the tip of a crack are presented for a family of incompressible solids in the context of the theory of finite anti-plane shear of an elastic material. The numerical model computes the near-field and far-field solutions simultaneously, enabling observations of both small-scale and large-scale nonlinearity. The computed near-field solution is compared with a lowest-order asymptotic solution. An approximation for the J-integral under conditions of very large loads is discussed and compared with numerical results. The size of the region over which the lowest-order solution applies is observed.

Numerical solutions are presented for the same crack problem with materials for which the equilibrium equation changes in type from elliptic to hyperbolic as a result of deformation. These results show the emergence of surfaces of discontinuity in the displacement field in some cases. In other cases they show a chaotic mixture of elliptic phases near the crack tip.

Analysis of the stability of such coexistent phases is carried out for a specific material, the trilinear material. It is shown that the Maxwell relation, and therefore local stability, cannot in general be satisfied exactly for an arbitrary boundary value problem with this material. However, in those cases where it cannot be satisfied exactly, it may be satisfied in the sense of a limit of a certain sequence of deformations. This sequence produces a progressively chaotic pattern of two coexistent elliptic phases, as was observed numerically. The phases mix over a definite region in a given boundary value problem. This region may be computed using a constitutive relation which characterizes the mixture in the limit of the sequence.

PREFACE

This dissertation is divided into two parts. Part I, "Numerical Studies of Anti-Plane Shear Crack Problems in the Theory of Finite Elastic Deformations," primarily concerns results of computer simulations of a nonlinear crack problem. Some of these results are for problems involving loss of ellipticity. Part II, "Consequences of the Maxwell Relation for a Family of Anti-Plane Shear Deformations," is devoted to interpretation of the results presented in Part I for cases in which ellipticity is lost. So that each of these parts may be read independently of the other, there is some redundancy between them.

CONTENTS

Part II:
Consequences of the Maxwell Relation for a Family
of Anti-Plane Shear Deformations

LIST OF FIGURES

Part I

Part II

PART I:

NUMERICAL STUDIES OF ANTI-PLANE SHEAR CRACK PROBLEMS IN THE THEORY OF FINITE ELASTIC DEFORMATIONS

Chapter 1. Introduction

The aim of this work is to explore numerically the equilibrium solutions of an anti-plane shear crack problem for a variety of incompressible hyperelastic materials. For some of these materials the equilibrium equation may change in type locally as a result of deformation from the usual elliptic case to parabolic or hyperbolic, a situation which will be referred to as *loss of ellipticity.*

The problem being modeled is that of a crack of finite length embedded in a homogeneous slab occupying the entire plane and subject to mode-III loading at infinity. This problem has been the subject of extensive analysis in the past. It has a known exact solution in the linear theory of elasticity which is readily found by conformal mapping methods.

The problem has also been analyzed for a variety of plastic materials and nonlinear elastic materials. The linear solution is also the exact solution for a neo-Hookean material in the theory of finite elastic deformations. The case of an elastic-perfectly plastic material was solved by Hult and McClintock [1] using the hodograph transformation. Rice [2] extended this technique to strain-hardening plastic materials. Both of the above solutions employed the assumption of small strains. Amazigo [3] applied the hodograph method to the crack problem for a pure power-law plastic material.

Knowles [4] addressed this crack problem for finite deformations of a family of hyperelastic materials by deriving an asymptotic solution valid near the crack tips. This asymptotic solution was found by assuming that the displacement near the crack tip has the form $u \sim r^m v(\theta)$, where m is a constant, $0 < m < 1$, v is an unknown function, and (r, θ) are the polar coordinates in a frame centered at the crack tip. For most of the materials in this family which do *not* lose ellipticity, this assumption together with the boundary conditions on the crack faces results in a nonlinear eigenvalue problem whose solution gives the asymptotic solution. Knowles found the exact solution to this eigenvalue problem.

In spite of the availability of the exact solution to this eigenvalue problem, there have remained some questions pertaining to this asymptotic solution, and these questions provide part of the motivation for the present work. One issue involves the role of higher order solutions to the eigenvalue problem and whether or not they have physical significance. Unlike the asymptotic solution for the linear theory of elasticity, in which the value $m = 1/2$ is the *unique* eigenvalue in the interval $(0, 1)$, Knowles shows that in some cases in the nonlinear problem there are multiple admissible values of m. So there is a possibility that higher order terms have significance in the nonlinear case. However, the numerical results presented here show that these higher order terms are apparently not important, and the lowest order solution provides an accurate description of the solution near the crack tip even when other admissible eigenvalues exist.

Another question about the solutions to the eigenvalue problem involves the region over which they are valid. It is easy to find the size of the region in which the asymptotic solution of the problem in the *linear* theory is an accurate approximation, since the exact solution is available. However, there has previously been no way to estimate where Knowles' low-order solution applies in the *nonlinear* problem. The present work provides direct numerical observations of this region. It also describes a simple way of estimating the size of this region for large applied loads. It is shown that this estimate also gives as a byproduct the value of the J-integral and hence the magnitude of the nonlinear analogue of the stress concentration factor of linear elastic fracture mechanics.

The results described above apply to the elliptic cases only. The numerical solutions to the crack problem involving loss of ellipticity are more surprising. In some cases they are characterized by a chaotic pattern of equilibrium shocks owing to the nonuniqueness of solutions to the problem. The numerical simulations of a "trilinear material" (to be defined in Chapter 2) may be regarded as a two-dimensional analogue of the arbitrary mixture of phases which Ericksen [5] predicted in a one-dimensional bar problem for a similar material.

There are some asymptotic solutions available for the cases of the crack problem involving loss of ellipticity [6, 7] but these differ fundamentally from the numerical results. In particular, these asymptotic solutions predict hyperbolic regions in the solution, while the numerical solutions never contain such regions. (In this work the term *hyperbolic region* means a region in which the system of partial differential equations is hyperbolic, and the term *hyperbolic solution* is defined similarly.) The reason for the lack of agreement is the dynamic instability of any hyperbolic solution in a hyperelastic body in anti-plane shear. The particular numerical method used in this study (dynamic relaxation) has the property that it predicts only dynamically stable solutions, since the method works by integrating the equation of motion in a suitably formulated dynamic problem over time. Therefore it can predict a solution involving a complex mixture of elliptic phases, but it never predicts a hyperbolic region. (The issue of the sense in which dynamic notions of stability are appropriate in solutions involving equilibrium shocks is not yet settled. Stability issues for loss of ellipticity are discussed further in Part II of this work.)

Part I of this dissertation is organized as follows. Chapter 2 reviews the basic equations of anti-plane shear and defines the constitutive relations used later. Chapter 3 describes the crack problem and summarizes the asymptotic solution by Knowles. Numerical methods are discussed in Chapter 4, and validation problems are presented there. Chapter 5 contains the numerical results for the crack problem in the elliptic cases and compares these results with asymptotic solutions. In Chapter 6 approximations for the J-integral and the size of the region of validity for the asymptotic solution are considered. Chapter 7 discusses numerical results in cases where ellipticity is lost, both for the crack problem and the simpler problem of a screw dislocation. Conclusions are presented in Chapter 8.

Part II is concerned with interpretation of the numerical results for loss of ellipticity. It shows how the chaotic numerical solutions may be interpreted using notions from

elastic stability theory and the theory of phase transitions.

Chapter 2. Anti-plane shear of a generalized neo-Hookean body

2.1 Basic equations

This section reviews the concepts of anti-plane shear of an incompressible hyperelastic body as applied to the generalized neo-Hookean family of materials. The next section will discuss the particular materials used in the numerical simulations described later in this work. The following is merely a summary of the basic equations, and a more detailed treatment may be found in reference [4].

Let a rectangular coordinate system (x_1, x_2, x_3) be given. Let B be a closed cylinder with generators parallel to the x_3-direction, and let R be the cross-section of B in the (x_1, x_2)-plane. An **anti-plane shear** deformation is a mapping of the form

$$y_1 = x_1, \quad y_2 = x_2, \quad y_3 = x_3 + u(x_1, x_2) \tag{2.1}$$

where (y_1, y_2, y_3) are the coordinates of the image of a material particle originally at (x_1, x_2, x_3), and u is a function on R called the **displacement field** or simply the **deformation**. The smoothness required of u will depend on the problem at hand.

The field ∇u defined at all points in R where u is differentiable will be called the **displacement gradient field** or simply the **gradient field**. The scalar field k on this same subset of R, defined by $k = |\nabla u|$, will be called the **amount of shear field** or simply the **shear field**.

Let $\mathbf{e}_i$ be the unit vector in the x_i-direction. At any point $\mathbf{x} \in R$ where the Cauchy stress tensor σ is defined (*i.e.*, wherever u is sufficiently smooth) let $\mathbf{T}(\mathbf{x})$ be the projection of $\sigma(\mathbf{x})\mathbf{e}_3$ into the (x_1, x_2)-plane. $\mathbf{T}$ will be called the **stress vector field**. Its components are $T_1 = \sigma_{13} = \sigma_{31}$ and $T_2 = \sigma_{23} = \sigma_{32}$. The scalar field T on R defined by $T = |\mathbf{T}|$ will be called the **shear stress field**.

A stress vector field will be called **equilibrated** if for every simple closed curve C in R,

$$\int_C \mathbf{T} \cdot \mathbf{n} ds = 0 \tag{2.2}$$

where $\mathbf{n}$ is the outward-directed unit vector normal to C and s denotes arc length. It will be assumed throughout this work that there are no body forces. Cauchy's theorem shows that if $\mathbf{T}$ is equilibrated, and if $\mathbf{x} \in R$ is a point at which $\mathbf{T}$ is differentiable, then

$$\nabla \cdot \mathbf{T}(\mathbf{x}) = \mathbf{0} \tag{2.3}$$

or equivalently

$$\frac{\partial T_1}{\partial x_1}(\mathbf{x}) + \frac{\partial T_2}{\partial x_2}(\mathbf{x}) = 0 \tag{2.4}$$

This work will be concerned exclusively with homogeneous, isotropic, hyperelastic bodies whose constitutive relations in terms of the stress vector field may be written as

$$\mathbf{T}(\mathbf{x}) = \mathbf{h}(\nabla u(\mathbf{x})) = \begin{cases} \mathbf{0}, & k(\mathbf{x}) = \mathbf{0} \\ \tau(k(\mathbf{x}))\nabla u(\mathbf{x})/k(\mathbf{x}), & k(\mathbf{x}) \neq \mathbf{0} \end{cases} \tag{2.5}$$

where τ is a piecewise continuously differentiable nonnegative scalar-valued function on $[0,\infty)$ such that $\tau(0) = 0$. $\mathbf{h}$ will be called the **constitutive relation**, and τ will be called the **stress-strain relation**.

One special class of materials of this type consists of the *generalized neo-Hookean* materials. For these materials the strain energy density is a function of the trace of the Green strain tensor only. In anti-plane shear, this means that the strain energy density may be expressed as $w(k)$ where $w \in C^2([0,\infty))$. The stress-strain relation is computed from w by

$$\tau(k) = w'(k), \qquad k \geq 0. \tag{2.6}$$

The equilibrium equation (2.3) may be locally elliptic, parabolic, or hyperbolic depending on the material and the deformation. Knowles [4] shows that the type is established from the local slope of the stress-strain relation as follows:

$$\begin{aligned} \tau' > 0 &\iff \text{elliptic} \\ \tau' = 0 &\iff \text{parabolic} \\ \tau' < 0 &\iff \text{hyperbolic} \end{aligned} \tag{2.7}$$

2.2 Stress-strain relations

Three types of generalized neo-Hookean materials will be considered here: a family of *linearizable power-law* materials, a family of *pure power-law* materials, and the *trilinear* material. These are described below.

2.2.1 Linearizable power-law materials. This family of generalized neo-Hookean materials was proposed by Knowles [4] for purposes of demonstrating the asymptotic nature of anti-plane shear deformations near the tip of a crack for various kinds of large-strain constitutive behavior. It is a three-parameter family of materials in which the large-strain behavior is determined by a *hardening parameter* n. Regardless of n, the material is linearizable in the sense that the slope of the stress-strain relation is finite and positive at zero shear.

The stress-strain relation will be denoted $\tau(k) = \tau_\ell(k;n)$ and is given by

$$\tau_\ell(k;n) = \mu k \left(1 + \frac{b}{n}k^2\right)^{n-1}, \qquad k > 0, \quad n > 0. \tag{2.8}$$

where μ is a positive constant (which equals the shear modulus after linearization near $k = 0$) and b is a positive constant. A corresponding strain energy density function is

$$w(k) = \frac{\mu}{2b}\left[\left(1 + \frac{b}{n}k^2\right)^n - 1\right]. \tag{2.9}$$

Because of scaling considerations to be discussed in Chapter 6, the parameters μ and b are not important in investigating the essential nature of the crack problem at hand. In all the numerical simulations for this family of materials the arbitrary values $\mu = 10^9$ and $b = 1$ were used. Six different values of n were used: 5, 1.5, 1, 0.6, 0.5, and 0.25. The stress-strain relations for these values are illustrated in Figure 2.1. Note that of these, only the case $n = 0.25$ can undergo a loss of ellipticity.

If $n > 1$, the material is a *hardening* material. If $n = 1$ the material is neo-Hookean, and the equilibrium equation (2.3) reduces to Laplace's equation. If $1/2 < n < 1$ the

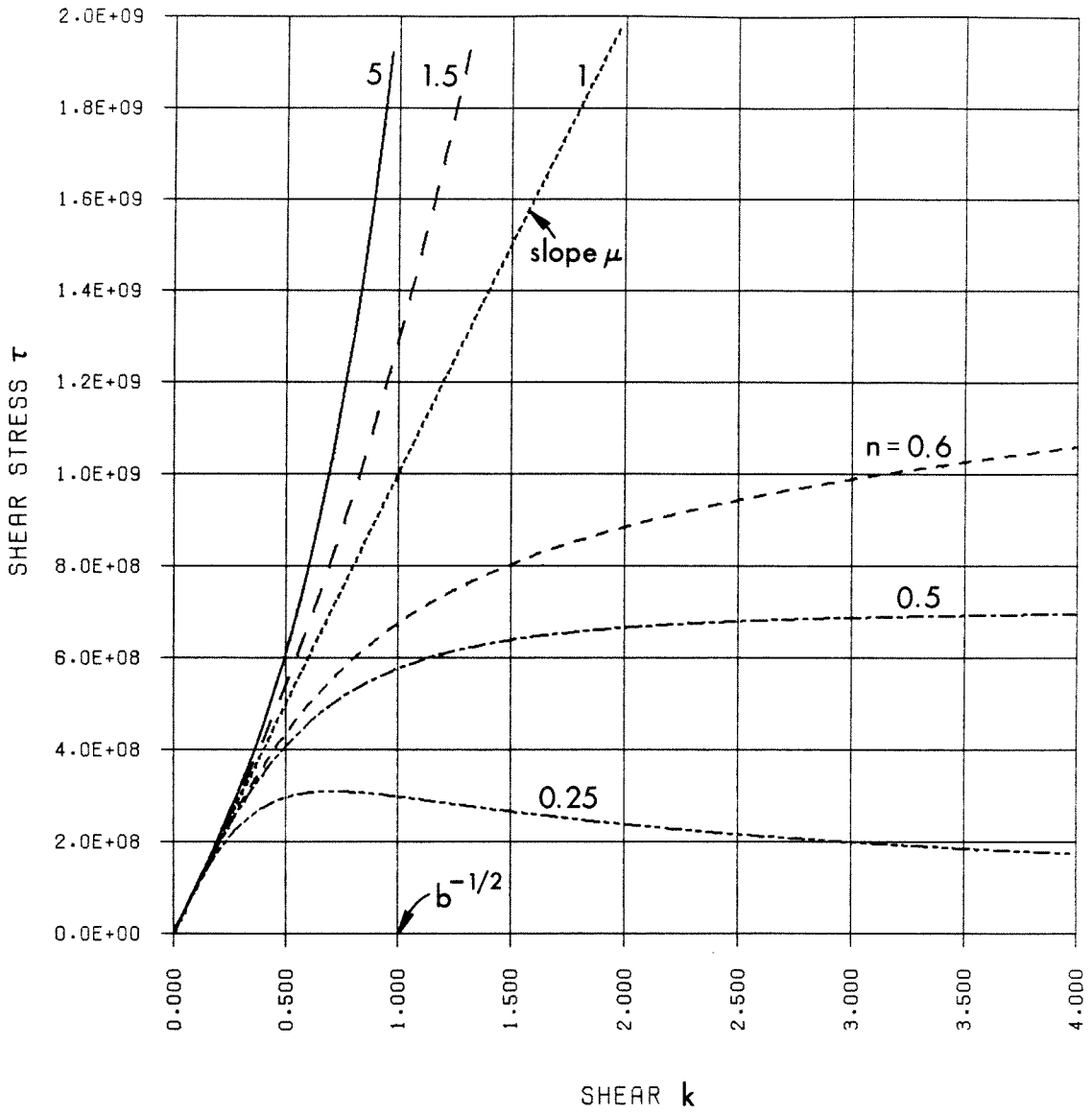

Figure 2.1. Stress-strain relation $\tau_\ell(k)$ for linearizable power-law material.

material is *softening*. If $n = 1/2$ the stress-strain relation approaches a constant positive value for large shear, but the equilibrium equation remains elliptic. The hyperbolic cases are provided by $0 < n < 1/2$, for which the stress-strain relation passes a maximum and asymptotically approaches zero for large shear.

2.2.2 Pure power-law materials. This family of materials is identical to the linearizable power-law materials for large-strain behavior. However, they do not in general have stress-strain relations with finite slope at $k = 0$, so they are not linearizable.

The stress-strain relation for this family of materials will be denoted $\tau(k) = \tau_p(k; n)$ and is given by

$$\tau_p(k; n) = \mu k \left(\frac{b}{n} k^2\right)^{n-1}, \qquad k > 0, \quad n > 0. \tag{2.10}$$

where μ is a positive constant (which equals the shear modulus after linearization near $k = 0$) and b is a positive constant. A corresponding strain energy density function is

$$w(k) = \frac{\mu}{2b} \left(\frac{b}{n} k^2\right)^n. \tag{2.11}$$

The pure power-law materials are used in this work solely in the context of validation problems for the numerical method, since there happen to be exact solutions available for certain crack problems with these materials.

2.2.3 Trilinear material. The stress-strain relation of the trilinear material will be denoted $\tau_\triangleleft$ and is given by

$$\tau_\triangleleft(k) = \begin{cases} \mu^- k, & 0 \le k \le K^- \\ \mu^- K^- + (k - K^-)\frac{\mu^+ K^+ - \mu^- K^-}{K^+ - K^-}, & K^- \le k \le K^+ \\ \mu^+ k, & K^+ \le k \end{cases} \tag{2.12}$$

and where K^+, K^-, μ^+, and μ^- are positive constants such that $K^- < K^+$, $\mu^- > \mu^+$, and $\mu^- K^- > \mu^+ K^+$. (See Figure 2.2.)

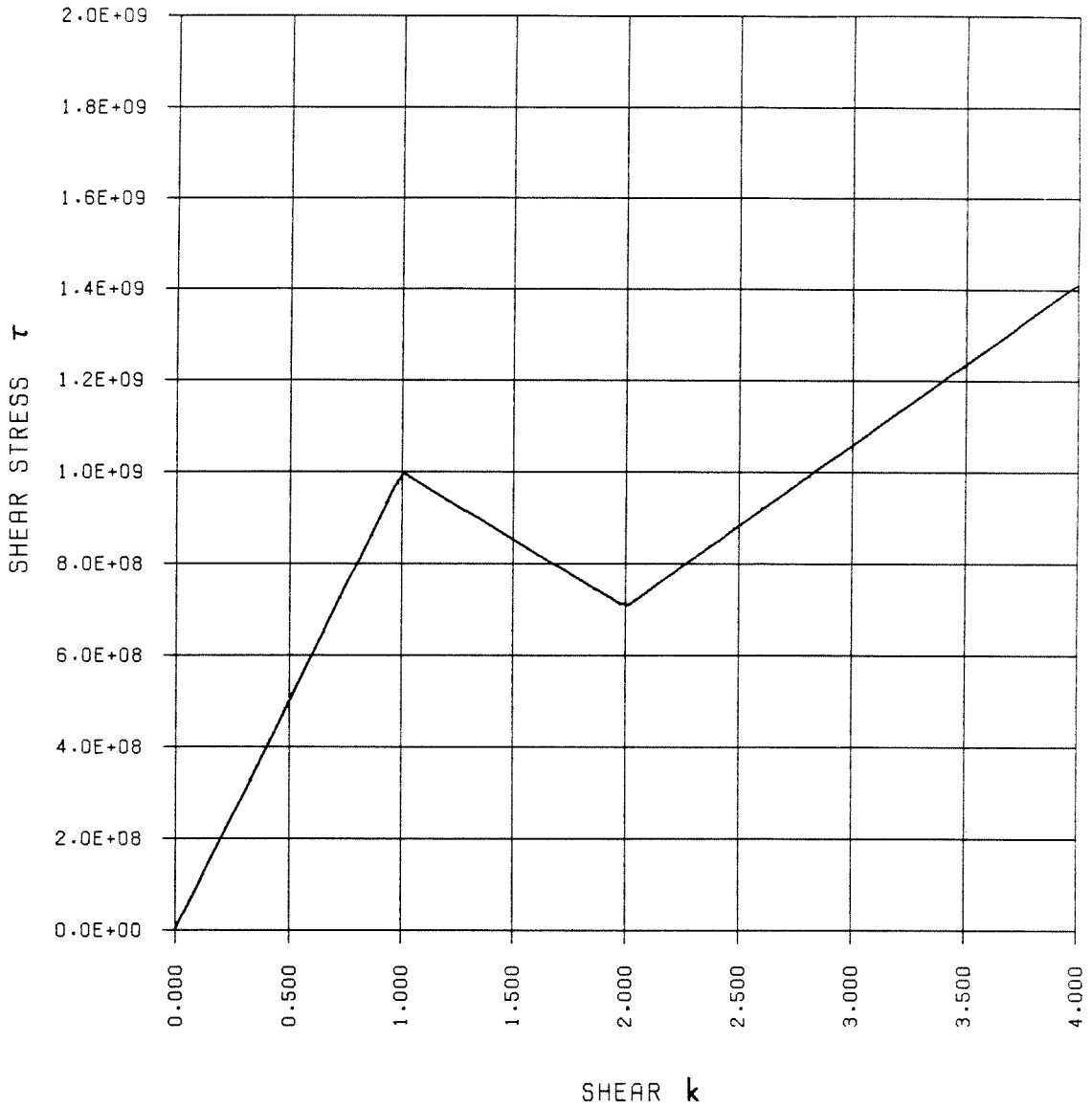

Figure 2.2. Stress-strain relation $\tau_{\triangleleft}(k)$ for trilinear material.

The strain energy density for the trilinear material is given by

$$w_{\triangleleft}(k) = \begin{cases} \dfrac{\mu^- k^2}{2}, & 0 \le k \le K^- \\ \dfrac{\mu^- K^{-2}}{2} + (k - K^-)\left[\mu^- K^- + \frac{1}{2}(k - K^-)\dfrac{\mu^+ K^+ - \mu^- K^-}{K^+ - K^-}\right], & K^- \le k \le K^+ \\ \dfrac{\mu^- K^{-2}}{2} + \dfrac{K^+ - K^-}{2}(\mu^+ K^+ + \mu^- K^-) + \dfrac{\mu^+}{2}\left(k^2 - K^{+2}\right), & K^+ \le k \end{cases} \tag{2.13}$$

The trilinear material is interesting to study for two reasons. First, unlike the hyperbolic cases of the power-law material, in the trilinear material the hyperbolic segment in the stress-strain relation (denoted H) is bounded and lies between low-strain and high-strain elliptic segments (denoted E^- and E^+ respectively). Second, for subregions in the body in which k is in either of the elliptic segments, the equilibrium equation (2.3) reduces to the Laplace equation.

The values of the constants used in the numerical simulations are as follows: $K^- = 1$, $K^+ = 2$, $\mu^- = 10^9$, and $\mu^+ = 10^9/\sqrt{8}$.

Numerical results involving the trilinear material are presented in Chapter 7 of Part I. Part II of this dissertation is devoted largely to interpreting these results in the context of the general theory of stability and phase changes.

Chapter 3. Anti-plane shear crack problem and asymptotic solution

Most of the remainder of this work will be concerned with the anti-plane shear crack problem specified below. Let R be the entire plane, and let a rectangular coordinate frame (x_1, x_2) be given. Let c be a positive number, and let the crack occupy the line segment $L = \{(x_1, x_2) \mid -c \le x_1 \le c,\ x_2 = 0\}$. Define D to be the complement of L in the plane. (See Figure 3.1.)

Call the displacement field u. We seek a field $u \in C^2(D)$ satisfying the equilibrium equation (2.3) and the constitutive relation $\mathbf{T}(\mathbf{x}) = \mathbf{h}(\nabla u(\mathbf{x}))$ subject to the following conditions:

$$\lim_{x_2 \to 0+} \frac{\partial u}{\partial x_2} = \lim_{x_2 \to 0-} \frac{\partial u}{\partial x_2} = 0, \qquad -c < x_1 < c \tag{3.1}$$

and

$$u \sim k_\infty x_2 \qquad \text{as } x_1^2 + x_2^2 \to \infty \tag{3.2a}$$

where k_∞ is a constant. Let $\tau_\infty = \tau(k_\infty)$. If the stress-strain relation is invertible at τ_∞, *i.e.*, if k_∞ is the only value of shear corresponding to τ_∞, then (3.2a) may be replaced by a stress condition at infinity:

$$T_1 \sim 0, \qquad T_2 \sim \tau_\infty \qquad \text{as } x_1^2 + x_2^2 \to \infty \tag{3.2b}$$

where $\tau_\infty = \tau(k_\infty)$.

From now on we will be concerned with the linearizable power-law material with hardening parameter n, so $\tau(\cdot) \equiv \tau_\ell(\cdot; n)$. There is no known exact solution for this crack problem except in the case of a neo-Hookean material ($n = 1$). However, Knowles [4] presents an asymptotic solution valid near the crack tips for the elliptic cases ($n \ge 1/2$). This asymptotic solution, which will also be called the *low-order* solution, is summarized below for later reference. Define a polar coordinate system (r, θ) centered at the right crack tip. For the case $n > 1/2$, the low-order solution is

$$u \sim r^m v(\theta) \qquad \text{as } r \to 0, \quad -\pi < \theta < \pi \tag{3.3}$$

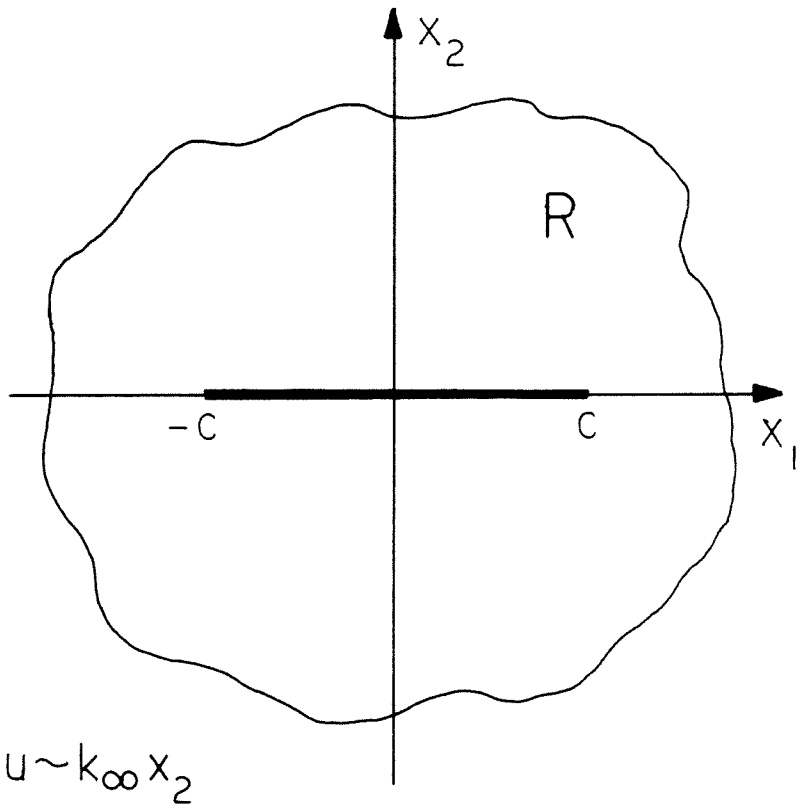

Figure 3.1. Anti-plane shear crack problem.

where

$$m = 1 - 1/2n, \tag{3.4}$$

$$v(\theta) = A \sin\frac{\theta}{2}\left[1 - \frac{2(1-1/n)^2\cos^2(\theta/2)}{1+\omega(\theta,n)}\right]^{1/2}\left[\omega(\theta,n) + (1-1/n)\cos\theta\right]^{(n-1)/2n}, \tag{3.5}$$

$$\omega(\theta,n) = \left[1 - (1-1/n)^2\sin^2\theta\right]^{1/2}, \qquad -\pi < \theta < \pi \tag{3.6}$$

and A is a constant which is determined by conditions far from the crack. The stress vector field components associated with this asymptotic solution are

$$T_\alpha \sim \mu\left(\frac{b}{n}\right)^{n-1} p^{n-1}(\theta)\left[mv(\theta)c_\alpha(\theta) + \dot{v}(\theta)\epsilon_{\beta\alpha}c_\beta(\theta)\right] r^{-m} \tag{3.7}$$

and the out-of-plane normal stress component is

$$\sigma_{33} \sim \mu\left(\frac{b}{n}\right)^{n-1} p^n(\theta) r^{-1} \tag{3.8}$$

where

$$c_1(\theta) = \cos\theta, \qquad c_2(\theta) = \sin\theta \tag{3.9}$$

and

$$p(\theta) = A^2\frac{(2n-1)^2}{4n^3}\left[\left(1-\frac{1}{n}\right)\cos\theta + \omega(\theta,n)\right]^{-1/n}. \tag{3.10}$$

The strain energy density is found to be

$$W \sim \frac{\mu}{2b}p^n(\theta)\left(\frac{b}{n}\right)^n r^{-1} \tag{3.11}$$

For the case $n = 1/2$ Knowles found an asymptotic solution by use of the hodograph transformation. The resulting displacement field is

$$u \sim \begin{cases} -c\sqrt{2b}\,k_\infty{}^2, & -\pi < \theta \le -\pi/2 \\ c\sqrt{2b}\,k_\infty{}^2\sin\theta, & -\pi/2 \le \theta \le \pi/2 \\ c\sqrt{2b}\,k_\infty{}^2, & \pi/2 \le \theta < \pi \end{cases} \tag{3.12}$$

The asymptotic solution quoted above requires evaluation of the constant A for the $n > 1/2$ case. For the case of small k_∞, Knowles accomplishes this using the path independence of the J-integral, which is computable from the linear solution to the global crack problem. This solution is assumed to be valid far from the crack. In the linear solution, for a contour surrounding the right crack tip,

$$J = \frac{\pi}{2}\mu c {k_\infty}^2 \tag{3.13}$$

while the corresponding integral over a small circle centered at the crack tip for the low-order solution is

$$J = \pi\mu b^{n-1} A^{2n} \frac{(2n-1)^{2n-1} n^3}{(4n^4)^n}. \tag{3.14}$$

Equating these two expressions leads to the estimate

$$A^{2n} = \frac{c}{2} b^{1-n} f(n) {k_\infty}^2 \tag{3.15}$$

where

$$f(n) = \frac{(4n^4)^n}{(2n-1)^{2n-1} n^3}. \tag{3.16}$$

This estimate holds only for small k_∞. An estimate for large k_∞ will be discussed in Chapter 6.

Chapter 4. Approximations and numerical methods

The numerical modeling of nonlinear crack problems continues to present difficulties in spite of the considerable advances that have been made in computer hardware and the technology of finite elements.

Various accurate and efficient numerical methods, such as the boundary integral method, are available for modeling singular problems in the *linear* theory of elasticity. The most common approach to representation of singularities in *nonlinear* problems is the use of singular elements. These elements are designed to provide the stiffness response of a given type of singularity located within the area represented by the element. Their limitation is that the properties of the singularity must be known or assumed. In the present work, the properties of the singularity are precisely what are being investigated, so it would be inappropriate to use such methods.

Another challenge presented by the nonlinear problems being investigated here is the inherent nonlinearizability of some of the problems. When ellipticity is lost in anti-plane shear problems, for example, the stress-strain relation may be locally downward-sloping. Simple hand calculations show that methods relying on linearization of the problem at any stage of the calculation would be expected to have difficulty in converging, and the physical significance of such solutions would be suspect even if they did converge. Therefore it is preferable not to use Newton-Raphson iteration or its derivatives or any of the incremental methods that are in wide use for conventional plasticity problems.

A third difficulty arising in the nonlinear elasticity problems considered here is the issue of elastic stability. Part II of this thesis discusses in detail the tremendous degree of nonuniqueness exhibited by boundary value problems involving loss of ellipticity and the role of elastic stability in choosing physically meaningful solutions. While the question of what is the correct notion of stability for these problems is far from resolved, it is reasonable to exclude those equilibrium solutions which spontaneously decay to other solutions when considered as initial conditions to a dynamic problem with the same

boundary conditions. Therefore a desirable trait of a numerical method would be that it predict only solutions that are dynamically stable in this sense. There is no reason to believe that methods such as Newton-Raphson iteration or incremental methods necessarily give solutions which have this stability property. (Note that nothing is being said here about minimization of potential energy, whose relation to dynamic stability is murky for equilibrium problems involving loss of ellipticity.)

The next section describes the numerical method developed for the present calculations.

4.1 The APE computer program

The APE program is the anti-plane shear version of CHIMP, which has been documented elsewhere [8]. The program uses a finite-difference method with dynamic relaxation and explicit integration in time. Spatial differencing in APE is accomplished using a Green's theorem formulation [9], which allows great flexibility with regard to mesh configuration. The displacement gradient vector field components are evaluated using the same spatial differencing method as for the stress tensor field components. Stress components are computed by substituting the displacement gradient components into the constitutive relation.

Dynamic relaxation [10] is the calculation of an equilibrium solution as the large-time limit of a damped dynamic problem. The equation of motion is integrated with a viscous damping term starting from some reasonable set of initial conditions. The viscous damping coefficient is chosen so as to provide critical damping for the fundamental vibrational mode of the mesh, since this value provides the fastest convergence rate.

Explicit central differencing in time is used in APE. This method allows great flexibility in the choice of constitutive relations, since there is no program modification necessary when a new material is introduced. The time integration method is conditionally stable. The stability condition is the Courant condition, which requires that the time step must be less than the minimum transit time for an infinitesimal wave through any zone in the mesh. In order to accommodate meshes in which the zone spacing varies

over orders of magnitude, APE exploits the dependence of speed of infinitesimal waves on mass density, a technique first suggested by Day [11]. Since the wave speed varies with the square root of density, and since the density field is irrelevant to an equilibrium solution, APE is able to assign zone mass densities so that the wave transit times are equal for all zones in the mesh in spite of any differences in spacing.

APE is adapted from methods such as HEMP [12] in wide use for moderate-distortion dynamic problems possibly involving interaction of many physical and chemical phenomena. While seldom used for equilibrium solid mechanics problems because of a lack of versatility compared with the finite-element method, this method has advantages with regard to the three difficulties mentioned at the beginning of this section.

Crack tips are readily modeled by APE as the ends of long thin elliptical holes. Logarithmic spacing of zones is used to focus greatest numerical resolution near the crack tip. For the present work, zone sizes near the ellipse tip were typically 10^{-5} times the size near the outer edges of the mesh. The validation problems presented elsewhere in this chapter show that this method of modeling a crack provides good resolution of the singularity except in the case of a severely hardening material close to the crack tip.

The APE method does not use linearization at any step of the calculation. As mentioned above, this is an inherent advantage because of the nonlinearizability of the problems considered here. APE also has the property of predicting only solutions that are dynamically stable with respect to the particular boundary value problem chosen. This is true because the program computes an equilibrium solution as the large-time limit of a dynamic problem. The viscous damping introduced as a means of achieving convergence does not affect the dynamic stability of the converged solution, since stability is a property of the solution itself rather than the means used to compute it.

4.2 Approximation of cracks by elliptical holes and leading term solutions

This section discusses the errors involved in the modeling of crack problems by elliptical hole problems and by asymptotic solutions. The following questions will be

addressed here:

(a) In what region should agreement between the exact solution and these approximations be expected?

(b) In this region, how close should the agreement be?

These questions cannot be answered *a priori* in the general nonlinear case, but it will be shown here that they can be answered with precision in the linear case. Although the quantitative answers for the linear case do not apply directly to the nonlinear problem, they help explain the qualitative nature of the agreement that is observed, at least in those problems where no loss of ellipticity is involved.

The leading term solution of the crack problem near the crack tip becomes *more* accurate as the crack tip is approached. The approximate solution obtained by treating the crack as an elliptical hole becomes *less* accurate as the crack tip is approached. Therefore one would expect the best agreement between the leading term solution and the elliptical hole solution in some annular region surrounding the crack tip.

In the linear theory of elasticity exact solutions are available for both the crack problem and the elliptical hole problem by conformal mapping techniques. The lowest order (leading term) solution near the crack tip is also readily obtained from this solution. These solutions will be used here to study the relation between the three problems quantitatively.

Denote the anti-plane shear crack problem defined in Chapter 3 as problem P. Now consider a second problem P' whose exact solution is to be used as an approximation to problem P. To decide how good the approximation is, it is necessary to define what an *error* is. For the crack problem, one suitable measure is as follows. Define a function ϵ on $(0, c)$ by

$$\epsilon(r) = \frac{\max\limits_{C_r} |\mathbf{T} - \mathbf{T}'|}{\max\limits_{C_r} |\mathbf{T}|}, \qquad 0 < r < c \tag{4.1}$$

where $\mathbf{T}$ and $\mathbf{T}'$ are the stress vector fields associated with P and P' respectively, and C_r is the circle of radius r centered at the crack tip. The quantity $\epsilon(r)$ will be called the *fractional error* of P' at radius r.

Suppose one wishes to find the region in which ϵ is less than some required value, say 0.20. To do this in the leading term and elliptical hole approximations, it will be convenient to consider the way ϵ scales according to the characteristic lengths that are present in the problems. In the leading term approximation the only characteristic length is c. As mentioned above, this approximation becomes better for small r. Therefore one expects there to be some number r_2/c independent of c such that $\epsilon(r) < 0.20$ whenever $r < r_2$.

For the moment assume that the elliptical hole model of the crack problem has the semi-major axis a equal to the crack length c. (It will be shown later that this is not in general the best model.) Then in the elliptical hole approximation there are two characteristic lengths: the semi-major axis of the ellipse, c, and the radius of curvature at the crack tip, ρ. (ρ is related to the semi-minor axis b by $\rho = b^2/c$.) Therefore there should be a number r_1/ρ, dependent only on ρ/c, such that $\epsilon(r) < 0.20$ whenever $r > r_1$.

So, to find the region of agreement, it is necessary to find the numbers r_1 and r_2 for only a single value of c and for variable ρ. Figure 4.1 shows $\epsilon(r)$ for $c = 1/2$ and for three values of ρ in the linear problem. Both axes are on logarithmic scales. r_1 and r_2 may be read off this figure for any desired value of ϵ. The results for $\epsilon = 0.20$ are shown in Table 4.1. The value of r_2/c for this ϵ is 0.30.

c/b	ρ/c	r_1/ρ	r_2/ρ
100	1.00×10^{-4}	1.50	3000
80	1.56×10^{-4}	1.51	1923
50	4.00×10^{-4}	1.55	750
30	1.11×10^{-3}	1.63	270
20	2.50×10^{-3}	1.76	120
10	1.00×10^{-2}	2.32	30

Table 4.1. Elliptical hole approximations, $\epsilon = 0.20$.

This table shows that for a desired accuracy of $\epsilon < 0.20$, one can use the elliptical hole approximation with any thinness ratio between 10 and 100 on the region $r > 2.32\rho$. For the leading term approximation, the desired accuracy is obtained if $r < 0.30c$.

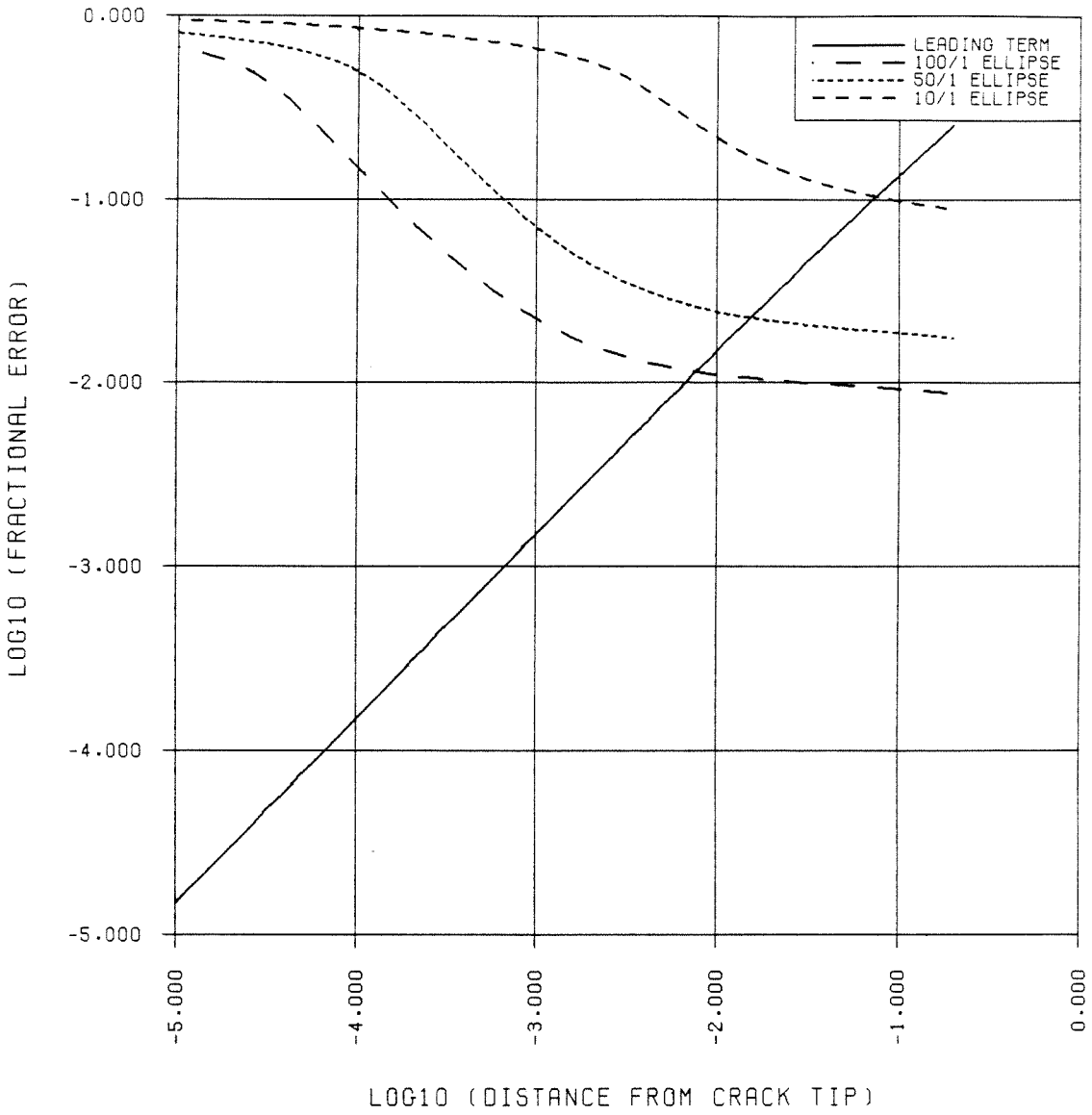

Figure 4.1. Fractional error ϵ as a function of distance r from crack tip for leading term and elliptical hole approximations in linear anti-plane shear crack problem.

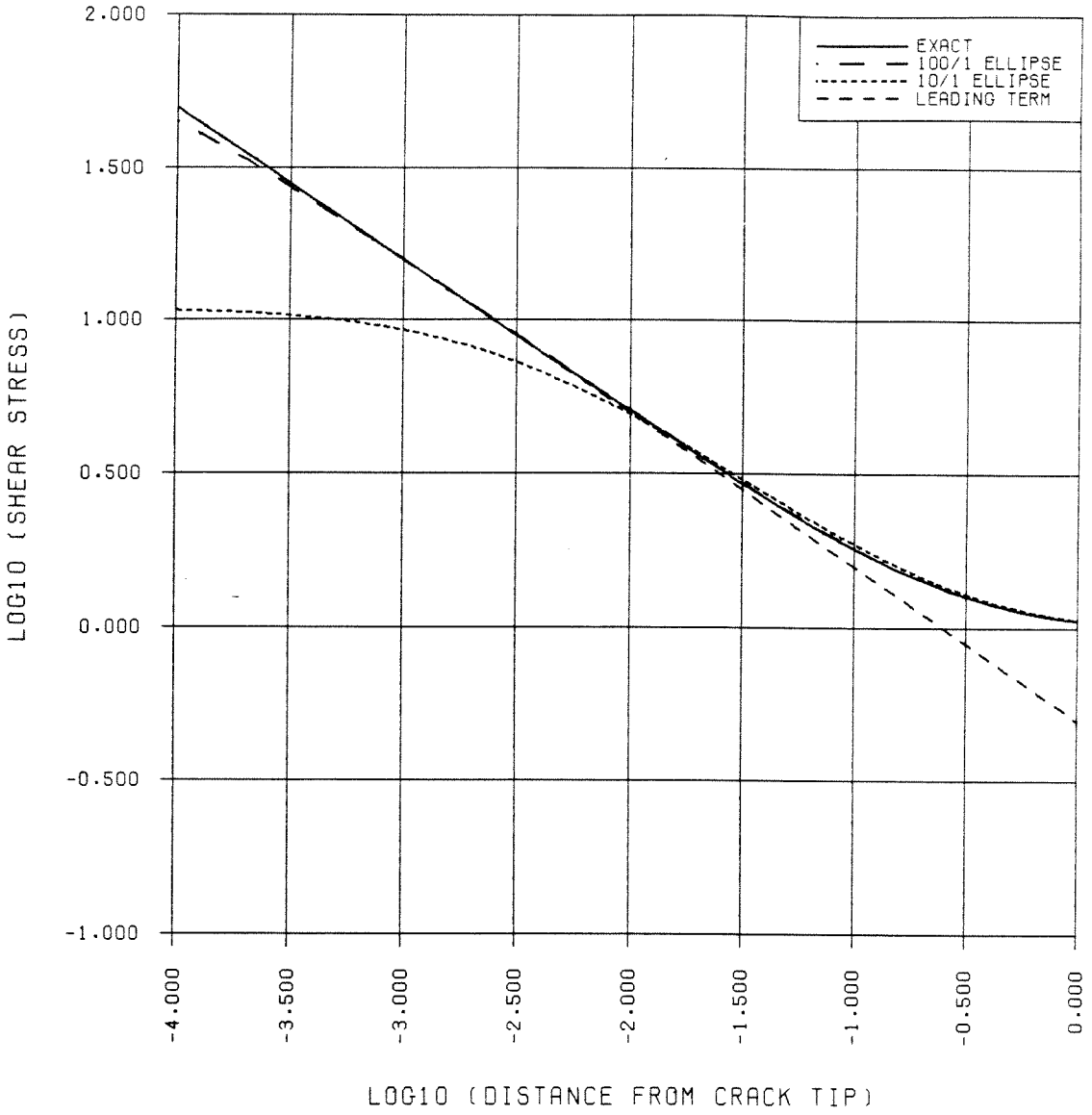

Figure 4.2. Shear stress T as a function of distance r from crack tip for leading term and elliptical hole approximations in linear anti-plane shear crack problem.

Figure 4.2 shows the shear stress T for the exact solution, the leading term approximation, and two ellipses along the crack axis near the crack tip with $c = 1/2$. Note that since both axes are on logarithmic scales, the leading term solution is a straight line of slope $-1/2$. The leading term solution becomes an excellent approximation close to the crack tip. The ellipses provide good approximations at distances greater than a few radii of curvature.

4.3 Optimum ellipse for nonlinear crack problems

Section 4.2 discussed approximation of the linear crack problem by an elliptical hole whose major axis precisely equals the crack length. However, it happens that the solution to the linear elliptical hole problem is an *exact* solution (at points where it is defined) to the crack problem in which the crack tips are located at the *foci* of the ellipse rather than at the endpoints. This property of the linear anti-plane shear problem may be confirmed by deriving the elliptical hole solution by the conformal mapping known as the Joukowski transformation [13]. It will be shown here that in the *nonlinear* case, while there is no elliptical hole problem which provides an exact solution to the crack problem, there is nevertheless a family of *optimum ellipses* for the crack problem which minimize errors near the crack tip.

Consider the crack problem for a linearizable power-law material with $n > 1/2$. Suppose one wishes to model the crack by a thin elliptical hole. The cost of numerical simulation of the elliptical hole problem increases with the thinness ratio a/b, where a is the semi-major axis and b is the semi-minor axis. Assume that the thinness ratio has been set by these cost considerations. It remains to find a for the given crack half-length c such the numerical solution is as close as possible to the crack solution near the crack tip.

Let a be the semi-major axis of the optimum ellipse for a given c and a given value of a/b. Let $\bar{r} = a - c$ (see Figure 4.3). Let ρ denote the radius of curvature of the ellipse at the tip, $\rho = b^2/a$. Consider a polar coordinate system (r, θ) centered at the right crack tip.

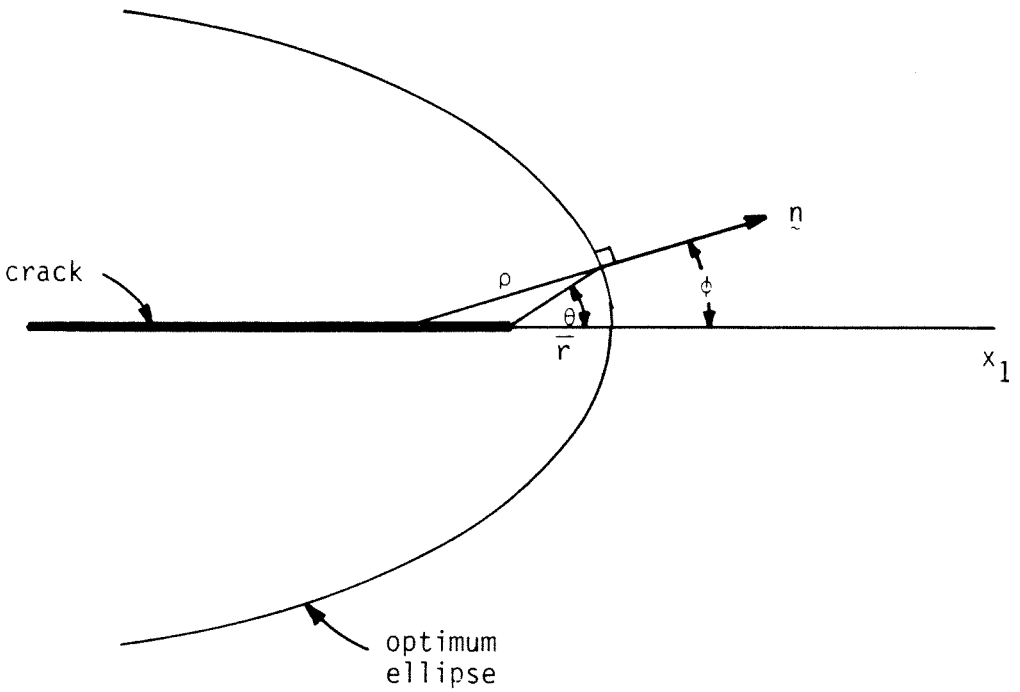

Figure 4.3. Optimum ellipse for a crack problem.

Assume that the low-order asymptotic solution by Knowles discussed in Chapter 3 holds near the crack tip. Let u be the displacement field associated with this asymptotic solution. Then

$$u = r^m v(\theta), \qquad m = 1 - 1/2n \tag{4.2}$$

where v is given in (3.5).

Associated with the asymptotic solution is a family of traction-free curves. An optimum ellipse is defined as an ellipse C whose curvature at the endpoint equals that of the traction-free curve which is tangent to it there. Therefore

$$\frac{\partial u}{\partial n} \approx 0 \qquad \text{on } C \text{ near } \theta = 0 \tag{4.3}$$

where n denotes the normal direction along C. Evaluation of the normal derivative leads to

$$\frac{\partial u}{\partial n} \approx \bar{r}^{m-1} \left[m v(\theta) n_r(\theta) + \dot{v}(\theta) n_\theta(\theta) \right] \tag{4.4}$$

where n_r and n_θ are the radial and tangential components of $\mathbf{n}$, the normal unit vector directed outward.

Let $\phi(\theta)$ be the angle that $\mathbf{n}$ makes with the x_1-axis at any θ. Then (4.3) and (4.4) imply that for $\theta \approx 0$,

$$\phi(\theta) \approx \theta + \frac{n_\theta(\theta)}{n_r(\theta)} \approx \theta - \frac{m v(\theta)}{\dot{v}(\theta)} \approx \theta - \frac{m \dot{v}(0) \theta}{\dot{v}(0)} = (1 - m)\theta \tag{4.5}$$

Referring to Figure 4.3, $\rho\phi \approx \bar{r}\theta$. Thus (4.5) implies

$$\frac{\bar{r}\theta}{\rho} \approx (1 - m)\theta. \tag{4.6}$$

Hence

$$\bar{r} \approx (1 - m)\rho \tag{4.7}$$

or equivalently

$$\bar{r} \equiv a - c = \frac{\rho}{2n}. \tag{4.8}$$

(4.8) gives the semi-major axis of the optimum ellipse, and the semi-minor axis is then computed from the known thinness ratio.

The efficacy of this choice of the ellipse geometry in modeling crack problems may be seen in the validation problems discussed in the next section, both of which use the optimum ellipse method.

4.4 Validation problems

This section presents numerical simulations of problems with known exact solutions for purposes of evaluating the accuracy of the numerical method. First, the numerical solution to the global crack problem is computed for the case of a linear (or a neo-Hookean) material. This is compared with the exact solution which is obtained by conformal mapping. The second test case is a boundary value problem whose *exact* solution is the low-order solution which Knowles introduced as an *approximate* solution to nonlinear crack problems (see Chapter 3).

4.4.1 Global solution to the linear crack problem. This validation problem assesses the accuracy of the numerical method in finding the near-field and far-field solutions simultaneously in the crack problem. The material modeled is a neo-Hookean material, for which the displacement field found from linear elasticity theory holds exactly. The exact solution to this problem may be found by a conformal mapping technique using the Schwartz-Christoffel transformation or the Joukowski transformation. The resulting field is most conveniently expressed as the real part of a complex function:

$$u(x_1, x_2) = \mathrm{Re}\left\{-ik_\infty \sqrt{z^2 - c^2}\right\}, \qquad z = x_1 + ix_2, \tag{4.9}$$

where the desired branch of the complex square root function is defined by $\sqrt{\varsigma} = |\varsigma|^{1/2} e^{i\theta/2}$, $\varsigma = |\varsigma| e^{i\theta}$, $-\pi < \theta \leq \pi$.

The numerical model for this validation problem was the same as the one used for the calculations presented later in this work for nonlinear cases. The mesh, shown in Figure 4.4, was generated in such a way that nodes lie along families of hyperbolas and ellipses. The total number of nodes was 1000. To model the condition at infinity, the crack was embedded in a mesh which was nearly circular at its outer boundary, and

whose radius was about $20c$. Tractions derived from the homogeneous deformation corresponding to the condition at infinity were applied at the outer circular boundary. The crack faces were traction-free, as was the x_2-axis. The x_1-axis was a zero-displacement boundary for $x_1 \geq c$.

Figure 4.5 compares the shear stress T along the crack axis for the numerical and the exact solutions. This graph employs the optimum ellipse method for making this comparison (see previous section). This means that the crack being modeled has tips on the foci of the ellipse. Figures 4.6(i)–(iv)compare the data for u, T, T_1, and T_2 along a circle of radius $0.02c$ centered at the right crack tip. Computation of the fractional error $\epsilon(r)$ defined previously shows that $\epsilon < 0.02$ near the crack tip.

4.4.2 A nonlinear singular problem. By identifying the terms in the equilibrium equation which are neglected in the derivation of Knowles' low-order solution for the *linearizable* power-law material, one can show that this solution is an *exact* solution to a suitably contrived boundary value problem for the *pure* power-law material. In this problem the displacements found from the low-order solution with an arbitrary value of A are taken as boundary conditions for the mesh shown in Figure 4.4 (except for the crack faces, which remain traction-free).

For this admittedly artificial boundary value problem, the low-order solution discussed in Chapter 3 provides an exact solution. This problem allows direct observation of the accuracy of the numerical method in nonlinear crack problems.

The same mesh used in the first validation problem was used here. The x_2-axis is no longer an axis of symmetry, and both this axis and the outer circular boundary have fixed displacements along them found from the low-order solution. The crack faces remain traction-free.

Figures 4.7(i)–(iv)compare the shearing stress T along the crack axis for four pure power-law materials: $n = 5$, 1.5, 1, and 0.6. It may be seen from the figures that there is some disagreement close to the crack tip for the nonlinear cases. This disagreement is caused by the fact that any ellipse, even the optimum ellipse discussed above, is an

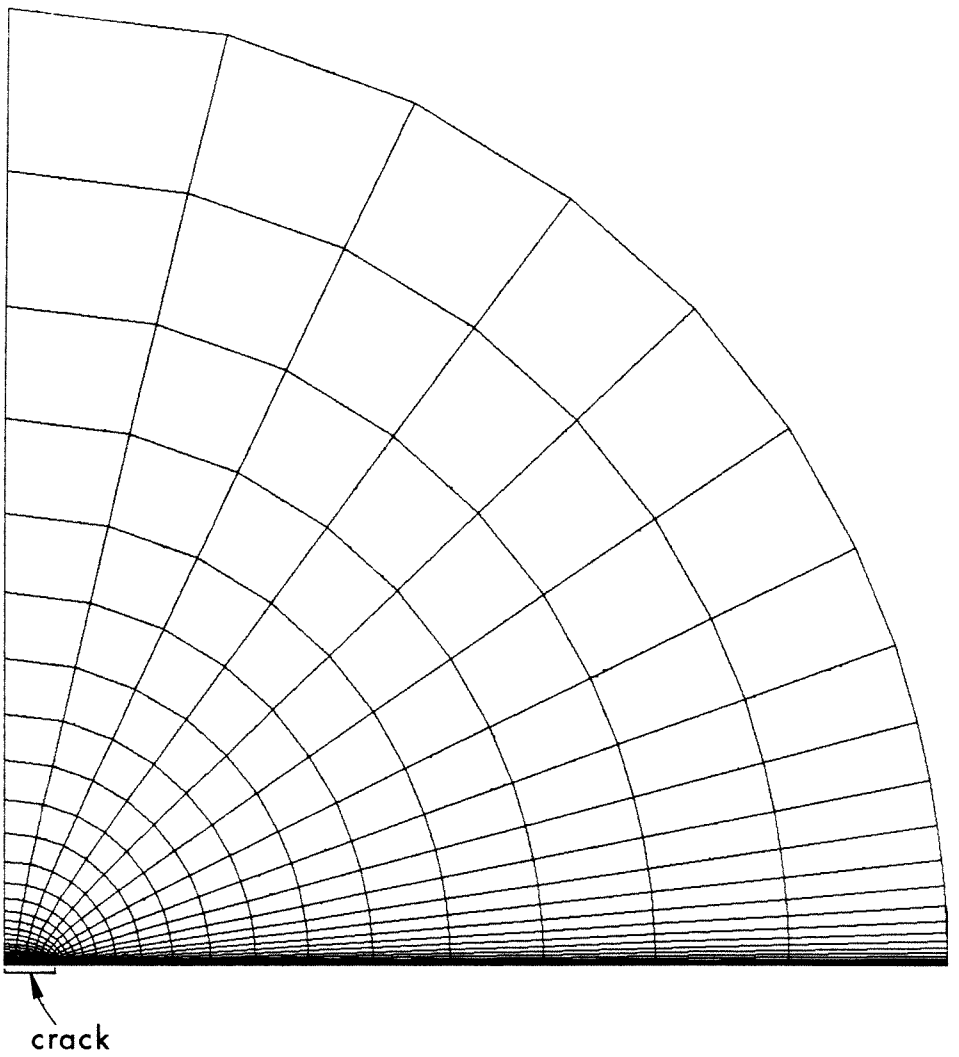

Figure 4.4. Numerical mesh used in crack problem simulations. Thinness ratio of elliptical hole is 50.

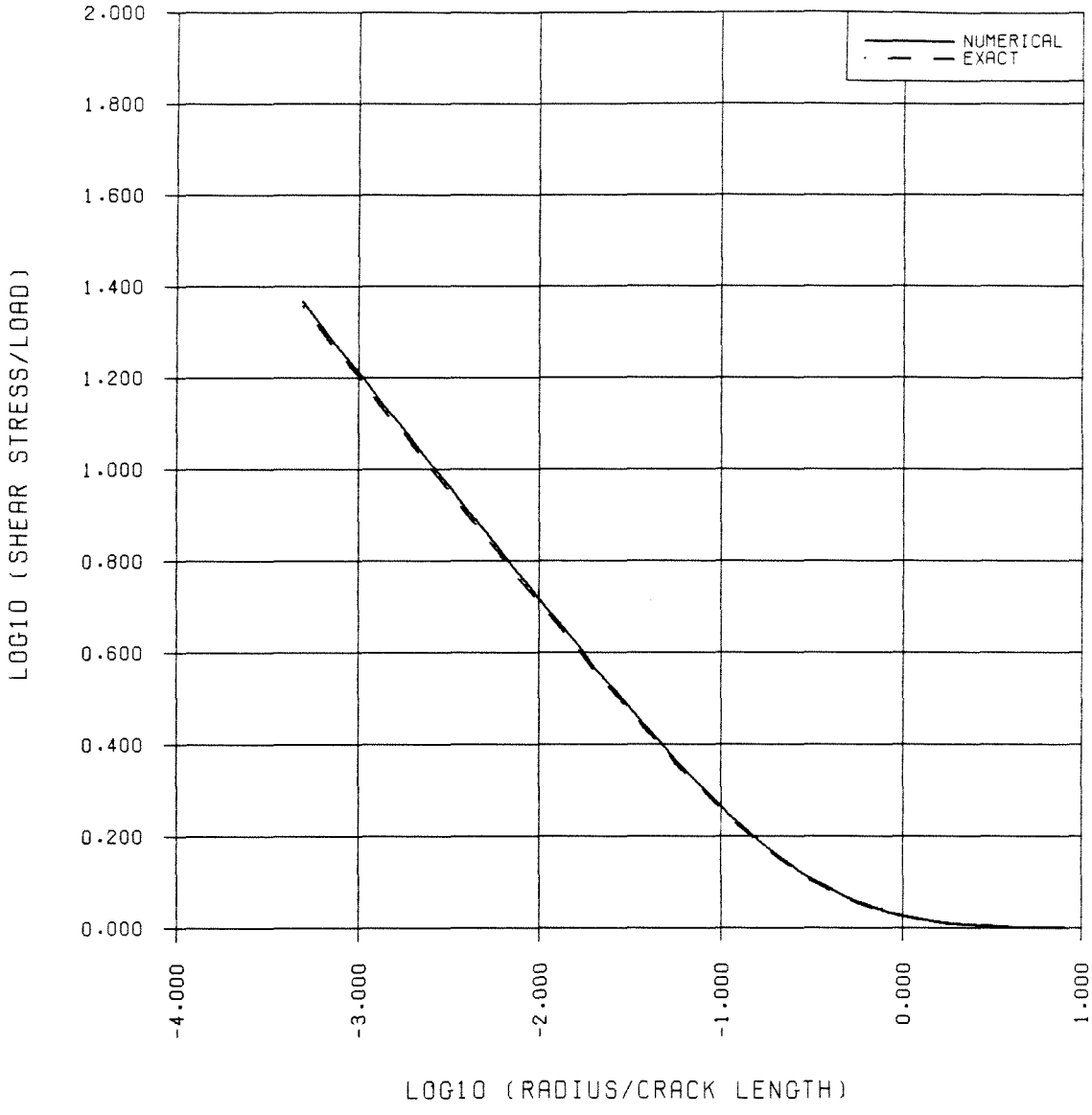

Figure 4.5. Numerical and exact solutions for crack problem in neo-Hookean material: shear stress T as a function of distance r from crack tip along crack axis.

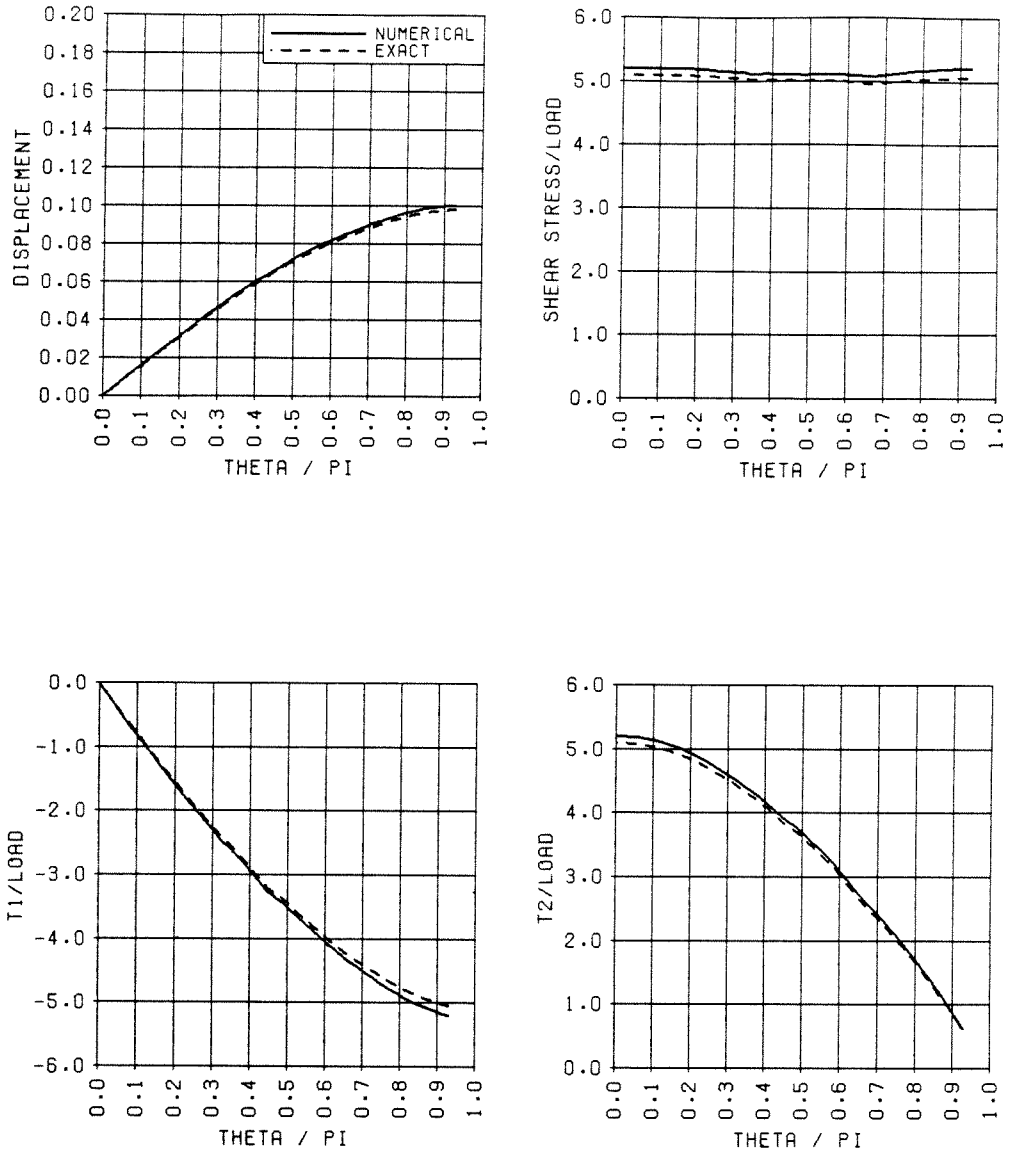

Figure 4.6. Numerical and exact solutions for crack problem in neo-Hookean material: θ-dependence of (i)u, (ii)T, (iii)T_1, (iv)T_2 along small circle centered at crack tip.

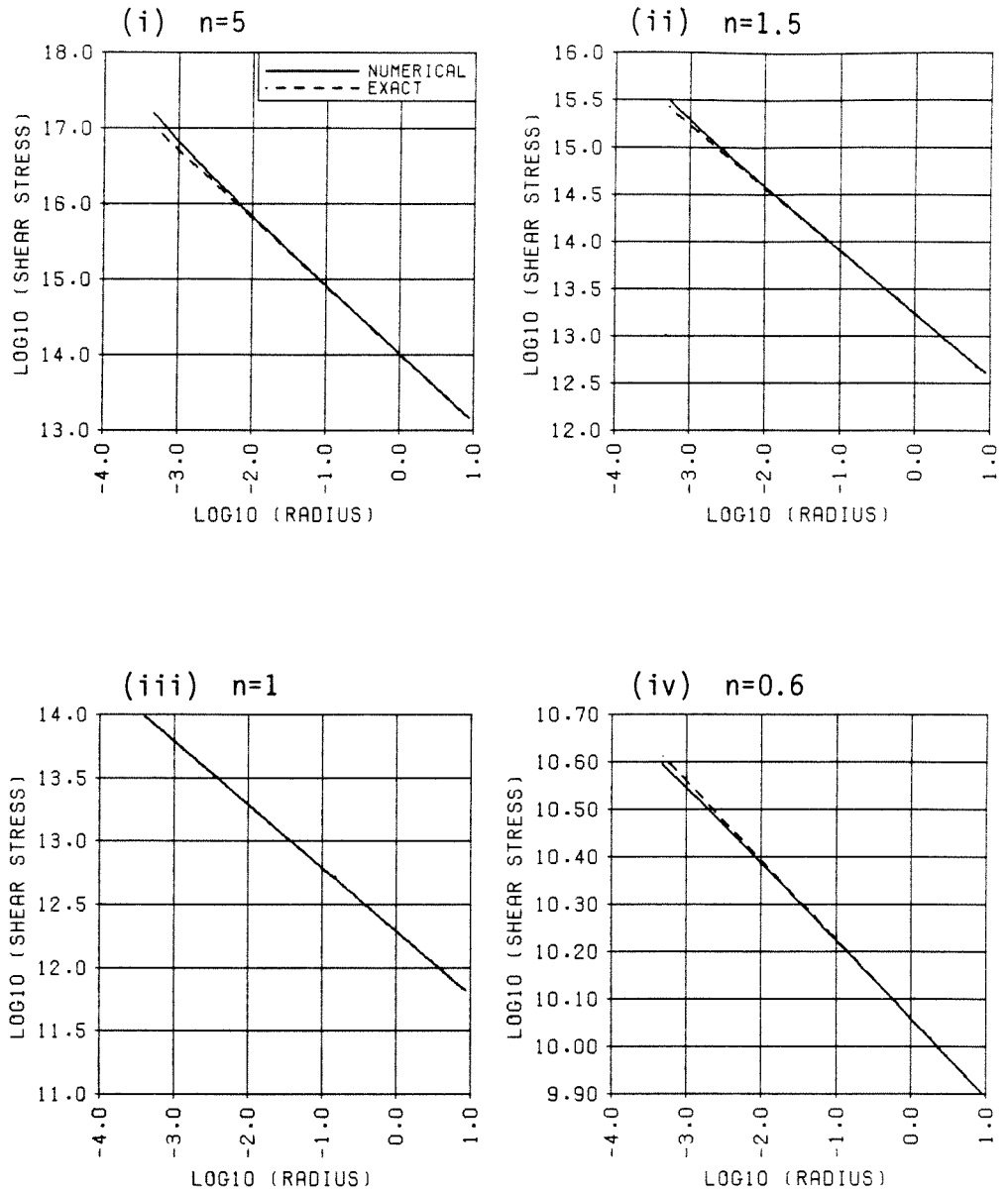

Figure 4.7. Numerical and exact solutions for second validation problem: shear stress T as a function of distance r from crack tip for pure power-law materials (i)$n = 5$, (ii), $n = 1.5$, (iii)$n = 1$, (iv)$n = 0.6$.

imperfect model for a crack in the nonlinear cases. As discussed in Section 4.3, the low-order solution for a given value of the hardening parameter is characterized by a family of curves along which $\partial u/\partial n = 0$. A more detailed analysis shows that the actual curves in this family are given by

$$r(\theta) = \bar{r} \exp\left\{ \int_0^\theta \frac{m v(t)}{\dot{v}(t)} dt \right\}, \qquad 0 \leq \theta < \pi \tag{4.10}$$

where $r(\theta)$ is the distance from the crack tip to the free surface and the other parameters are as discussed in Section 4.3. The optimum ellipse is the ellipse which provides the best fit to one of these curves. Numerical tests have shown that the second validation problem yields excellent agreement similar to that seen in the linear case (Figure 4.7(iii)) when the optimum ellipse is replaced by the curve described by (4.10). However, the optimum ellipse solutions are sufficiently accurate for purposes of this work at distances beyond about $0.001c$, so use of a mesh based on (4.10) is not regarded as necessary.

Chapter 5. Numerical solutions for elliptic cases

5.1 Results

This chapter presents numerical solutions for anti-plane shear crack problems which do *not* involve loss of ellipticity. Cases in which ellipticity is lost are treated in Chapter 7. The purpose of the present section is to compare qualitative features of the solutions for various values of the hardening parameter n for the linearizable power law material. Properties of the J-integral and the low-order zone size are discussed in Chapter 6.

The following values of n are treated here: 5, 1.5, 1, 0.6, and 0.5. The properties of these materials were discussed in Chapter 2. All simulations were done using the APE program with the same numerical mesh used for the validation problems described in section 4.4.

One property of interest in fracture mechanics, especially from the point of view of predicting crack growth, is how the region of highest shear stress is oriented with respect to the crack tip. Figures 5.1a-e illustrate this pattern, which will be called the "stress concentration pattern," for variable n. All cases shown are for loads large enough so that the problem is fully nonlinear. Figure 5.1a shows the stress concentration pattern in the $n = 5$ case. The shaded region represents the area in which the shearing stress exceeds that at infinity by a certain ratio, specifically $T > 6\tau_\infty$. The local density of dots in the figure increases with T up to a value of $T = 12\tau_\infty$, above which the density is constant. Figures 5.1b-d show similar data for the $n = 1.5$, 1, 0.6, and 0.5 materials.

For the case of a neo-Hookean material ($n = 1$, Figure 5.1c) the stress concentration is circular in shape and centered at the crack tip, regardless of load. The region of highest shear stress in located *behind* the crack tip in the hardening materials or *ahead* of the crack tip in the softening materials. The present counterpart of the elliptical pattern of the yielded region predicted by Rice [2] for the elastic-perfectly plastic material in a deformation theory of plasticity may be observed in the $n = 0.5$ case, Figure 5.1e.

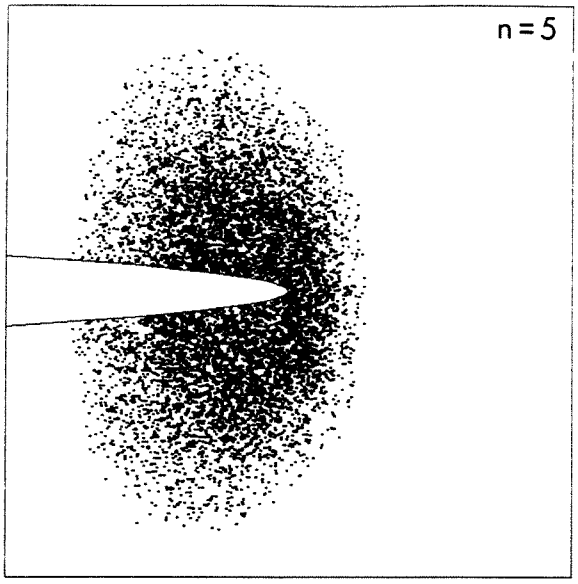

a

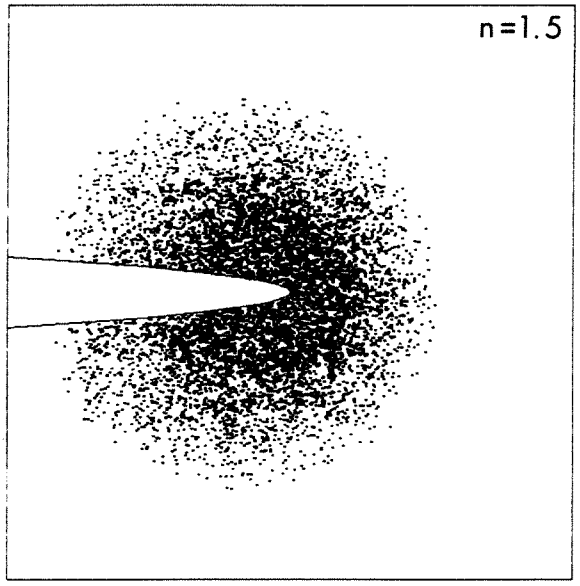

b

Figure 5.1a,b. Stress concentration pattern for (a) $n = 5$, (b) $n = 1.5$.

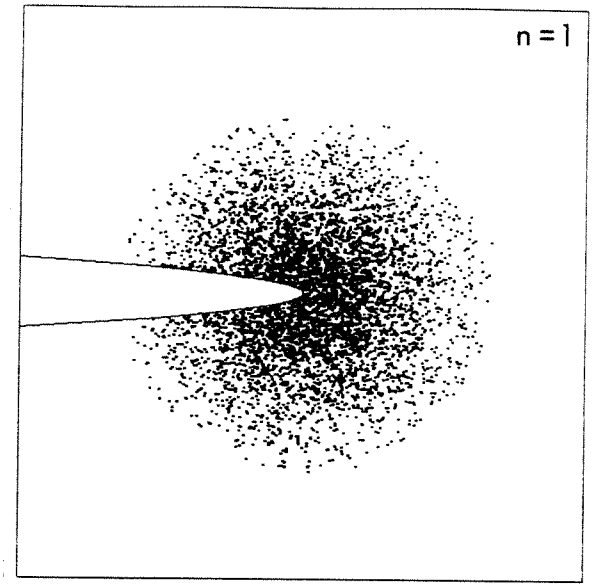

c

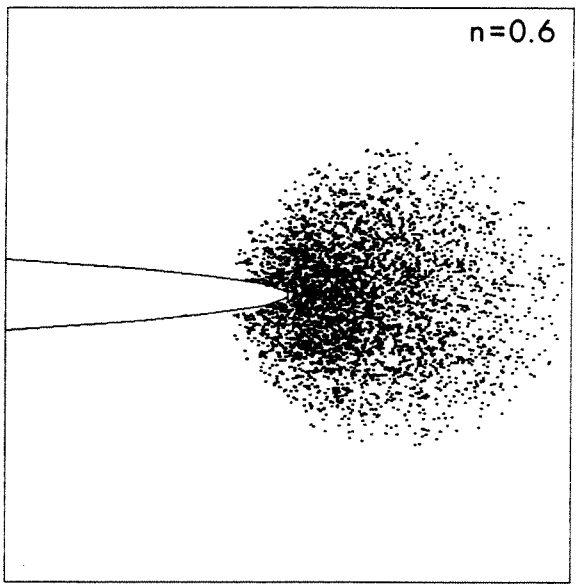

d

Figure 5.1c,d. Stress concentration pattern for (c) $n = 1$, (d) $n = 0.6$.

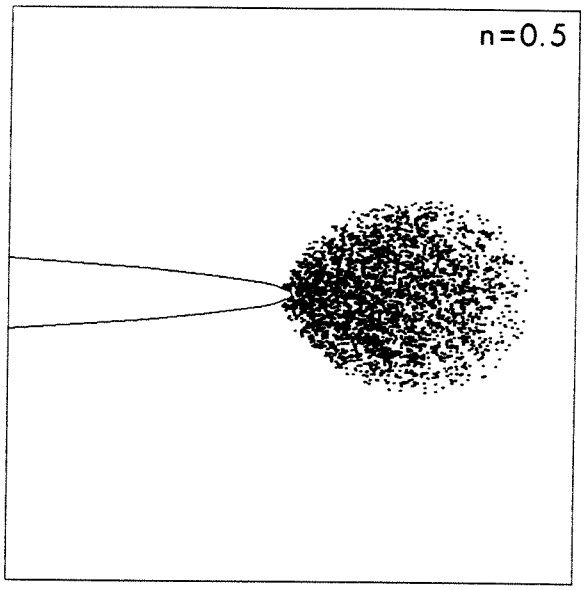

Figure 5.1e. Stress concentration pattern for (e) $n = 0.5$.

Figures 5.2a-e compare the displacement fields near the crack tip for $n = 5$, 1.5, 1, 0.6, and 0.5 for large values of τ_∞. The surface depicted in each figure represents the shape into which an initially flat sheet in the plane is deformed. The tear along the left side of the surface corresponds to the crack faces. It should be noted that each of the five surfaces is normalized separately and is on a separate vertical scale. The two plots on each page show the same surface from a different view, the second being from a point directly ahead of the crack.

Figures 5.2a-e clearly illustrate the qualitative differences in the singularities in displacement fields between the different materials. The hardening material has the "smoothest" displacement field, while the softening materials have more violent behavior near the crack tip. This trend is predicted by the asymptotic solution discussed in Chapter 3. Recall that in the low-order solution for $n > 0.5$, Knowles found that $u \sim r^m$ near the crack tip, where $m = 1 - 1/2n$. Thus the weakest singularity in displacement, *i.e.*, the largest value of m, is found for the largest value of n. In the case $n = 0.5$, Knowles found that the asymptotic solution for u depends on θ only, and therefore u is *discontinuous* at the crack tip. The numerical solution for $n = 0.5$ may be readily interpreted as representing such a discontinuity.

Having considered some qualitative features of the numerical solutions near the crack tip for some nonlinear materials, we now turn to quantitative observations of the singularities. Figure 5.3a displays the variation of shear stress T along the crack axis for $n = 5$. Each of the four graphs on the page corresponds to a different load τ_∞. Figures 5.3b-e display similar data for $n = 1.5$, 1, 0.6, and 0.5. The solid line on each graph is the numerical solution. Also shown are the asymptotic solution discussed in Chapter 3 (the r^{-m} singularity) and the global solution from linear elasticity. Note that the axes are both on $\log_{10}$ scales, so that a straight line with slope $-m$ represents a variation with r^{-m}.

The asymptotic solutions shown in Figures 5.3a-e employ *numerically computed*

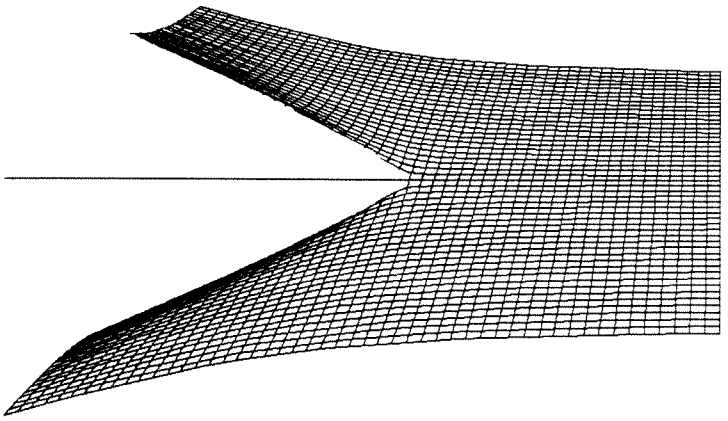

n = 5

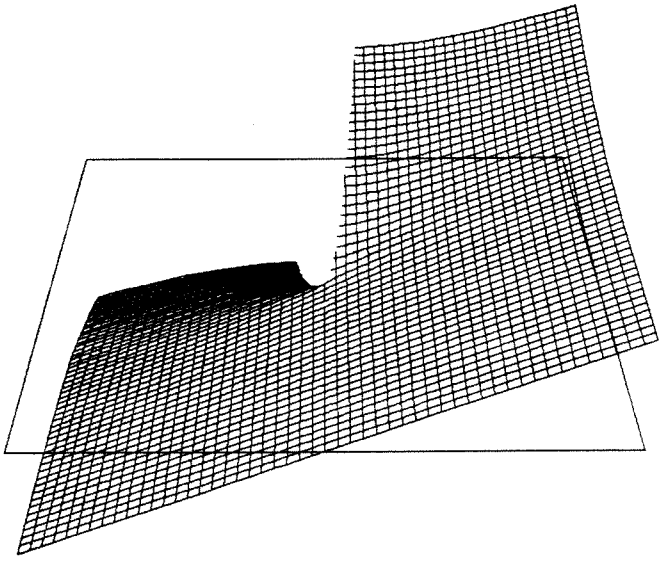

Figure 5.2a. Deformation near crack tip for $n = 5$.

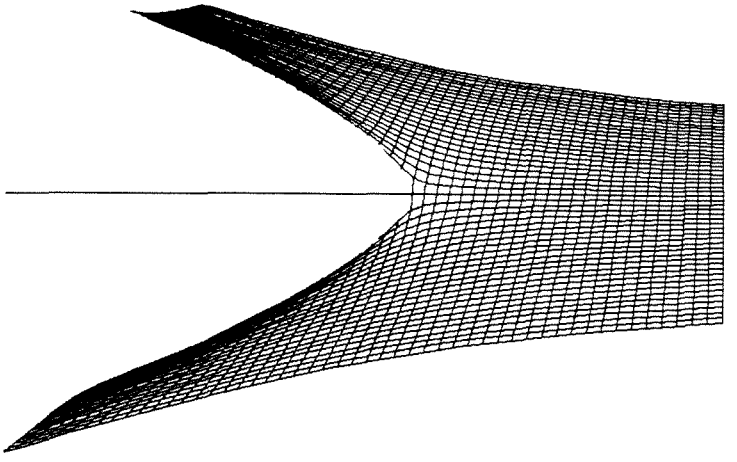

n=1.5

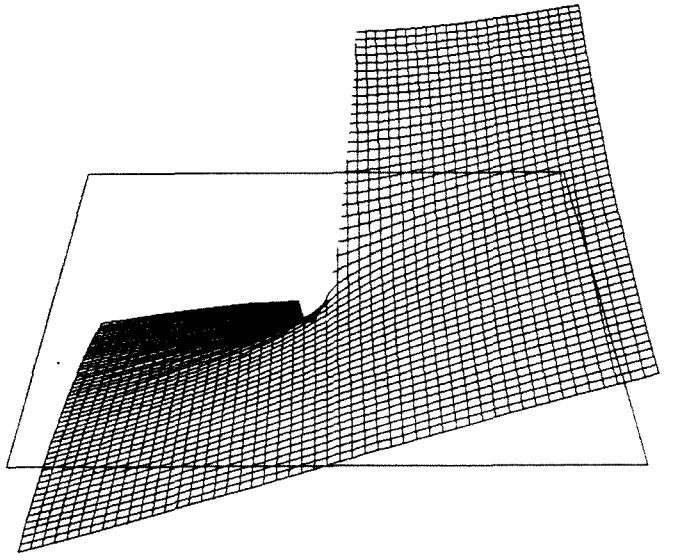

Figure 5.2b. Deformation near crack tip for $n = 1.5$.

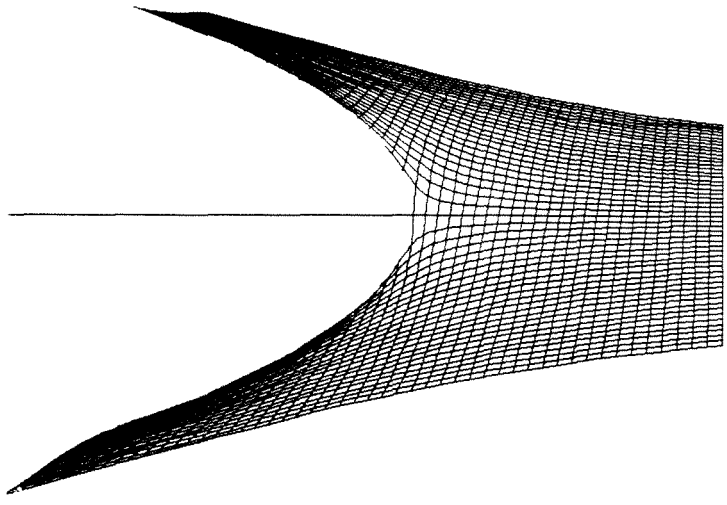

n = 1

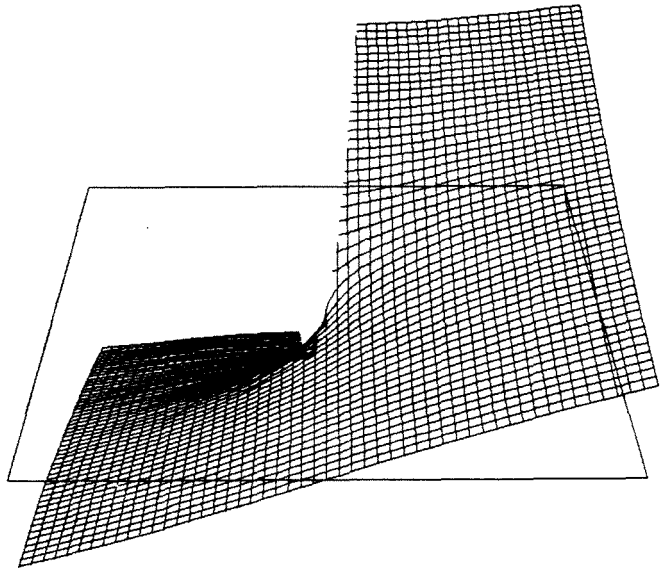

Figure 5.2c. Deformation near crack tip for $n = 1$.

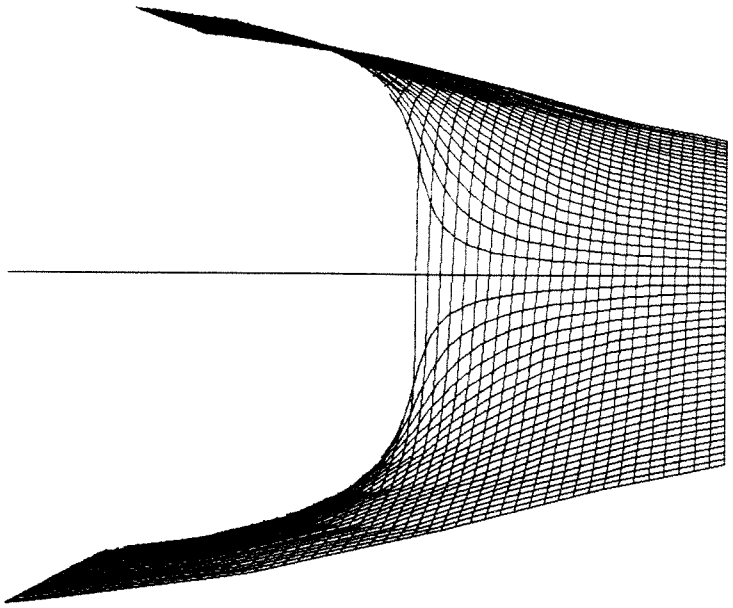

n=0.6

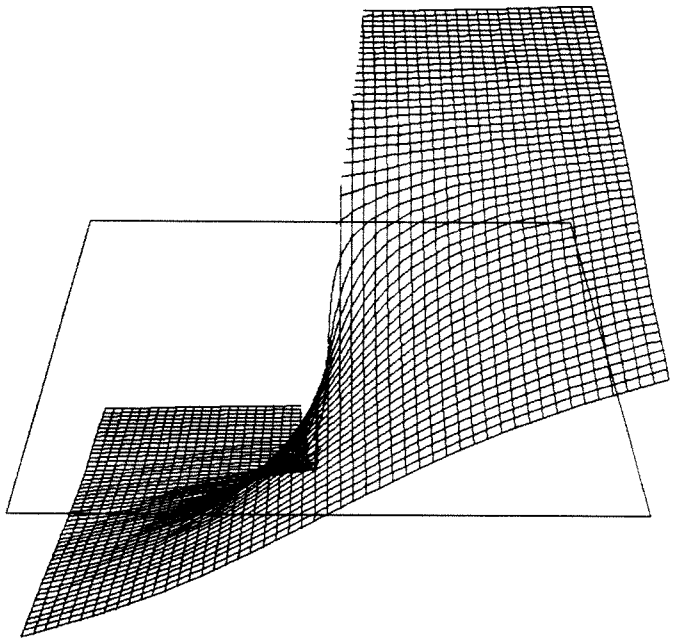

Figure 5.2d. Deformation near crack tip for $n = 0.6$.

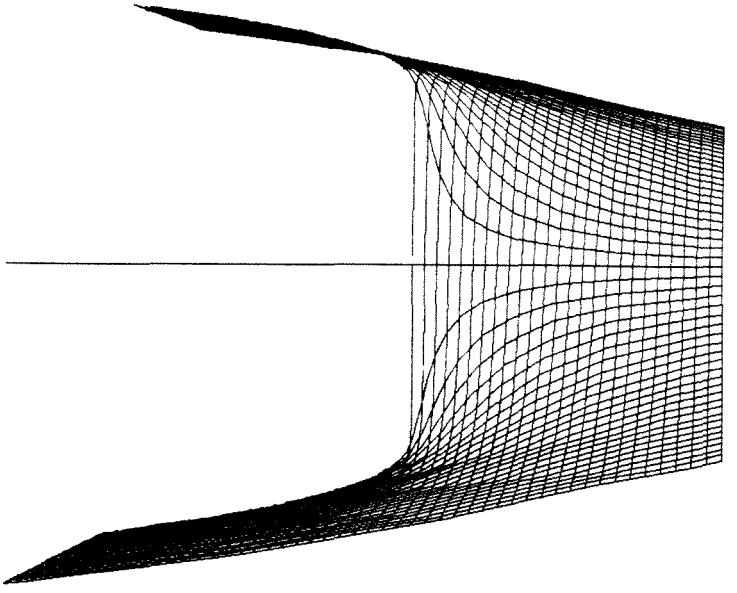

n=0.5

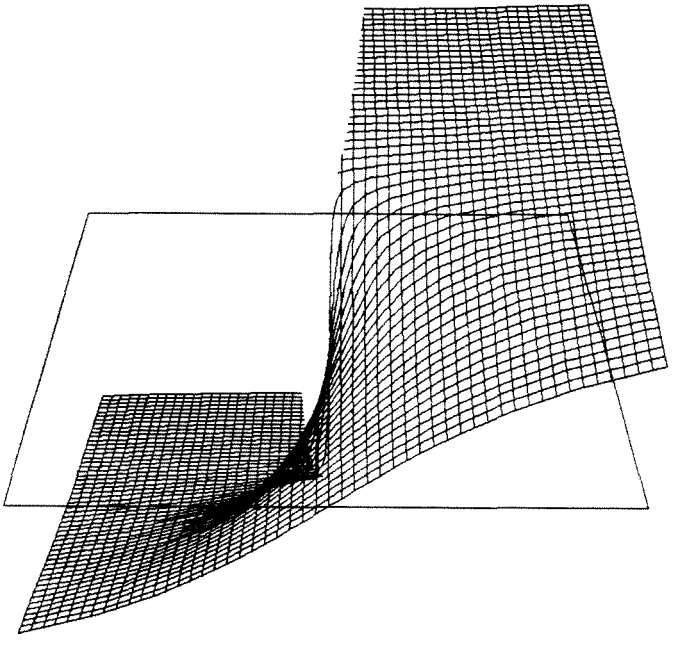

Figure 5.2e. Deformation near crack tip for $n = 0.5$.

n=5

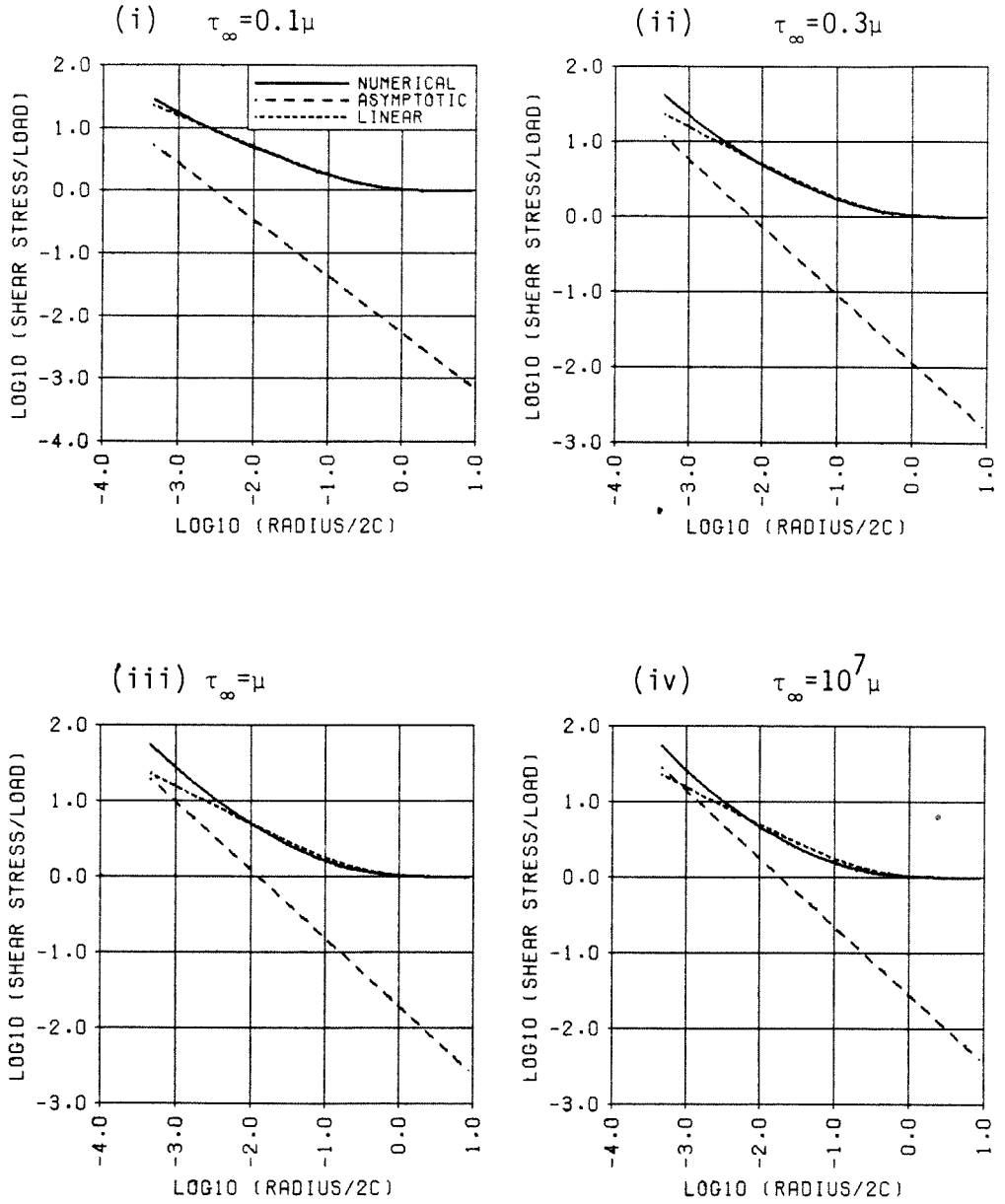

Figure 5.3a. Dependence of T/τ_∞ on $r/2c$ for $n = 5$: (i)$\tau_\infty = 0.1\mu$, (ii)$\tau_\infty = 0.3\mu$, (iii)$\tau_\infty = \mu$, (iv)$\tau_\infty = 10^7\mu$.

n=1.5

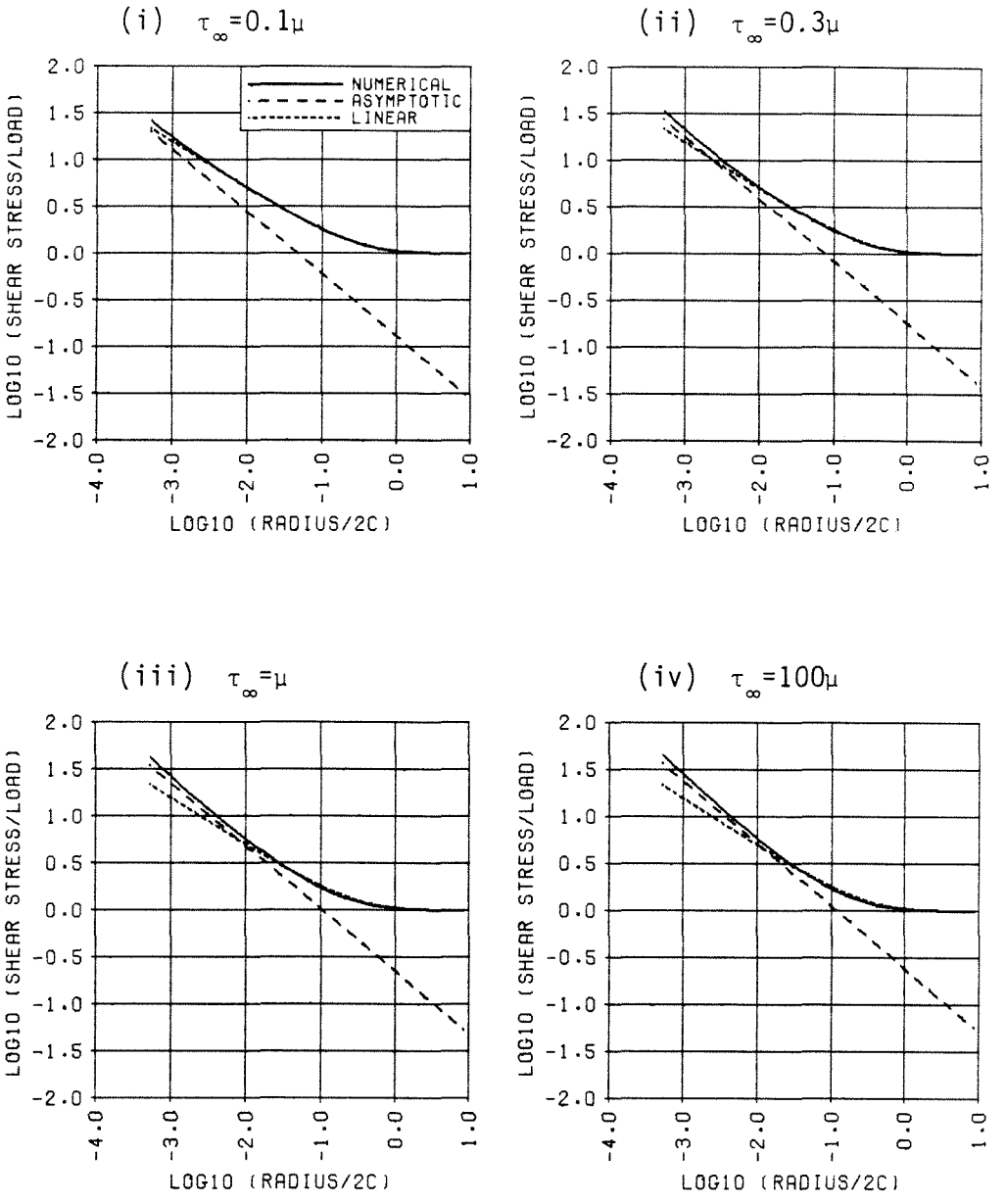

Figure 5.3b. Dependence of T/τ_∞ on $r/2c$ for $n = 1.5$: (i)$\tau_\infty = 0.1\mu$, (ii)$\tau_\infty = 0.3\mu$, (iii)$\tau_\infty = \mu$, (iv)$\tau_\infty = 100\mu$.

n=1

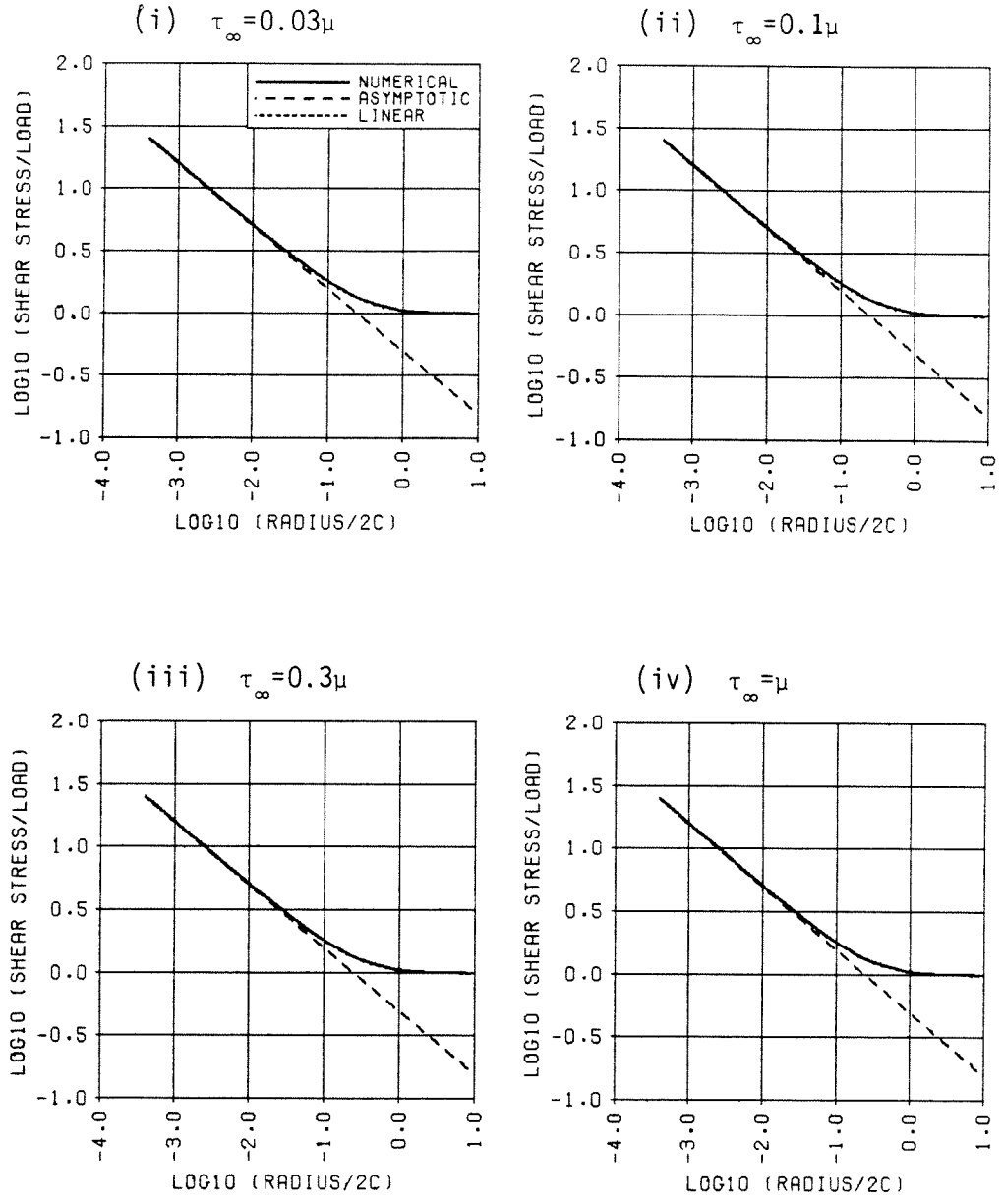

Figure 5.3c. Dependence of T/τ_∞ on $r/2c$ for $n = 1$: (i)$\tau_\infty = 0.03\mu$, (ii)$\tau_\infty = 0.1\mu$, (iii)$\tau_\infty = 0.3\mu$, (iv)$\tau_\infty = \mu$.

n = 0.6

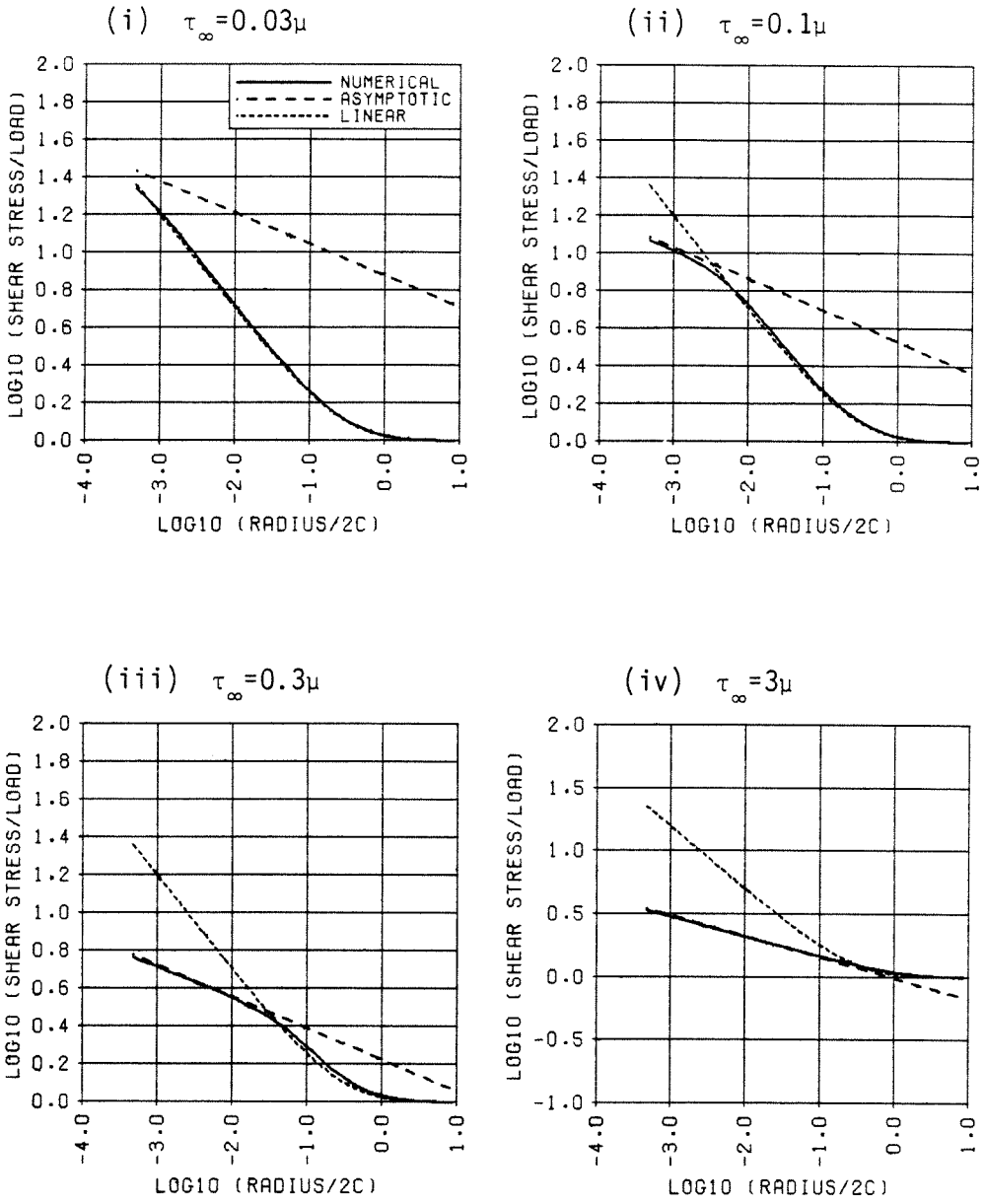

Figure 5.3d. Dependence of T/τ_∞ on $r/2c$ for $n = 0.6$: (i)$\tau_\infty = 0.03\mu$, (ii)$\tau_\infty = 0.1\mu$, (iii)$\tau_\infty = 0.3\mu$, (iv)$\tau_\infty = 3\mu$.

n=0.5

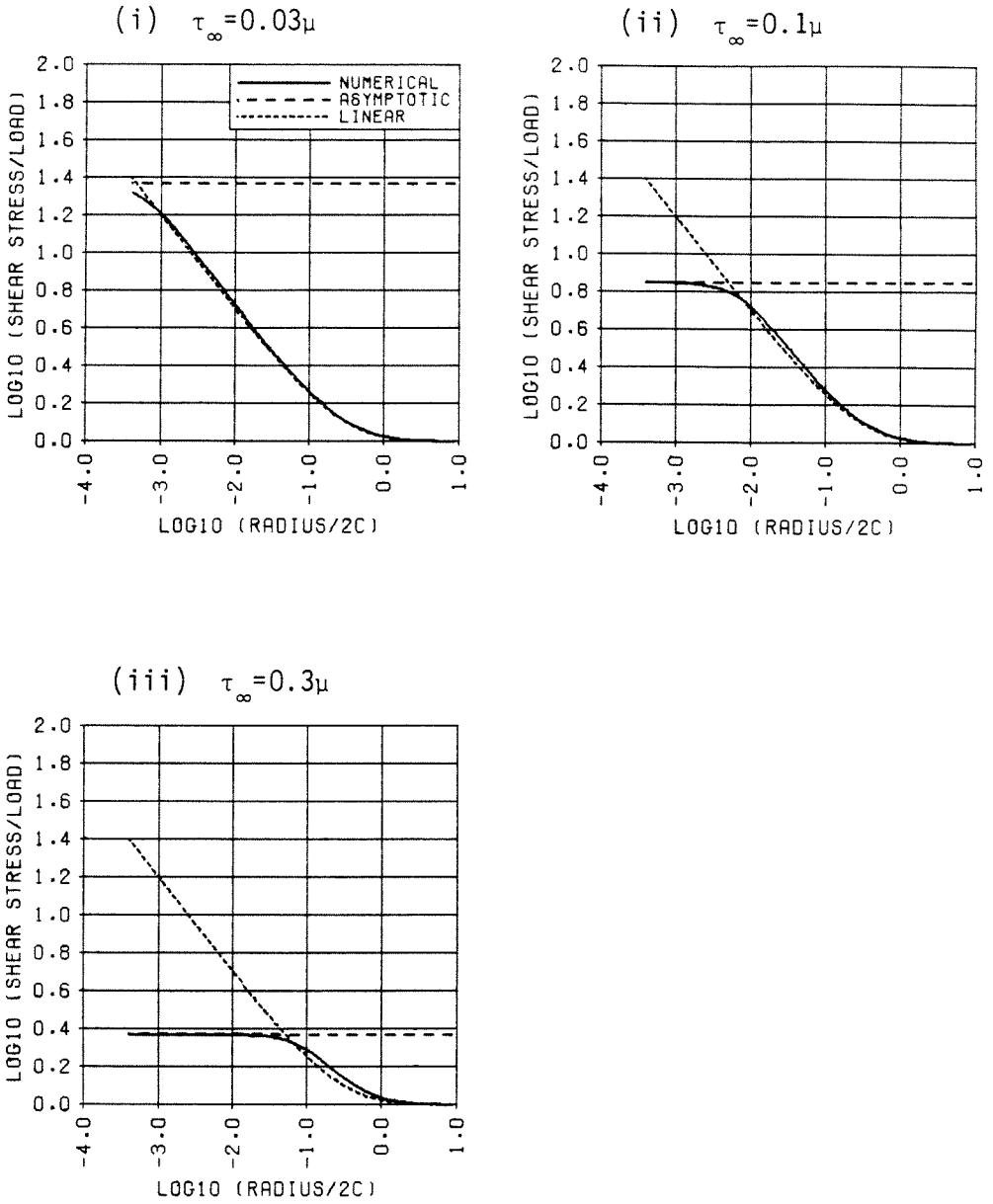

Figure 5.3e. Dependence of T/τ_∞ on $r/2c$ for $n = 0.5$: (i)$\tau_\infty = 0.03\mu$, (ii)$\tau_\infty = 0.1\mu$, (iii)$\tau_\infty = 0.3\mu$.

values of the J-integral from the computer simulations which are represented by the solid lines. This is necessary because the asymptotic solution contains an arbitrary constant A (see Chapter 3) which must somehow be assigned in order to evaluate the asymptotic solution explicitly. Approximate methods of finding A will be discussed in Chapter 6, but for present purposes it is evaluated using (3.14) with numerically determined values of J.

Figures 5.4a-e compare the angular dependence of the displacement and stress fields along a small circle centered at the crack tip. For the material $n = 5$, Figure 5.4a shows the variation of u, T, T_1, and T_2 with θ, $\theta = 0$ being the crack axis. The radius of the circle is 0.006c, sufficiently small that the asymptotic solution may be regarded as fully developed there. The low-order asymptotic solution is also shown. Note that the axes are *not* logarithmic here. Figures 5.4b-e show similar data for the other materials. The $n = 0.5$ case includes a comparison with the Hult-McClintock solution [1] for an elastic-perfectly plastic material. The radii of the circles used in these plots for each of the five materials differ slightly and were assigned in order to best illustrate the asymptotic behavior of the solution.

5.2. Discussion

The above results show that the low-order solution is generally valid for all the materials considered. There is no evidence that any higher-order terms are significant in the asymptotic solutions.

However, there are certain aspects of the extreme cases $n = 5$ and $n = 0.5$ that require further explanation. The $n = 5$ curves (Figures 5.3a and 5.4a) show some deviation from the low-order solution. Some further analysis was carried out to help explain this. The primary contributor to the difference is that the simulations are for the *linearizable* power-law material rather than for the *pure* power-law material. The low-order solution assumes that k is large asymptotically. Thus the stress-strain relation

n=5

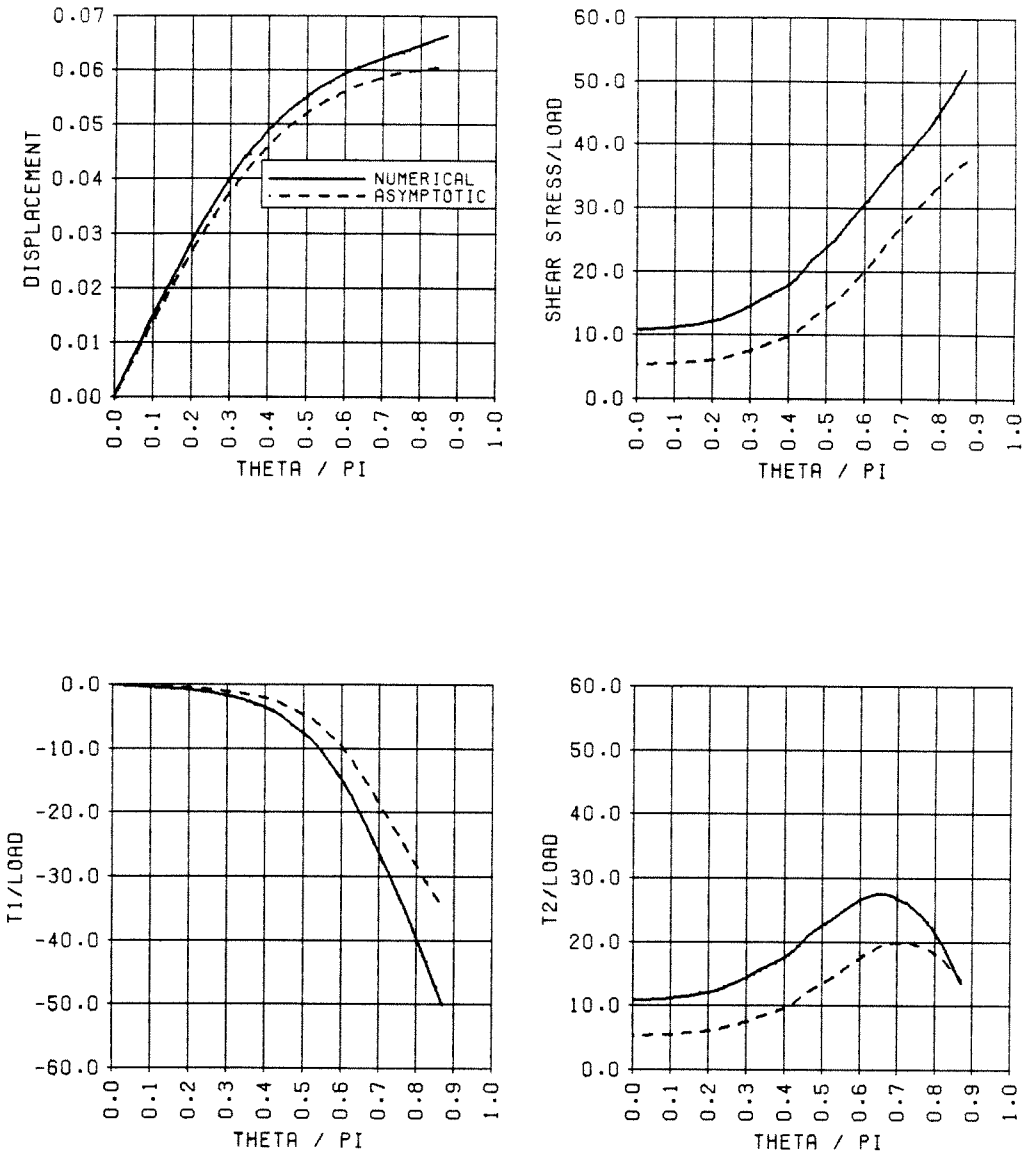

Figure 5.4a. Dependence of fields on angle on a circle of radius $0.006c$ centered at the crack tip for $n = 5$, large load case: (i)u, (ii)T/τ_∞, (iii)T_1/τ_∞, (iv)T_2/τ_∞.

n=1.5

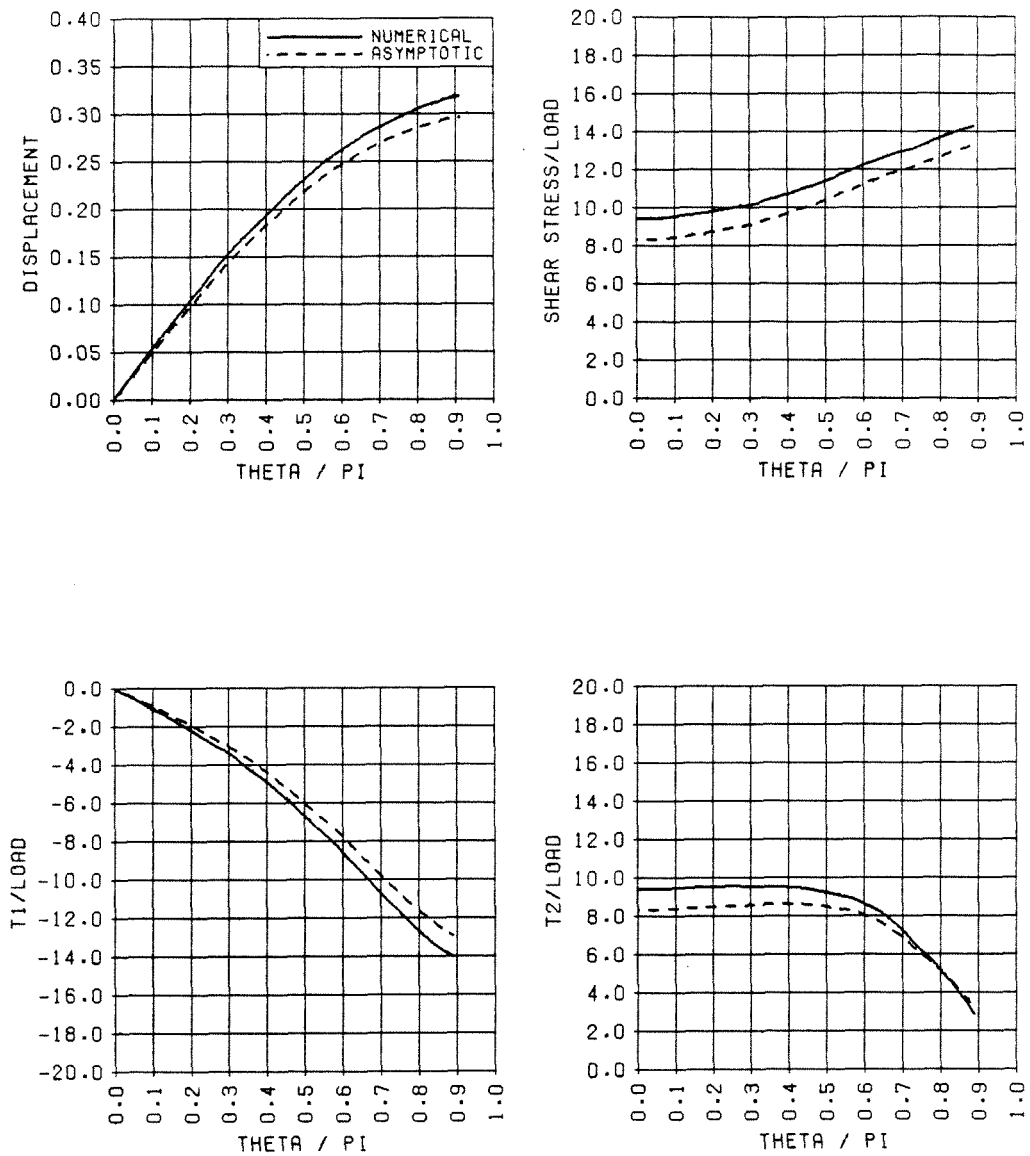

Figure 5.4b. Dependence of fields on angle on a circle of radius $0.01c$ centered at the crack tip for $n = 1.5$, large load case: (i)u, (ii)T/τ_∞, (iii)T_1/τ_∞, (iv)T_2/τ_∞.

n = 1

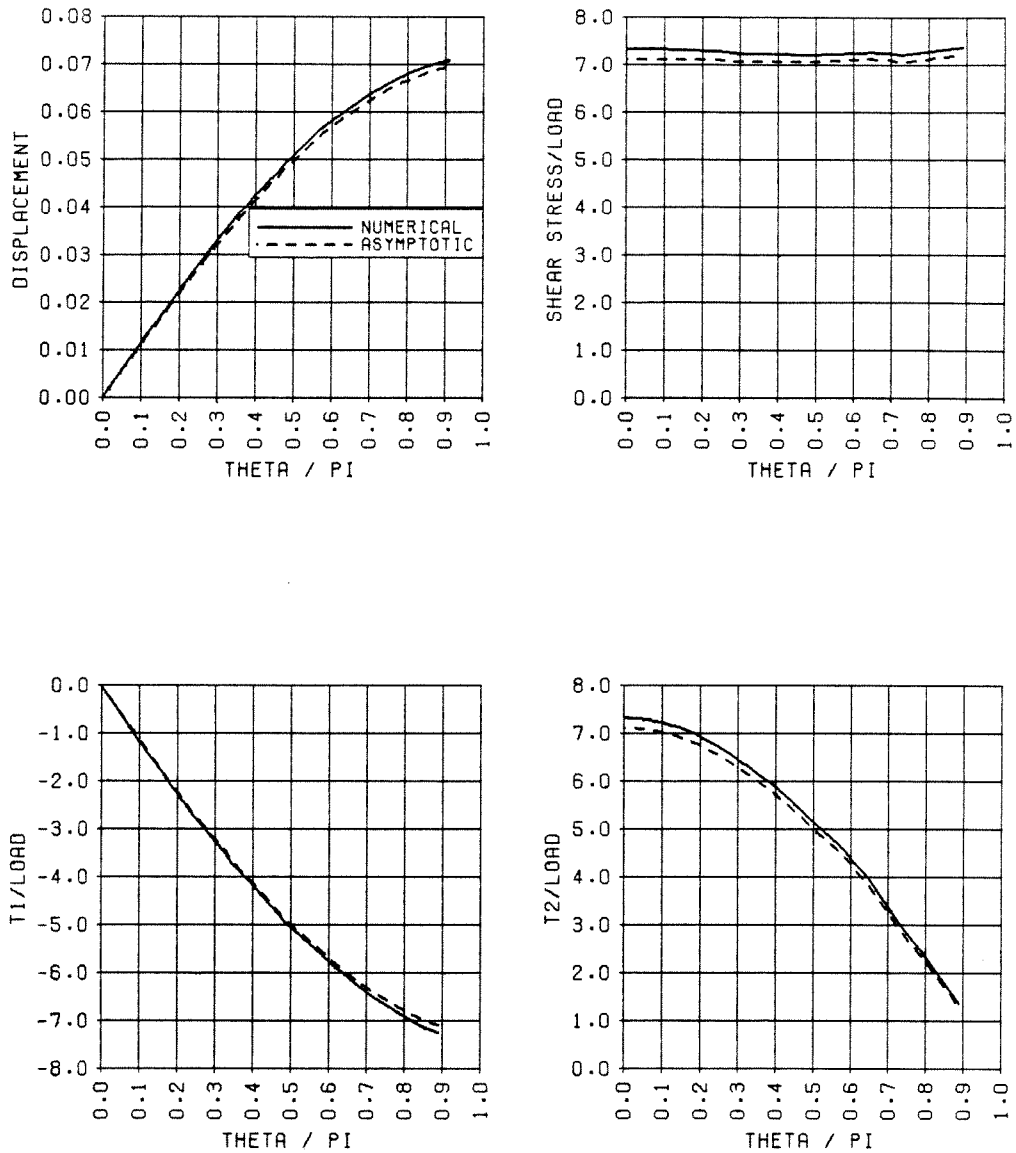

Figure 5.4c. Dependence of fields on angle on a circle of radius $0.01c$ centered at the crack tip for $n = 1$, large load case: (i)u, (ii)T/τ_∞, (iii)T_1/τ_∞, (iv)T_2/τ_∞.

n=0.6

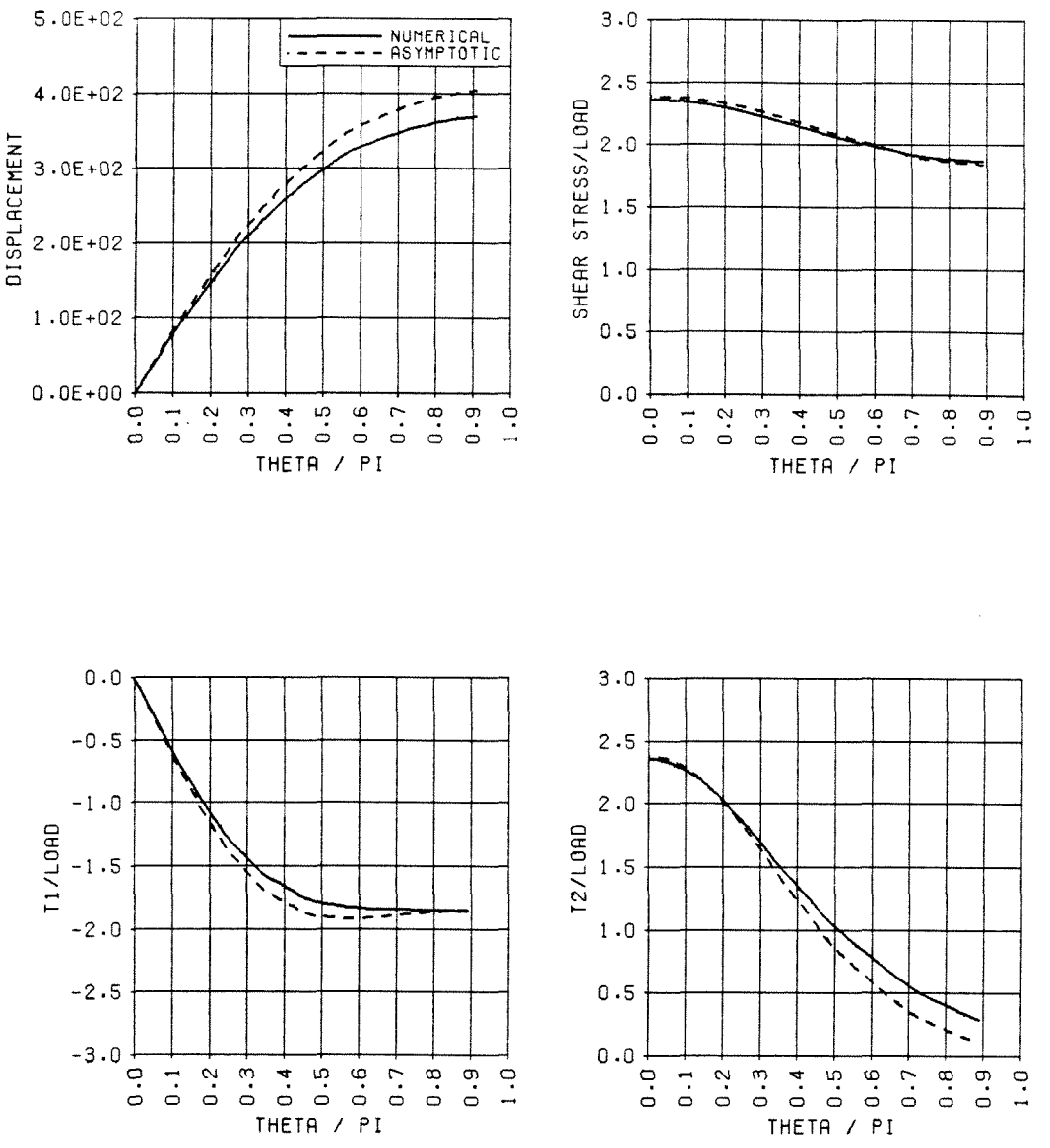

Figure 5.4d. Dependence of fields on angle on a circle of radius $0.01c$ centered at the crack tip for $n = 0.6$, large load case: (i)u, (ii)T/τ_∞, (iii)T_1/τ_∞, (iv)T_2/τ_∞.

n = 0.5

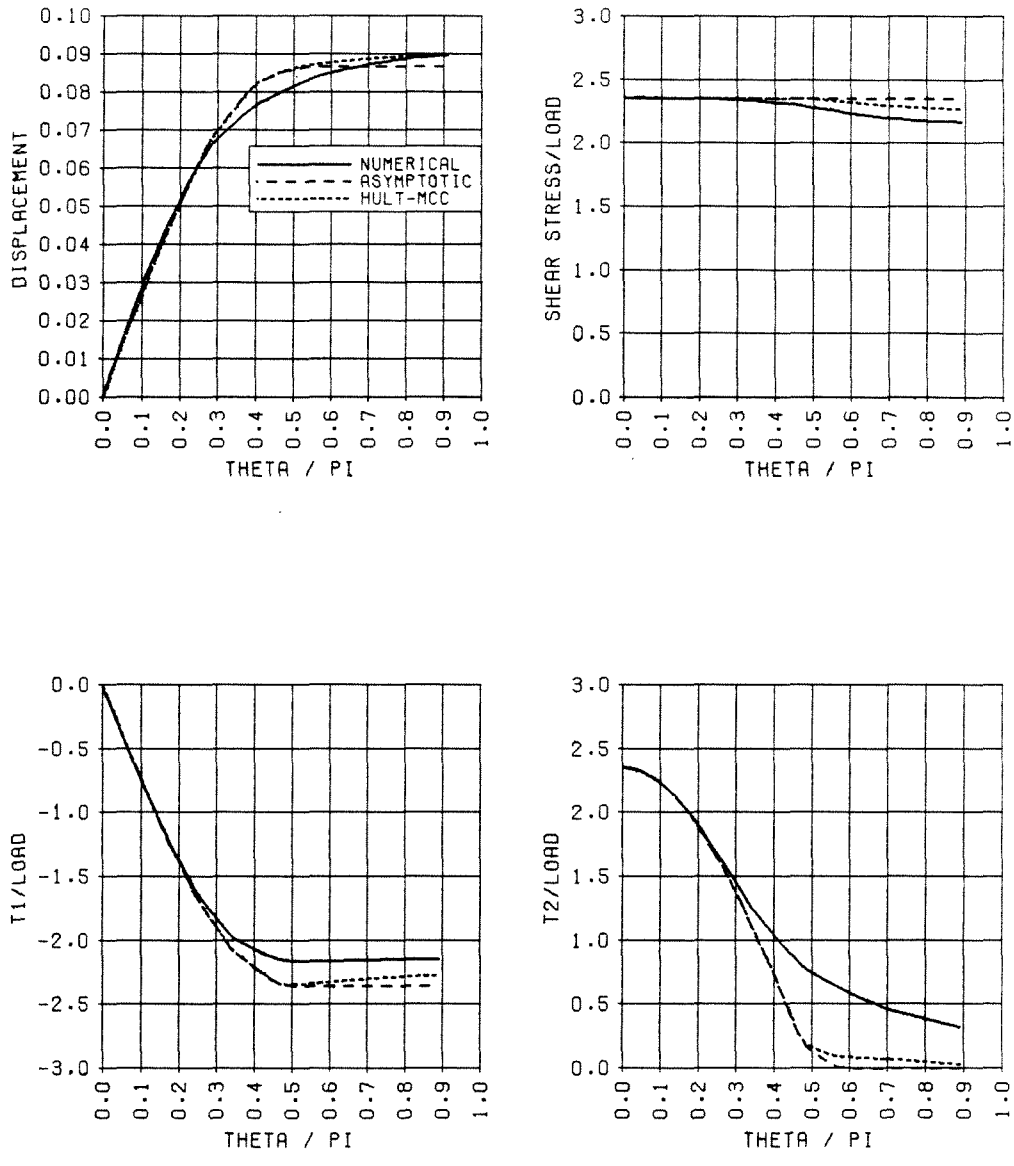

Figure 5.4e. Dependence of fields on angle on a circle of radius $0.01c$ centered at the crack tip for $n = 0.5$, large load case: (i)u, (ii)T/τ_∞, (iii)T_1/τ_∞, (iv)T_2/τ_∞.

of the linearized power-law material is, in effect, formally replaced by the pure power-law relation in the derivation of the low-order solution. This replacement is valid except in two cases.

In the case of a severely hardening material, such as $n = 5$, the shears are not high except at points very close to the crack tip. This occurs because although the stresses become large at moderate distances, the shear stress varies with k^9. Thus the strains are relatively small even for large stresses. Therefore the low-order solution does not become valid except at very small radii, too small to be observed with the numerical mesh used here. To confirm that this explanation of the discrepancy is correct, the second validation problem of Chapter 4 was run for both the linearizable and pure power-law materials for $n = 5$. The resulting differences were comparable to those seen in the results shown in this chapter for $n = 5$.

The other case in which the assumption of large strains is flawed is in the $n = 0.5$ case for the linearizable power-law material. The large-k assumption underlying the low-order solution effectively means that the $n = 0.5$ material is treated like a rigid-perfectly plastic material. In fact, the $n = 0.5$ constitutive relation more closely resembles that of the elastic-perfectly plastic material considered by Hult and McClintock [1]. This difference may be seen in Figure 5.4e(i), in which the numerical simulation shows u varying near the crack faces while the low-order solution predicts constant u in those regions. This difference occurs because the stresses are low there, and the low-stress end of the stress-strain relation is where the difference between the linearizable and pure power-law materials is the most prominent. The Hult-McClintock solution is plotted along with the other solutions in Figure 5.4e, and while this does not provide perfect agreement, it does show variation of u with θ near $\theta = \pi$.

It should also be noted that the use of an elliptical hole to model a crack is expected to cause more significant errors for the $n = 0.5$ material than for the "more linear" materials, since the exact free surface predicted by (4.10) for $n = 0.5$ is a slit with

straight sides and a semicircular tip. This effect may be observed especially in Figure 5.4e(iv), which shows a larger value of T_2 for $\theta \approx \pi$ than is predicted by the low-order solution.

Chapter 6. Approximations for the low-order zone size

In the use of asymptotic solutions such as the low-order solutions discussed in Chapter 3, it is important to know the region of validity of the approximation. It is apparent from the results of the previous section that there is in general a sizable transition zone between the region near the crack tip in which the low-order solution is valid (the *low-order zone*) and the far-field solution. In the $n = 5$ case, for example, Figure 5.3a(i)shows that this transition region is at least an order of magnitude larger in radius than the low-order zone. (The reason for the large size of the transition zone in this case was discussed in Section 5.2.) The situation is additionally complicated by the fact that for small loads with the *linearizable* power-law material, there is an intermediate region in which the asymptotic solution of linear elasticity holds, a situation known as *small-scale nonlinearity*.

The above considerations suggest that it is not a worthwhile endeavor to attempt to observe the size of the region of validity of the asymptotic solution directly from the numerical data. Instead, the discussion below uses a notion of the low-order zone size derived by fitting an asymptotic solution to the numerical data and observing where this solution takes on the value τ_∞ along the crack axis. This notion of the low-order zone size will be defined more precisely below.

It will be shown that the low-order zone size determines the J-integral and A, the nonlinear analogue of the stress concentration factor. The two extreme cases of very small loads and large loads allow approximations of these parameters (the former was discussed in Chapter 3), and these approximations will be compared with numerical data below.

6.1 Scaling considerations

Before discussing observations of the low-order zone size, it is useful to apply dimensional analysis to help shed light on its dependence on the various parameters which

characterize a problem.

First, let us define the low-order zone size R. Recall that in the low-order zone, τ is given asymptotically on the crack axis by $T \sim Cr^{-m}$, where C and m are positive constants, $0 < m < 1$. At points far from the crack tip, the condition at infinity requires $T \sim \tau_\infty$. Define the **low-order zone size** R as the point on the crack axis at which the two solutions would intersect if they were extended into the transition zone, *i.e.*, $CR^{-m} = \tau_\infty$. (See Figure 6.1.) Therefore the low-order solution for stress on the crack axis may be written

$$T \sim \tau_\infty (r/R)^{-m}. \tag{6.1}$$

To apply dimensional analysis to the evaluation of R, first consider all the parameters that the stress vector $\mathbf{T}$ could depend on at a fixed point (x_1, x_2). For the linearizable power-law material with $n > 1/2$, these are as follows: x_1, x_2, n, k_∞, μ, b, and c. Consider the dimensions of these quantities. Displacement is a variable that has its own dimension, like temperature in a heat conduction problem, and should not be regarded as a length even though it represents the distance traveled by a particle. Rather than using displacement as a fundamental dimension, it will be more convenient to use *strain*, meaning displacement/length.

Taking stress (σ), length (L), and strain (ϵ) as the fundamental dimensions, the dimensions of the related quantities may be immediately written down: $[T_1] = \sigma$, $[T_2] = \sigma$, $[x_1] = L$, $[x_2] = L$, $[k_\infty] = \epsilon$, $[\mu] = \sigma/\epsilon$, $[b] = \epsilon^{-1/2}$, $[c] = L$, $[R] = L$, $[n] = 1$.

In the following discussion, the notation $X = F(Y_1, Y_2, \ldots, Y_i)$ will mean that a quantity X depends only on i numbers $Y_1, Y_2, \ldots, Y_i$.

Taking the parameters c, k_∞, and μk_∞ as the fundamental groups with dimensions of length, strain, and stress respectively, the following nondimensional groups may be formed: $T_1/\mu k_\infty$, $T_2/\mu k_\infty$, x_1/c, x_2/c, n, R/c, and $bk_\infty{}^2$. Thus

$$\frac{\mathbf{T}}{\mu k_\infty{}^2} = F\left(\frac{x_1}{c}, \frac{x_2}{c}, n, bk_\infty{}^2\right). \tag{6.2}$$

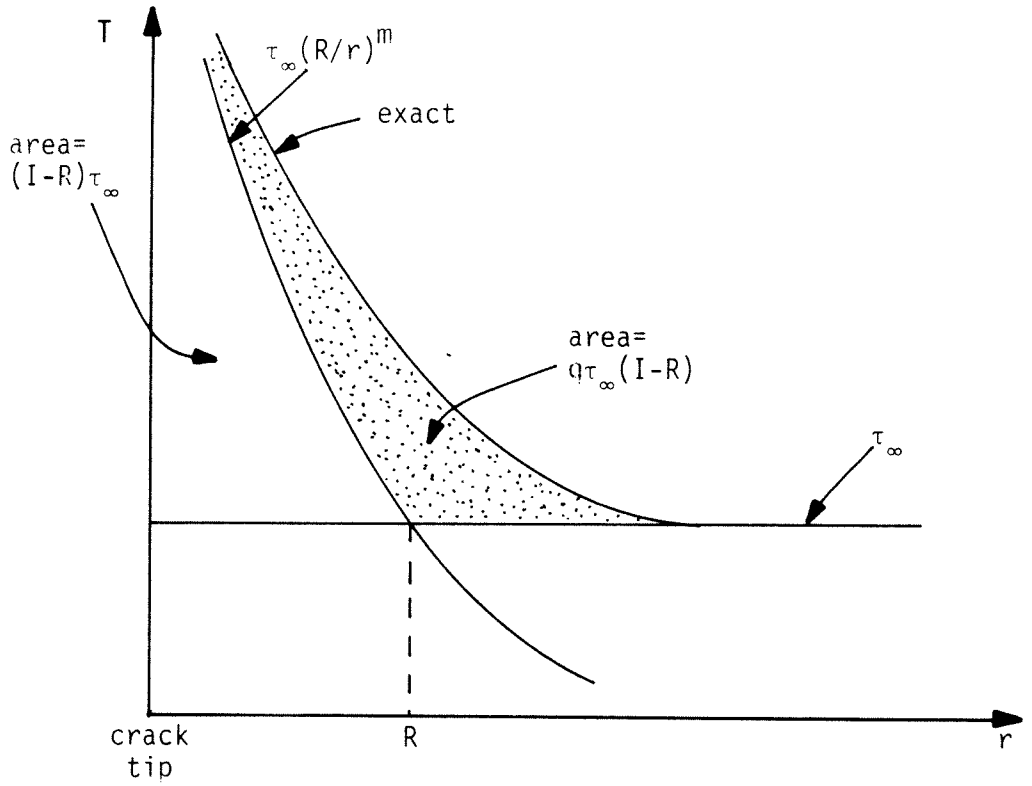

Figure 6.1. Model for estimation of low-order zone size for large loads. R is just large enough so that the $T(r)$ curve, after accounting for the transition terms, transfers the correct vertical force through the crack axis.

Noting that by the constitutive relation, $\tau_\infty = F(\mu k_\infty, n, bk_\infty{}^2)$, and it follows that $\mu k_\infty = F(\tau_\infty, n, bk_\infty{}^2)$. (The unique invertibility of the constitutive relation has been used here.) So (6.2) implies

$$\frac{\mathbf{T}}{\tau_\infty} = F\left(\frac{x_1}{c}, \frac{x_2}{c}, n, bk_\infty{}^2\right). \tag{6.3}$$

Along the crack axis, it follows that

$$T = \tau_\infty F\left(\frac{r}{c}, n, bk_\infty{}^2\right). \tag{6.4}$$

Using the definition of R, this implies

$$\tau_\infty \left(\frac{R}{r}\right)^m \sim \tau_\infty F\left(\frac{r}{c}, n, bk_\infty{}^2\right) \quad \text{as } r \to 0. \tag{6.5}$$

Since m depends only on n (recall $m = 1 - 1/2n$) (6.5) implies

$$\frac{R}{c} = F(n, bk_\infty{}^2). \tag{6.6}$$

The quantity $bk_\infty{}^2$ appears in (6.6) because it represents "how nonlinear" the problem is at infinity. It therefore determines whether there is an intermediate zone where the asymptotic solution of the *linear* theory holds (small-scale nonlinearity). A similar analysis of the *pure* power law material, in which there cannot be small-scale nonlinearity, results in (6.6) being replaced by $R/c = F(n)$. This additional simplification is significant because for large shears, the linearizable power law material behaves like the pure power law material:

$$\mu k\left(1 + \frac{b}{n}k^2\right)^{n-1} \approx \mu k\left(\frac{b}{n}k^2\right)^{n-1}. \tag{6.7}$$

Thus for very large loads in the linearizable power law material, R should depend only on n. This is indeed observed in the numerical results, as may be seen in Figures 5.3a(iii)and (iv). The curves of shear stress as a function of distance along the crack axis have roughly the same shape although the loads differ by a factor of 10^7.

6.2 Small load approximation

For small loads with $n > 1/2$, the nonlinearity is expected to be small-scale, so the low-order zone is contained within some larger zone in which the $r^{-1/2}$ singularity of linear elasticity theory is present. Evaluation of the shearing stress along the crack axis in the low-order zone using Knowles's solution discussed in Chapter 3 leads to

$$T = \mu \left(\frac{b}{n}\right)^{n-1} g(n) A^{2n-1} r^{-m} \tag{6.8}$$

where

$$g(n) = \left(\frac{1}{4n}\right)^{n-\frac{1}{2}} \left(\frac{2n-1}{n}\right)^{(2n-1)^2/2n}, \tag{6.9}$$

$$A = \left[\frac{c}{2} b^{1-n} f(n) {k_\infty}^2\right]^{1/2n}, \tag{6.10}$$

and

$$f(n) = \frac{(4n^4)^n}{(2n-1)^{2n-1} n^3}. \tag{6.11}$$

Requiring $T = \mu k_\infty$ at radius R in (6.8) and using (6.9)–(6.11) gives the small-load estimate for R:

$$R = \left(\frac{b {k_\infty}^2}{n^{2n}}\right)^{(n-1)/(2n-1)} \left(\frac{c}{2}\right) f(n) g^{2n/(2n-1)}(n) \tag{6.12}$$

Of more interest in the small-load case is the radius at which the low-order solution changes to the $r^{-1/2}$ behavior of the linear elastic solution. Call this point of transition R_*. The asymptotic solution in the linear theory provides the following approximation T_* for shearing stress along the crack axis:

$$T_*(r) = \mu k_\infty \sqrt{\frac{c}{2r}}. \tag{6.13}$$

Now require $T = T_*$ at R_* along the crack axis making use of (6.8)–(6.11) and (6.13). Carrying out the indicated computations leads to

$$R_* = \frac{c b {k_\infty}^2}{2} \left(\frac{1}{n}\right)^{(3n-2)/(n-1)}. \tag{6.14}$$

The J-integral associated with the small-load approximation is that of the linear theory,

$$J = \frac{\mu c \pi {k_\infty}^2}{2}. \tag{6.15}$$

6.3 Large-load approximation

For large loads with $n > 1/2$, there is no annulus in which the $r^{-1/2}$ singularity of linear elasticity is present. Instead, the problem is entirely nonlinear.

An attempt to evaluate the constant A by use of the J-integral, as was done in the small-load case, fails in the large-load case because J cannot be evaluated without knowing the complete global solution to the nonlinear problem. Various methods have been proposed to evaluate J in special cases (see [3] and [14], for example). The following describes a simple way of estimating R and J based on a force balance through the crack axis. This simple approximation is based on a model similar to that used by Irwin [15] to estimate the plastic zone size in elastic-plastic materials.

Instead of the crack problem in an unbounded domain, consider the analogous problem in a large circular disk of radius $B >> c$ with a traction field corresponding to the conditions at infinity applied on the outer circumference. Consider the variation of shear stress T along the crack axis extending from the right crack tip. Suppose one ignores the terms which give rise to the transition region separating the low-order zone from the homogeneous region. Then the following approximation holds on the crack axis (see Figure 6.1):

$$T = \begin{cases} \tau_\infty (r/R)^{-m}, & 0 < r \leq R \\ \tau_\infty, & R \leq r \leq B - c. \end{cases} \tag{6.16}$$

Suppose further that all the force which would be transferred across the segment $-c \leq x_1 \leq c$ along the crack axis if the crack were *not* present is instead transferred by the singular terms near the crack tip. Define the quantity I by

$$I = \int_0^R \left(\frac{r}{R}\right)^{-m} dr = \frac{R}{1-m} \tag{6.17}$$

so that $\tau_\infty I$ is the area under the low-order singularity curve in Figure 6.1.

The above model immediately needs modification because numerical simulations indicate that the transition terms contribute significantly to the total transferred force.

To account for them, assume that there is a constant q independent of n such that the force carried by the transition terms is $q\tau_\infty(I-R)$. Geometrically, this means that the transition force is q times the force carried by the low-order singularity in excess of the homogeneous term. This approximation for the transition terms has no justification except that it is geometrically plausible and gives reasonably good agreement with numerical data.

The total force out of the plane exerted on the quarter disk at the outer boundary is $B\tau_\infty$. Making the assumptions described above, a force balance along the crack axis is expressed as

$$B\tau_\infty = \tau_\infty I + q\tau_\infty(I-R) + \tau_\infty(B-R-c) \tag{6.18}$$

in which the terms on the right represent forces carried by the low-order singularity, the transition terms, and the homogeneous term in that order. Solving (6.18) for R/c using (6.17) yields

$$\frac{R}{c} = \frac{1}{(1+q)(2n-1)}. \tag{6.19}$$

Since q is assumed to be independent of n, it may be evaluated using the known global solution in the neo-Hookean case (n=1), which is $R = c/2$. Thus $q = 1$. So the large-load approximation for R is

$$\frac{R}{c} = \frac{1}{2(2n-1)}, \qquad n > \frac{1}{2}. \tag{6.20}$$

Other quantities of interest which follow from this approximation and (3.7), (3.14), and (6.1) are given below:

$$A = \left\{ \frac{W_\infty b^{1-n} c (4n^4)^n}{\mu n (2n-1)^{2n}} \right\}^{1/2n}, \tag{6.21}$$

$$J = \frac{W_\infty c \pi n^2}{2n-1}, \tag{6.22}$$

$$\tau \sim \tau_\infty \left[2(2n-1)\frac{r}{c} \right]^{-m} \qquad \text{as } r \to 0,\ \theta = 0, \tag{6.23}$$

and

$$W \sim W_\infty \left[2(2n-1)\frac{r}{c} \right]^{-1} \qquad \text{as } r \to 0,\ \theta = 0, \tag{6.24}$$

where W_∞ is the value of strain energy density corresponding to the condition at infinity.

The large-load approximation given above provides the correct near-field behavior in the neo-Hookean case. Its adequacy in other cases will be discussed below.

6.4 Comparison with numerical results

Figures 6.2a-b(i)-(ii)compare the numerically observed values for J, R, and R_* with the small-load and large-load approximations discussed above for two materials: $n = 5$ and $n = 0.6$. The plots show the applied shear k_∞ on the horizontal axis. Note that for large loads, R becomes independent of the load, a fact that was predicted earlier from scaling considerations alone. For very small loads it is not possible to observe R and R_* using the current numerical model because the low-order zone is smaller than the radius of curvature of the elliptical hole.

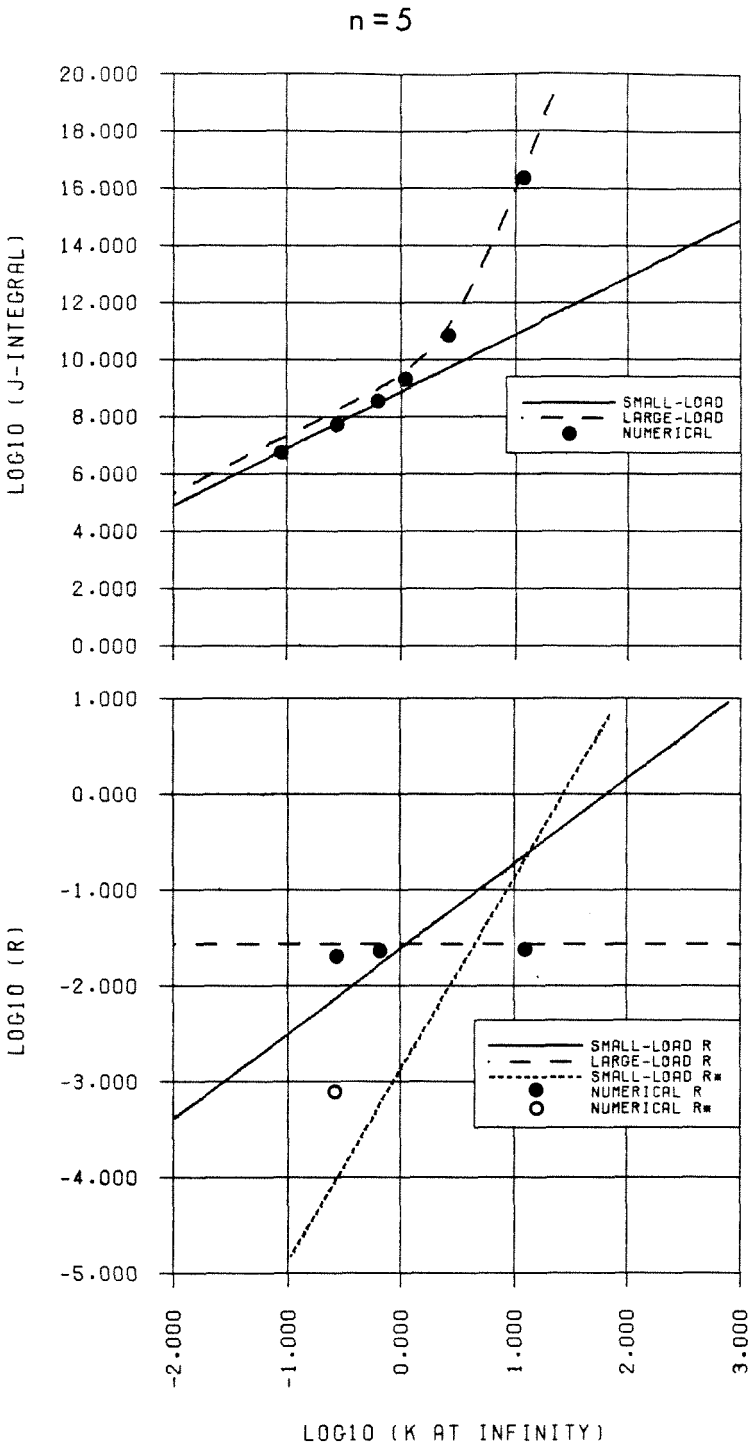

Figure 6.2a. Small-load and large-load estimates along with numerical results for J, R, and R_* as a function of k_∞ with $n = 5$.

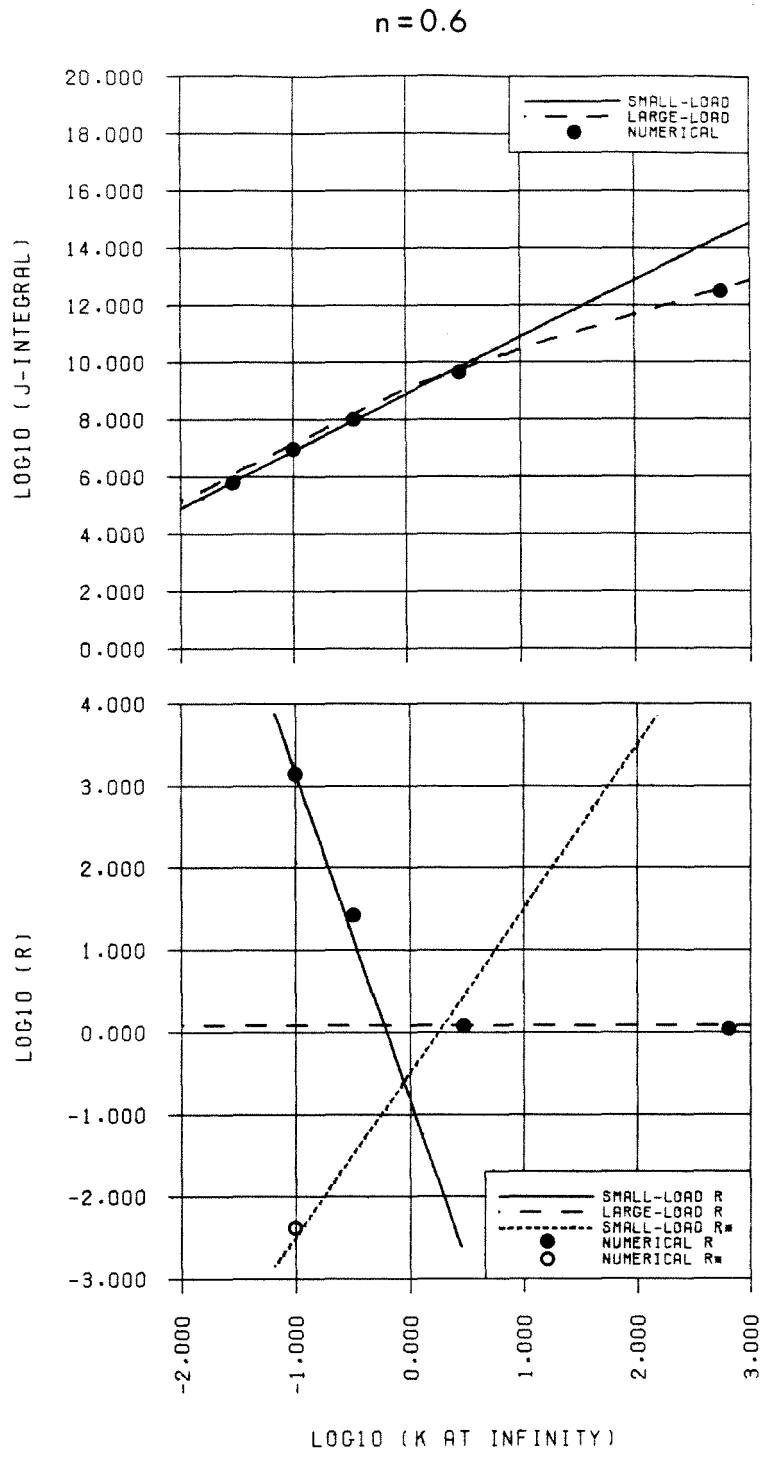

Figure 6.2b. Small-load and large-load estimates along with numerical results for J, R, and R_* as a function of k_∞ with $n = 0.6$.

Chapter 7. Loss of ellipticity: Numerical results

This section presents numerical results for the anti-plane shear crack problem with materials in which the underlying partial differential equation describing the equilibrium of the body may lose ellipticity as a result of deformation. Two materials will be considered here: the linearizable power-law material with $n = 1/4$ and the trilinear material described in Chapter 2.

7.1 Linearizable power-law material, $n = 1/4$

The stress-strain relation for this material is shown in Figure 2.1. The curve has a maximum at $k_0 = \sqrt{1/2b}$, corresponding to a shearing stress of $\tau_0 = \mu\sqrt{1/2b}\, 3^{-3/4}$. For shears greater than k_0, the curve is monotonically strictly decreasing, and it asymptotically approaches zero for large shears. As mentioned in Chapter 2, a locally decreasing stress-strain curve in simple shear corresponds to a locally hyperbolic solution of the equilibrium equation.

The numerical simulation of the crack problem for this material was carried out for a loading of $\tau_\infty = 0.1\mu$, corresponding to a shear of $k_\infty = 0.1$. The shear at infinity is small compared with the shear at the maximum of the stress-strain curve, which for the current case is $k_0 = 1/\sqrt{2}$. However, the load is large enough so that shears larger than k_0 are expected to occur near the tip of the ellipse.

In the simulations which did not involve loss of ellipticity, experience has suggested that the solution of the anti-plane shear crack problem is unique except for rigid deformations. This apparent uniqueness is not surprising, since a slight modification to the Kirchhoff uniqueness proof in linear elastostatics, assuming strong ellipticity, suffices to prove infinitesimal uniqueness in a large class of boundary value problems for finite anti-plane shear. This is not the case in problems in which ellipticity is lost, and experience has shown that the numerical solutions are sensitive to initial conditions and the way boundary conditions are applied over time.

In the simulation of the $n = 1/4$ crack problem, the initial conditions were quiescent. A traction field s at the outer edge of the mesh was applied according to a ramp function of time as follows. Denoting the angle in a polar coordinate system centered at the crack midpoint by ϕ, the traction field $s(\phi, t)$ was computed as

$$s(\phi, t) = \tau_\infty \min(1, t/\lambda) \sin\phi, \qquad t > 0,\ 0 \leq \phi \leq \pi/2 \tag{7.1}$$

where λ is a constant and t is time.

In this simulation a value of $\lambda = 400$ was used. This value is about 10 times as large as the transit time for small waves from the origin to the outer edge of the mesh. Therefore the simulation should be nearly quasi-static.

Figure 7.1 shows the distribution of shear at the time when the calculation was terminated. Note the long, narrow band of intense shear extending from the crack tip along the crack axis. This band occupies one finite-difference zone in width, and it may therefore be regarded as having infinitesimal thickness. The band will be called a "shear band" in an analogy with the localization phenomenon in plasticity. The shear in this band is so large that there is effectively zero shearing stress inside the band. The band is therefore essentially a fracture.

Although the dynamic relaxation technique is not designed to provide an accurate model of the dynamics of the problem, it is nevertheless of interest to consider the evolution of the band during the calculation. The discontinuity first appears at the ellipse tip at the time when the shearing stress there first exceeds τ_0. The band then propagates rapidly forward from the ellipse tip much in the manner of a propagating crack.

The calculation fails to converge fully because the problem has no stable equilibrium solution. The band evidently propagates unboundedly, and each half-plane moves more or less as a rigid body into or out of the plane. Stability considerations will be discussed further in Section 7.3 below.

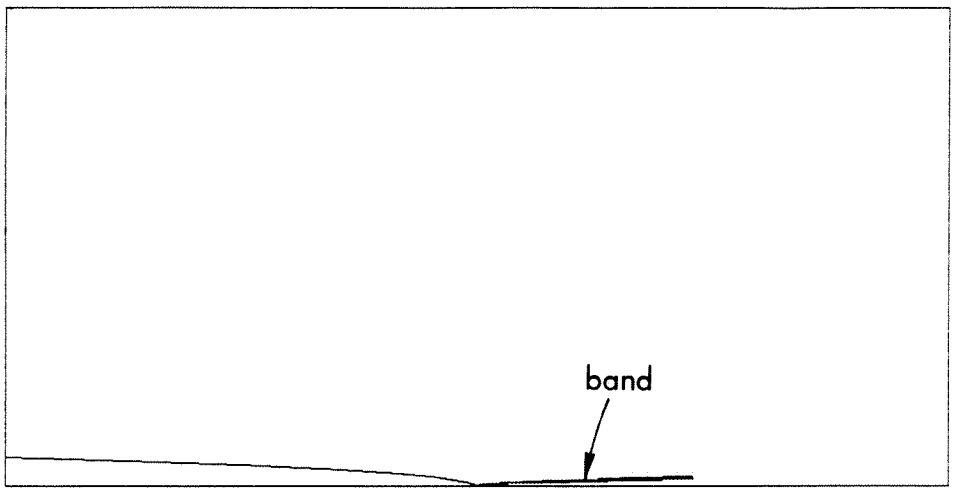

Figure 7.1. Shear band in crack problem for $n = 1/4$ material. Darkness increases with shear.

Figure 7.2 shows the displacement field near the ellipse tip at the time when the calculation was stopped. Note the line of discontinuity of displacement. Figures 7.3a-d show u, T/μ, T_1/μ, and T_2/μ as functions of angle along a small circle centered at the right crack tip.

7.2 Trilinear material

The trilinear material was described in Chapter 2. The downward-sloping segment $[K^-, K^+]$ in the stress-strain curve corresponds to locally hyperbolic solutions to the equilibrium equation. The following discussion first presents numerical simulations of the anti-plane shear crack problem for the trilinear material. It then presents numerical simulations of a screw dislocation problem, whose solution is easier to interpret than that of the crack problem.

7.2.1. Crack problem. The anti-plane shear crack problem was simulated for the case $k_\infty = 0.3$, $\tau_\infty = 0.3\mu^-$. Some modifications in the mesh were made for this material. Because of a greater than usual need for resolution at intermediate distances from the crack tip, it was feasible to model only the region near the crack tip (see Figure 7.4). Because of an expected breakdown in symmetry across the crack axis, both upper and lower half planes were modeled. The mesh contained 3,339 nodes.

Initial conditions were quiescent. Displacement boundary conditions were applied as a ramp function of time as follows. Denoting the exact solution to the *linear* elliptical hole problem by u_{lin}, the displacements at nodes along the outer edge of the mesh were computed from

$$u(x_1, x_2, t) = u_{\text{lin}} \min(1, t/\lambda), \qquad t \geq 0 \tag{7.2}$$

where λ is a positive constant. For this simulation $\lambda = 100$, a time interval on the order of the wave transit time for the mesh, which is 62.

Figure 7.5 shows the distribution of the three phases (low-strain elliptic E^-, hyperbolic H, and high-strain elliptic E^+) in the converged solution. Note the chaotic

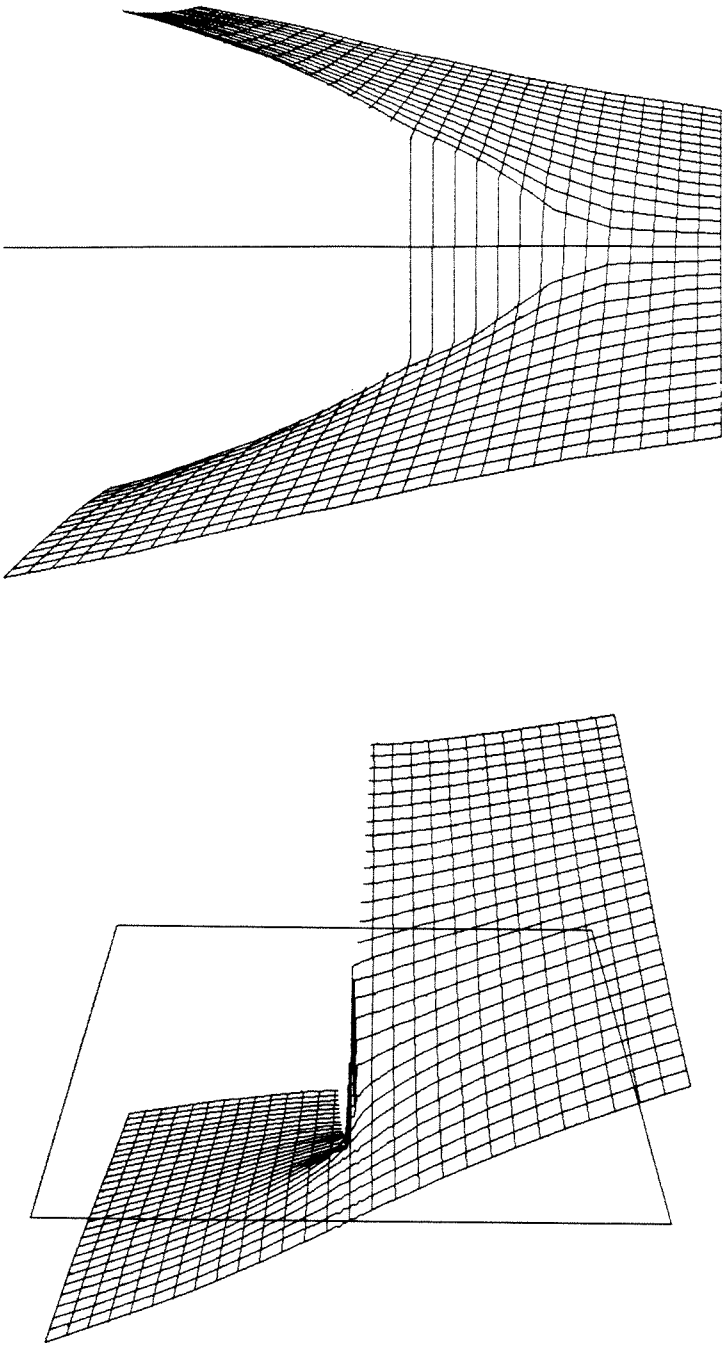

Figure 7.2. Deformation of a sheet initially in the plane in crack problem, $n = 1/4$ material.

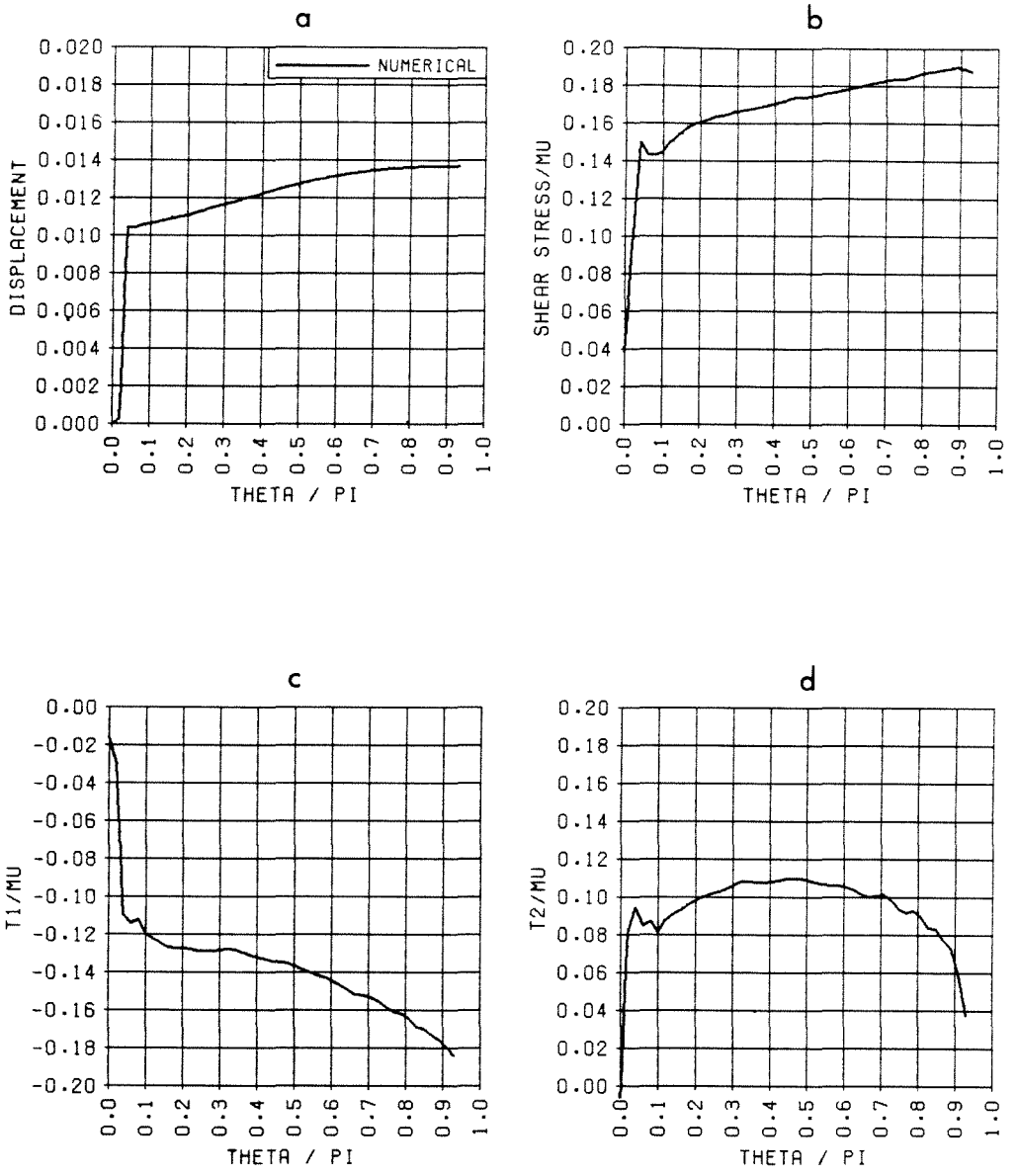

Figure 7.3. Dependence on θ of (a) u, (b) T/μ, (c) T_1/μ, (d) T_2/μ along circle centered at crack tip for $n = 1/4$ material.

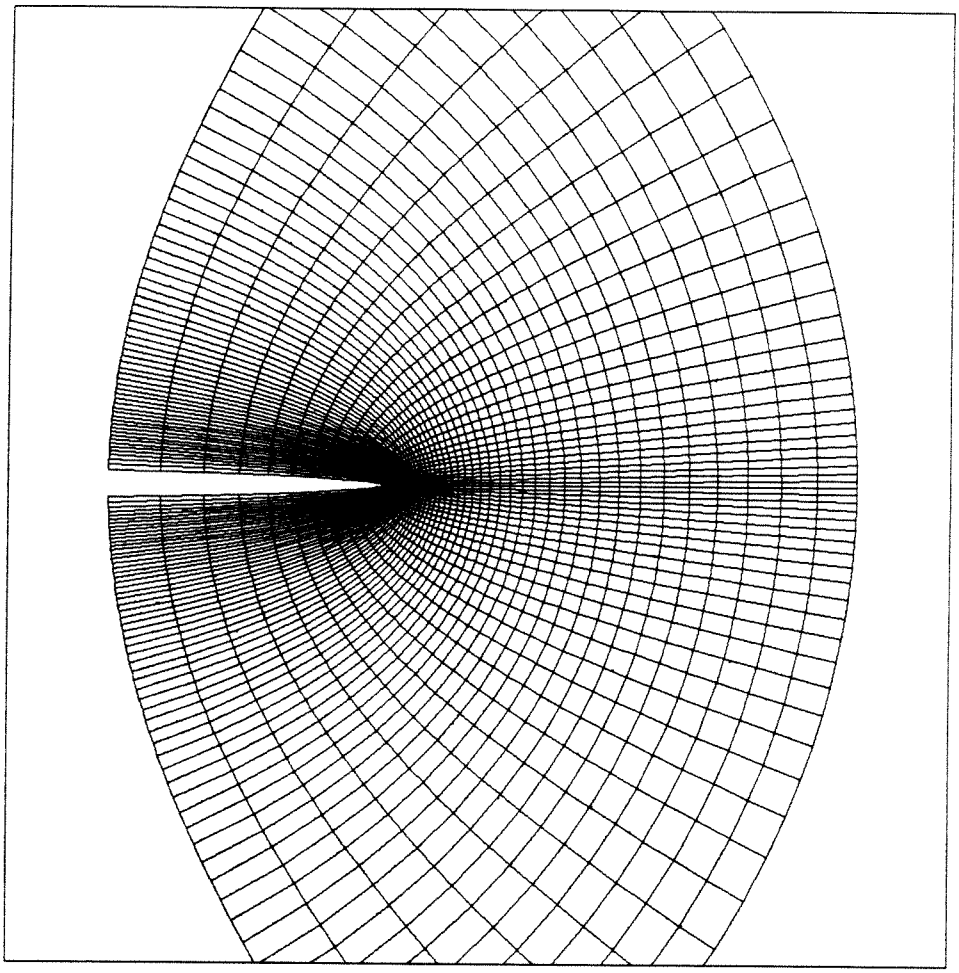

Figure 7.4. Numerical mesh used for simulation of crack problem in trilinear material.

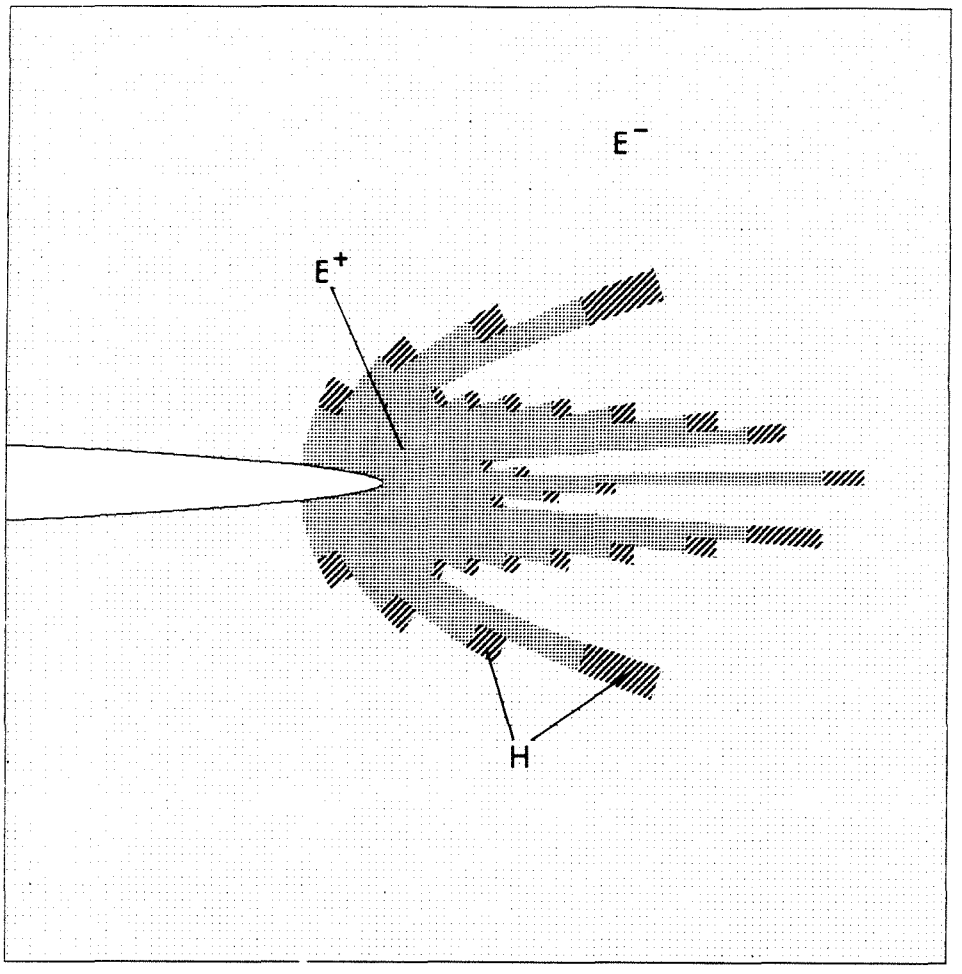

Figure 7.5. Distribution of phases in simulation of crack problem, trilinear material. E^- =low-strain elliptic, H =hyperbolic, E^+ =high-strain elliptic.

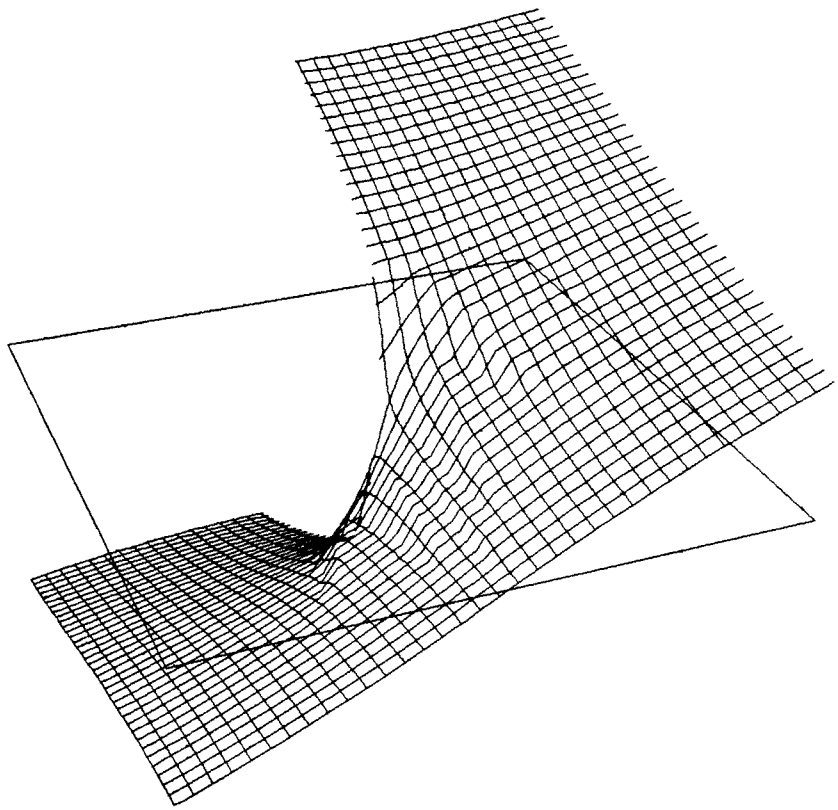

Figure 7.6. Deformation of a sheet initially in the plane in crack problem, trilinear material.

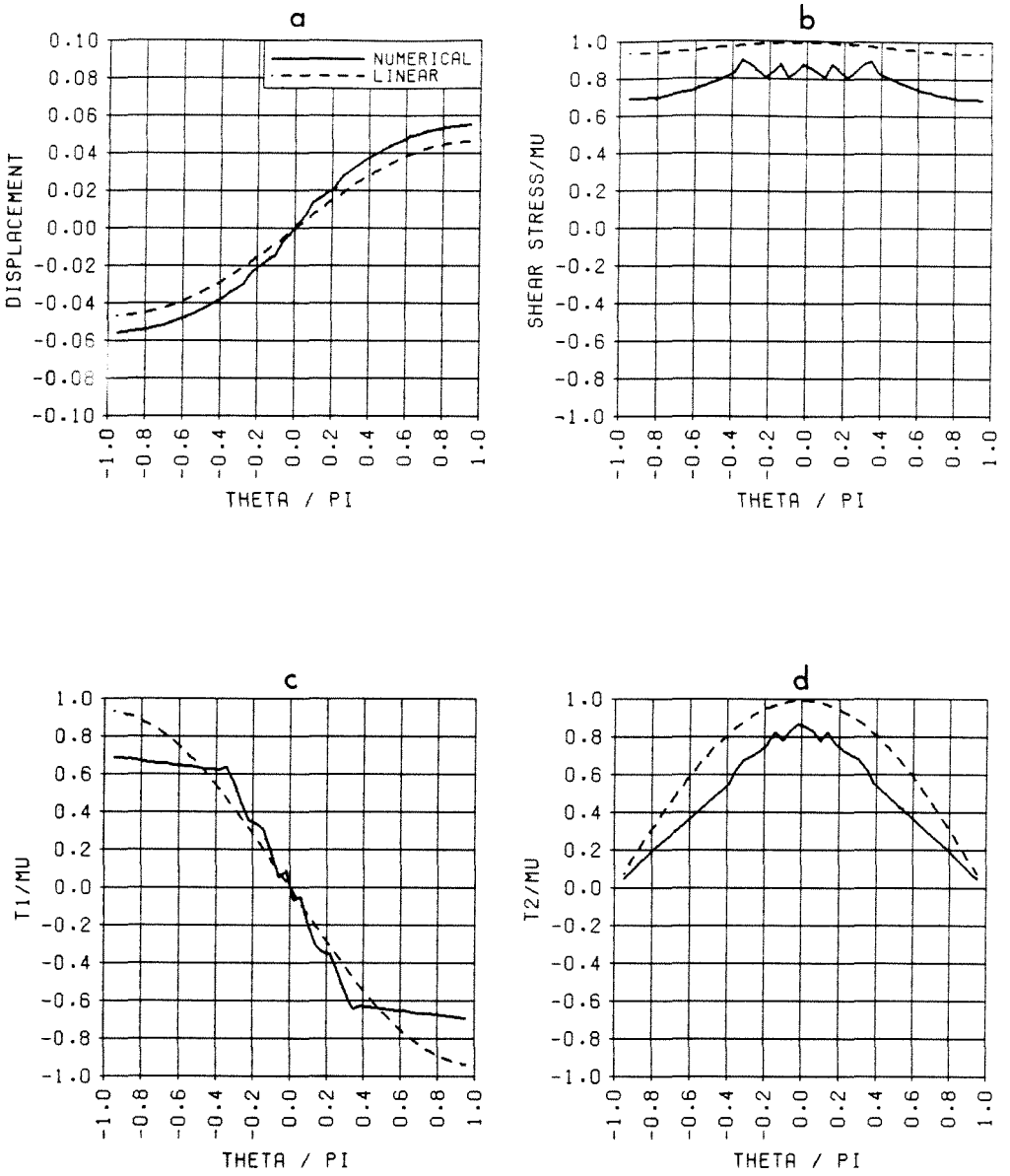

Figure 7.7. Dependence on θ of (a) u, (b) T/μ, (c) T_1/μ, (d) T_2/μ along circle centered at crack tip for trilinear material.

appearance of the phases. Of particular interest is the almost complete absence of a hyperbolic phase. Alteration of the initial or boundary conditions in the simulation changes the details of the converged numerical solution but not the general features. There is always a similar pattern of "dendrites" of the two elliptic phases extending into each other in a region at intermediate distance ahead of the crack. The thickness of these dendrites is always on the order of the finite-difference zone width, and they invariably end in cusps. Using a finer mesh merely results in more dendrites rather than enabling a closer look at any structure within them.

Figure 7.6 shows the displacement field near the crack tip. The wrinkled appearance of the field is caused by the dendrites issuing from the high-strain elliptic region at the crack tip. Figures 7.7a-d show u, T/μ, T_1/μ, and T_2/μ as functions of angle along a small circle centered at the right crack tip.

7.2.2. Screw dislocation problem. A simpler boundary value problem which retains many of the features of the crack problem is that of a screw dislocation, shown in Figure 7.8. In a body occupying the entire plane, a cut is made along the positive x_1-axis, and the lower face is displaced out of the plane by a constant amount u_0. The upper face is held fixed. It is also required that $u \sim u_0\theta/2\pi$ as $r \to \infty$.

The screw dislocation problem has the interesting property that for *any* generalized neo-Hookean material, linear or nonlinear, the field

$$u = u_0\theta/2\pi, \qquad r > 0, \quad 0 \le \theta < 2\pi \tag{7.3}$$

provides a solution of the boundary value problem. This fact was apparently first observed by Kachanov [16].

Numerical simulation of the screw dislocation problem for the trilinear material was carried out using a mesh which modeled the first quadrant only. The mesh had 25 radial lines of nodes and 40 circular lines. Initial conditions were provided by (7.3), and displacement boundary conditions derived from (7.3) were used around the entire

boundary.

Figure 7.9a shows the distribution of the three phases (low-strain elliptic E^-, hyperbolic H, and high-strain elliptic E^+) for the numerical simulation. Note the pattern of dendrites very similar to that found in the crack problem.

In order to investigate the effect of mesh spacing on the solution, the screw dislocation problem was also run using a higher density of radial lines (but modeling a narrower wedge, occupying $0 \leq \theta \leq \pi/8$). The displacement boundary condition on the wedge was modified to correspond to the same u_0 as in the coarse mesh simulation. The distribution of phases for the simulation with a fine mesh is shown in Figure 7.9b.

Figure 7.10 shows the quantity

$$\frac{2}{\pi}\int_0^{\pi/2} T(r,\theta)\, d\theta \tag{7.4}$$

as a function of r in the fine mesh simulation. Over a certain interval this average stress is near the Maxwell stress, which is $2^{-1/4}\mu^- \approx 0.8409\mu^-$ for the trilinear material. Since the Maxwell stress plays a prominent role in the stability of coexistent phases in anti-plane shear, its appearance in the numerical solution suggests that the formation of dendrites is related to stability. The significance of stability in these solutions is the subject of Part II of this work. It will be shown there that the dendrites form in a way that is geometrically predictable from stability considerations.

7.3 Discussion

Part II of this dissertation is devoted to explaining the behavior of the trilinear material by considerations of elastic stability. However, some preliminary points will be made here.

An asymptotic solution of the crack problem for a special material similar to the $n = 1/4$ material was developed by Knowles and Sternberg [17,18]. This solution differs in a fundamental way from the numerical results described above. The asymptotic

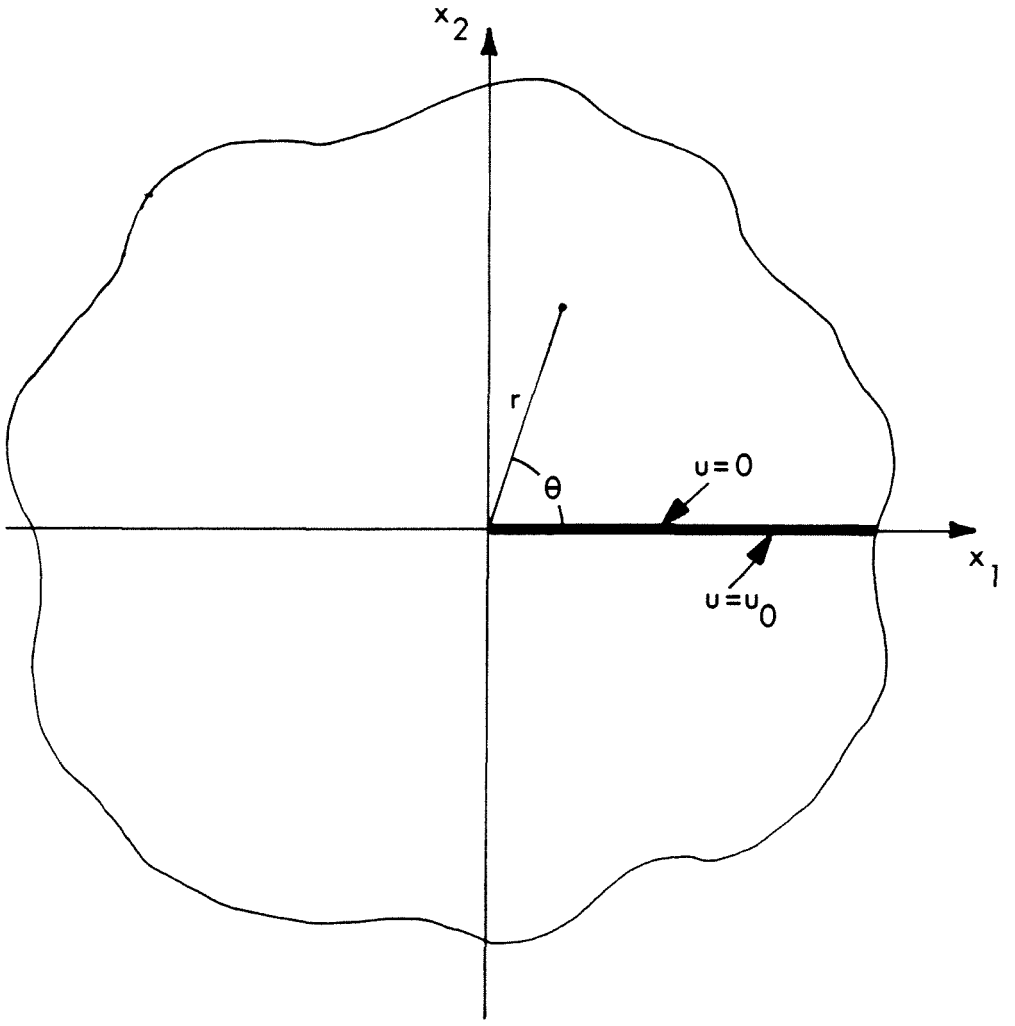

Figure 7.8. Screw dislocation problem. Only the first quadrant is modeled numerically.

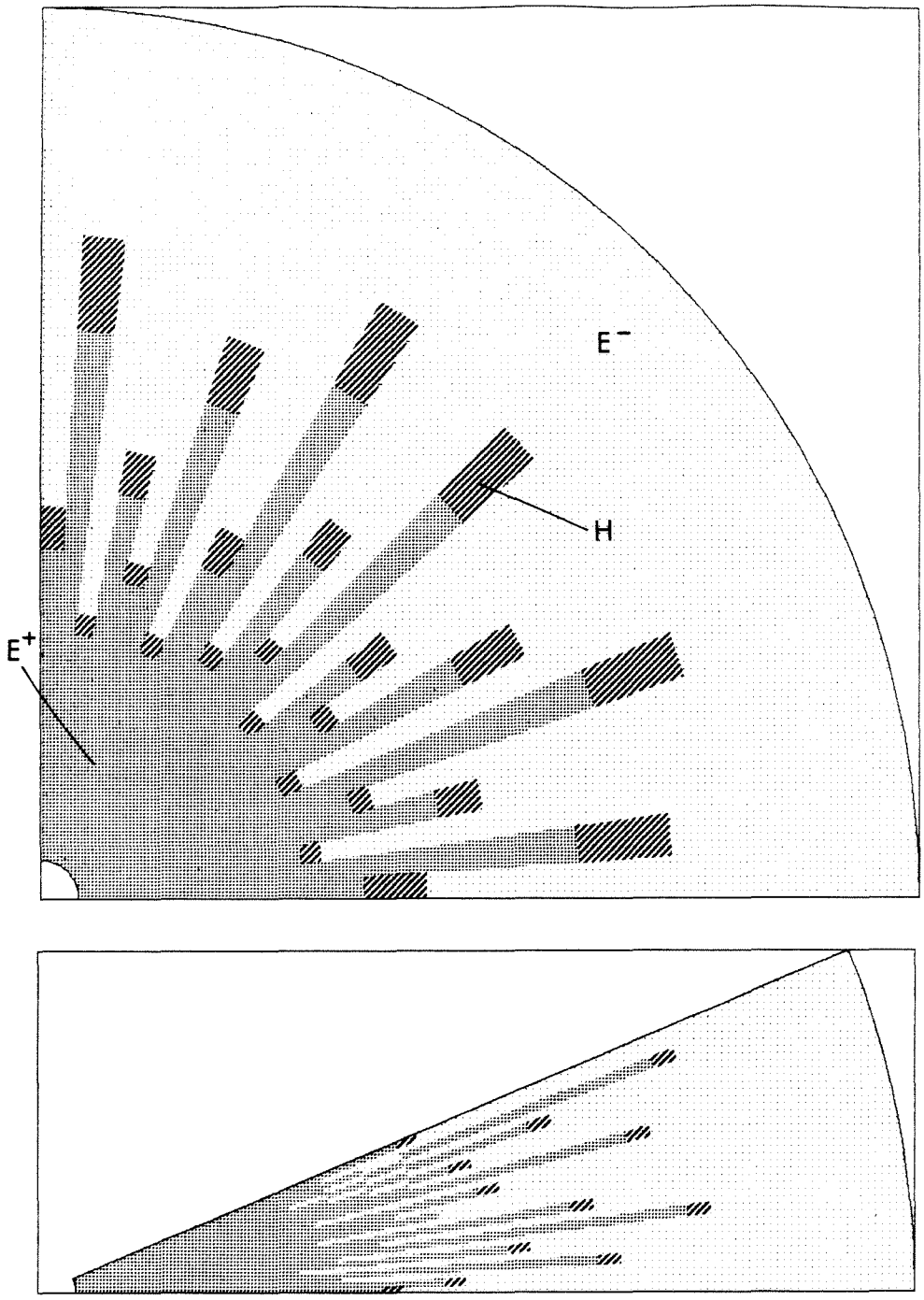

Figure 7.9. Distribution of phases in simulation of the screw dislocation problem, trilinear material. E^- =low-strain elliptic, H =hyperbolic, E^+ =high-strain elliptic: (a) coarse mesh, (b) fine mesh.

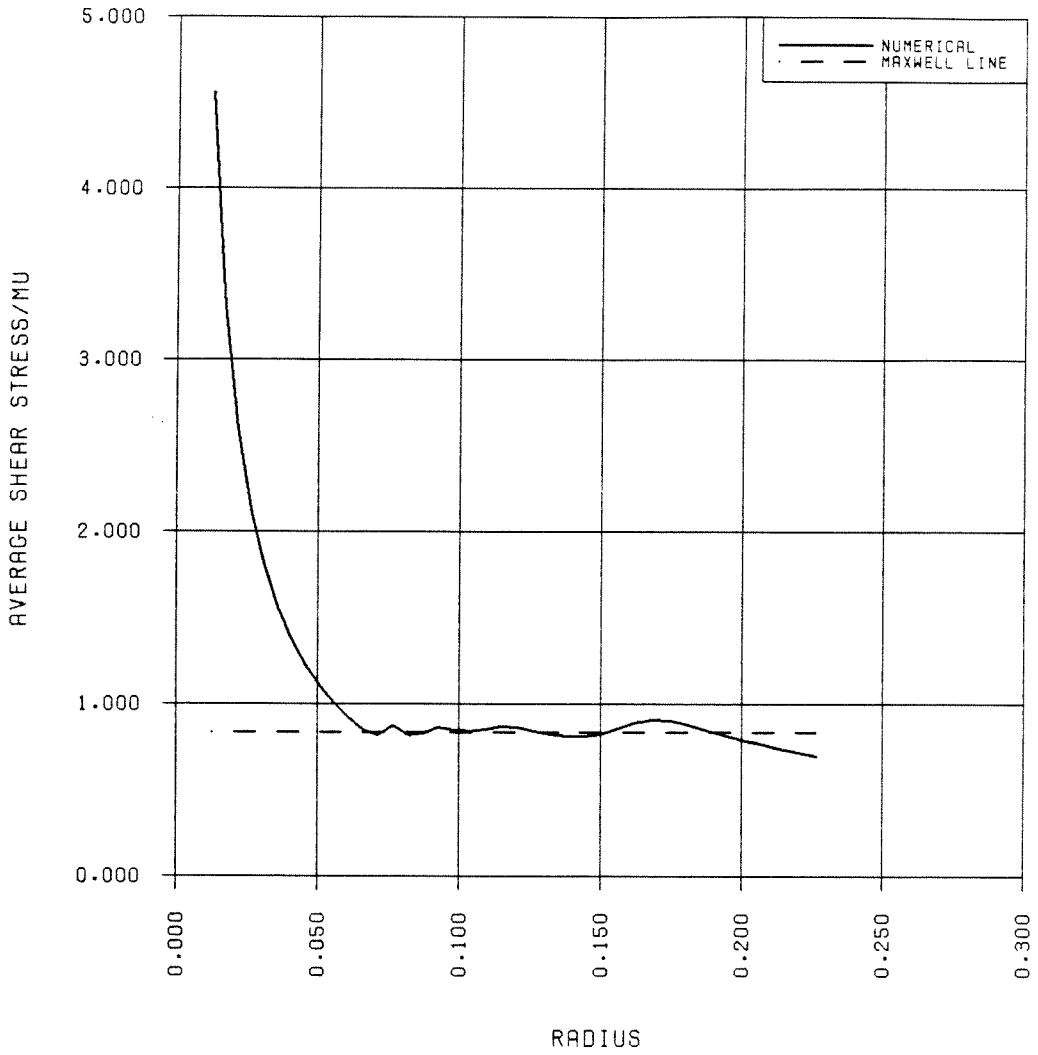

Figure 7.10. Average value of shear stress T/μ^- on a circular arc of radius r in screw disclocation problem, trilinear material, fine mesh. Flat part of curve is at the Maxwell stress, $0.8409\mu^-$.

solution, while containing equilibrium shocks, has continuous displacements and does not contain a shear band. A solution for a material similar to the trilinear material was developed by Abeyaratne [7]. This solution also contains equilibrium shocks but does not predict the chaotic pattern of dendrites observed numerically. Both of the above asymptotic solutions contain hyperbolic regions, which are never seen in the numerical results.

It is straightforward to show that any hyperbolic solution of the equilibrium equation in anti-plane shear for a hyperelastic body cannot be a minimizer of potential energy. It is also a simple matter to show that if such a hyperbolic solution exists in some region, then small plane-waves grow unboundedly in that region since strong ellipticity is lost there [19,20]. (This statement assumes that the constitutive behavior is the same in the dynamic case as in the equilibrium case.) Recall that the dynamic relaxation method predicts locally stable solutions, solutions that do not spontaneously change when used as initial conditions in the dynamic problem. It therefore makes sense that this numerical method does not predict solutions that are hyperbolic in any region.

The emergence of a curve of discontinuity in ∇u, *i.e.*, an equilibrium shock, is not at all surprising when ellipticity is lost [21–24]. However, a curve of discontinuity in u, as is seen in the $n = 1/4$ simulation, is perhaps unexpected. One might expect that the propagation of such a band would entail the expenditure of surface energy, as in the propagation of fractures. However, the following simple analysis shows that no such energy is required. Suppose the band has a small thickness δ, and suppose the difference in displacement across the band is U. Assuming that shear is constant across the width of the band, the shear is $k = U/\delta$. The total strain energy per unit length of the band is $\Phi = \delta w(k)$ where w is given by (2.9). Letting δ become small,

$$\Phi \sim \delta \frac{\mu}{2} \left(\frac{b}{n} k^2 \right)^n \sim \delta \frac{\mu}{2} \left(\frac{b}{n} \right)^n \left(\frac{U}{\delta} \right)^{2n} \sim \frac{\mu}{2} \left(\frac{b}{n} \right)^n U^{2n} \delta^{1-2n} \quad \text{as } \delta \to 0. \tag{7.5}$$

So, for $n > 1/2$, the surface energy Φ increases unboundedly as δ becomes small. For $n = 1/2$, Φ remains constant, which makes intuitive sense because the material in the band

is in effect flowing like a perfectly plastic material. But for $n < 1/2$, Φ approaches zero for small δ, indicating that no surface energy is required to propagate the band. Thus the numerical simulation of the $n = 1/4$ material showing the unbounded development of the band is quite plausible.

A vivid demonstration of the dynamic instability of hyperbolic solutions is shown in Figure 7.11, which shows the maximum magnitude of velocity of any node in the screw dislocation problem as a function of time. The initial conditions for this problem were quiescent and were given by the classical displacement field (7.3), which is an exact solution to the nonlinear problem. Thus, if the classical solution were dynamically stable, there would be no motion induced in the numerical mesh except for the effects of truncation and roundoff error. Since the shear field associated with this displacement field is $k = u_0/2\pi r$, there is initially an annulus in which the shears occupy the downward-sloping segment H of the stress-strain curve. Therefore in this annulus the equilibrium equation is hyperbolic initially. Figure 7.11 shows exponential growth in velocity during the early stages of the simulation. These velocities are initially on the order of the roundoff error in the calculations, but they soon grow into sizable waves. These waves decay only after the body separates into the two elliptic phases and the hyperbolic phase disappears.

The above argument that a stable hyperbolic solution is not to be expected in any *region* does not preclude loss of ellipticity along a *curve* in a stable equilibrium solution. This is precisely what is seen in the $n = 1/4$ simulation in the shear band extending from the crack tip. It is also seen in the equilibrium shocks which form the boundaries of the dendrites in the trilinear material, since the existence of shocks necessarily means a loss of ellipticity there.

It is apparent from Figure 7.5 that the solution to the trilinear crack problem is not symmetric about the x_1-axis. This loss of symmetry is consistent with the above considerations regarding elastic stability. Gurtin [25] shows that a necessary condition

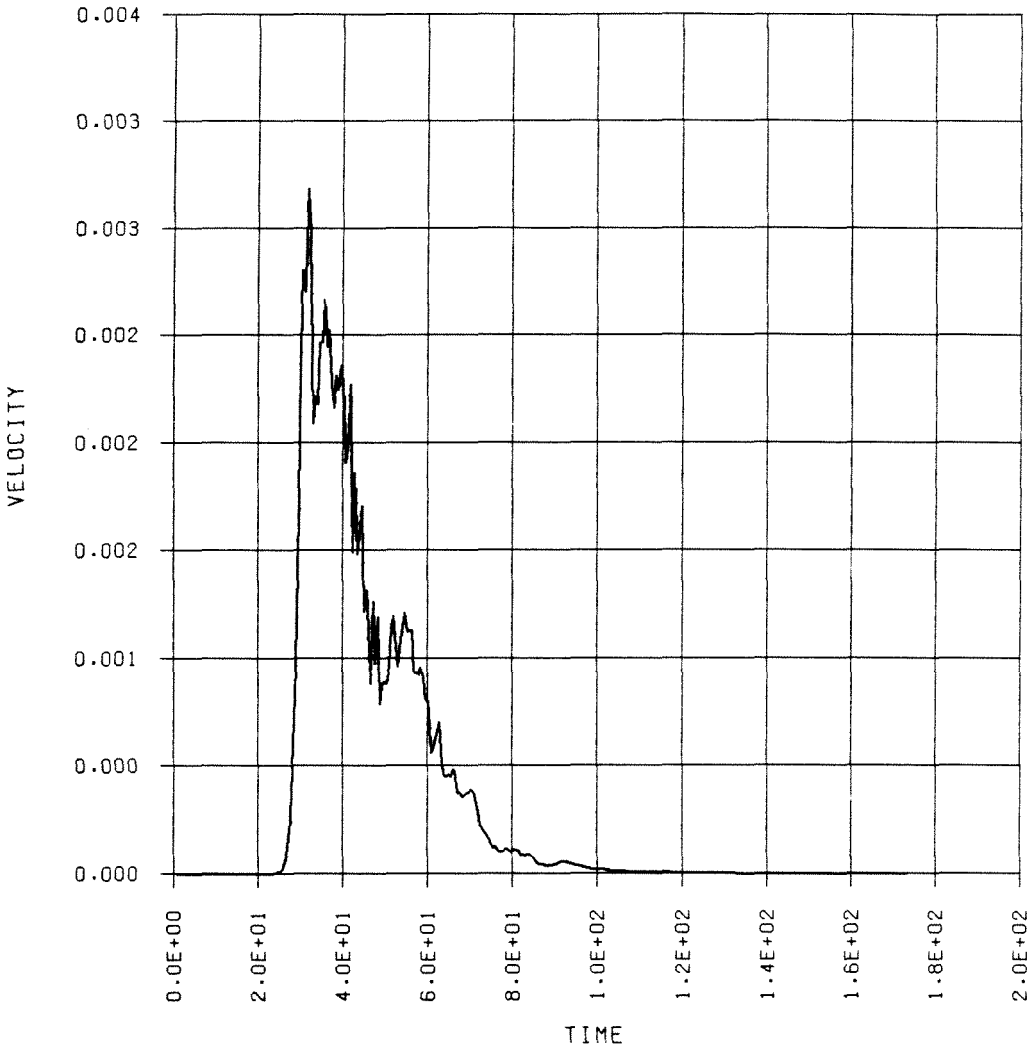

Figure 7.11. Maximum magnitude of velocity anywhere in mesh as a function of time in screw dislocation problem, coarse mesh. Exponential growth in velocity indicates dynamic instability of the initial condition.

for loss of uniqueness during a quasi-static process (*i.e.*, a bifurcation) is that the process pass through an unstable state. Indeed, loss of uniqueness is to be expected when such an unstable state is reached. Gurtin uses the example of a buckling Euler beam to illustrate this point. As a compressive force on the ends of the beam is slowly increased, a force equal to the buckling load results in an unstable state of the body, heralding a loss of uniqueness during further loading. This loss of uniqueness causes a lack of symmetry in the process, as evinced by the fact the beam can buckle in any of an infinite number of directions.

Since hyperbolic solutions are dynamically unstable, the trilinear crack problem passes through an unstable state at some point along the loading path. Therefore uniqueness and symmetry are expected to be lost. The actual path followed by the numerical simulation depends on details of the calculation such as roundoff error. Experience with various types of meshes and loading conditions has suggested that there are in fact an infinite number of solutions. Part II of this dissertation will show that among this infinite number of solutions, those that are stable may be approximated by assuming that the elliptic phases are very finely mixed.

Chapter 8. Conclusions

The numerical simulations of elliptic cases for the anti-plane shear crack problem have confirmed the low-order asymptotic solutions presented in Chapter 3. They have also provided direct observations of the low-order zone size and the dependence of the J-integral on load. It has been shown in Chapter 6 that a crude model of the force balance near the singularity provides reasonably accurate approximations for these quantities in large-load cases for $n = 1/2$. The main feature of the observed low-order zone sizes for $n > 1/2$ is that for small loads the zone size is proportional to ${k_\infty}^2$, while for large loads it approaches a constant value. Similarly, computations of J show that for small loads J is proportional to ${k_\infty}^2$ (the small-scale yielding case) while it is proportional to W_∞, or equivalently to ${k_\infty}^{2n}$, in the large-load case. For the $n = 1/2$ material the Hult-McClintock estimate for plastic zone size provides a good estimate of the low-order zone size for small loads. There is no large-load case for the $n = 1/2$ material.

The numerical simulations of materials which do lose ellipticity in the crack problem have yielded unexpected results. In the $n = 1/4$ material, which becomes hyperbolic for sufficiently large strains, the instability of the hyperbolic solutions results in a collapse of the non-elliptic region onto a single band of very small thickness and very high strain. The displacement field is discontinuous across this band. This band propagates apparently unboundedly in the dynamic relaxation solution much in the manner of a propagating crack.

In the trilinear material, unlike the $n = 1/4$ material, the portion of the stress-strain curve which yields hyperbolic solutions is confined to a bounded interval. Therefore the band which appears in the $n = 1/4$ material is not a possibility. Instead, a chaotic pattern of equilibrium shocks separating the two elliptic phases emerges. It will be shown in Part II of this dissertation that this pattern is predictable from considerations of elastic stability. Potential energy is minimized only in the limit of an infinitely fine mixture of the two phases such that neighboring shocks are always parallel to each

other. This mixture occurs in a definite region which may be computed by finding the solution to the crack problem in an "elastic-plastic-elastic" material in which the yield stress occurs at the Maxwell line of the original trilinear material.

Preliminary work has shown that many of the phenomena observed in anti-plane shear simulations of loss of ellipticity also occur in plane-strain conditions. In particular, plane-strain crack problems for the Blatz-Ko material [26–28], a compressible hyperelastic material which loses ellipticity under uniaxial stress conditions for sufficiently high stretches, show failure at the crack tip similar to the $n = 1/4$ case in anti-plane shear. This work will be documented separately.

References for Part I

[1] J. A. H. Hult and F. A. McClintock, "Elastic-plastic stress and strain distribution around sharp notches under repeated shear," *Proceedings of the Ninth International Congress of Applied Mechanics, Brussels, Belgium* **8** (1956) 51-58

[2] J. R. Rice, "Stresses due to a sharp notch in a work-hardening elastic-plastic material loaded by longitudinal shear," *Journal of Applied Mechanics* **34** (1967) 287-298

[3] J. C. Amazigo, "Fully plastic crack in an infinite body under anti-plane shear," *International Journal of Solids and Structures* **10** (1974) 1003-1015

[4] J. K. Knowles, "The finite anti-plane shear field near the tip of a crack for a class of incompressible elastic solids," *International Journal of Fracture* **13** (1977) 611-639

[5] J. L. Ericksen, "Equilibrium of bars," *Journal of Elasticity* **5** (1975) 191-201

[6] J. K. Knowles and Eli Sternberg, "Anti-plane shear fields with discontinuous deformation gradients near the tip of a crack in finite elastostatics," *Journal of Elasticity* **11** (1981) 129-164

[7] R. Abeyaratne, "Discontinuous deformation gradients away from the tip of a crack in anti-plane shear," *Journal of Elasticity* **11** (1981) 373-393

[8] S. A. Silling, "CHIMP — a computer program for finite elastostatics," to appear

[9] W. Hermann and L. D. Bertholf, "Explicit Lagrangian finite-difference methods," in *Computer Methods for Transient Analysis*, T. Belytschko and T. J. R. Hughes, eds., Amsterdam: Elsevier (1983) 361-416

[10] P. Underwood, "Dynamic relaxation," in *Computer Methods for Transient Analysis*, T. Belytschko and T. J. R. Hughes, eds., Amsterdam: Elsevier (1983) 245-265

[11] A. S. Day, "An introduction to dynamic relaxation," *The Engineer (London)* **219** (1965) 218-221

[12] M. L. Wilkins, "Calculation of elastic-plastic flow," Lawrence Radiation Laboratory report UCRL-7322 (1969)

[13] I. G. Currie, *Fundamental Mechanics of Fluids*, New York: McGraw-Hill (1974) 100

[14] R. Abeyaratne, "On the estimation of energy release rates," *Journal of Applied Mechanics* **50** (1983) 19-23

[15] G. R. Irwin, J. A. Kies, and H. L. Smith, "Fracture strengths relative to onset and arrest of crack propagation," *Proceedings of the American Society for Testing and Materials* **58** (1958) 640-657

[16] M. L. Kachanov, "Screw dislocation in a non-linear elastic continuum," *International Journal of Solids and Structures* **18** (1982) 917-918

[17] J. K. Knowles and Eli Sternberg, "Discontinuous deformation gradients near the tip of a crack in finite anti-plane shear: an example," *Journal of Elasticity* **10** (1980) 81-110

[18] J. K. Knowles and Eli Sternberg, "Anti-plane shear fields with discontinuous deformation gradients near the tip of a crack in finite elastostatics," *Journal of Elasticity* **11** (1981) 129-164

[19] J. Hadamard, "Sur quelques questions du calcul des variation," *Bull. Soc. Math. France* **30** (1902) 253-256

[20] C. Truesdell and W. Noll, "The non-linear field theories of mechanics," *Handbuch der Physik*, vol. III/3, Berlin: Springer (1965) Sec. 68 bis.

[21] J. R. Rice, "The localization of plastic deformation," in *Theoretical and Applied Mechanics, Proceedings of the 14th IUTAM Congress, Delft, The Netherlands*, Amsterdam: North Holland (1976)

[22] R. Hill and J. W. Hutchinson, "Bifurcation phenomena in the plane tensile test," *Journal of the Mechanics and Physics of Solids* **23** (1975) 239-264

[23] J. K. Knowles and Eli Sternberg, "On the ellipticity of the equations of nonlinear elastostatics for a special material," *Journal of Elasticity* **5** (1975) 341-361

[24] J. K. Knowles and Eli Sternberg, "On the failure of ellipticity and the emergence

of discontinuous deformation gradients in plane finite elastostatics," *Journal of Elasticity* **8** (1978) 329-379

[25] M. E. Gurtin and S. J. Spector, "On stability and uniqueness in finite elasticity," *Archive for Rational Mechanics and Analysis* **70** (1979) 153-165

[26] P. J. Blatz and W. L. Ko, "Application of finite elastic theory to the deformation of rubbery materials," *Transactions of the Society of Rheology* **6** (1962) 223

[27] J. K. Knowles and Eli Sternberg, "An asymptotic finite-deformation analysis of the elastostatic field near the tip of a crack," *Journal of Elasticity* **3** (1973) 67

[28] J. K. Knowles and Eli Sternberg, "Finite-deformation analysis of the elastostatic field near the tip of a crack: reconsideration and higher-order results," *Journal of Elasticity* **4** (1974) 201

PART II:

CONSEQUENCES OF THE MAXWELL RELATION FOR A FAMILY OF ANTI-PLANE SHEAR DEFORMATIONS

Chapter 9. Introduction

The investigation of phase changes in solids is currently an active area in continuum mechanics. One component of this field of research is the study of equilibrium deformations of elastic bodies which contain jump discontinuities in the first derivatives of displacement. Because boundary value problems may admit an infinite number of solutions with such discontinuities, conditions of elastic stability have been proposed as one means of identifying those solutions which are physically meaningful. However, there are several different notions of elastic stability, and it is not known which of these, if any, provides an appropriate criterion.

Even if one adopts the traditional notion of minimum potential energy as a condition for stability, one must identify a class of variations with respect to which a stable solution is required to be a minimizer [1]. For example, for *infinitesimal* stability one requires a stable solution to be a minimizer with respect to variations with sufficiently small *displacement gradients*. For *local* stability one requires that it be a minimizer with respect to variations with sufficently small *displacements*. These two requirements lead to very different practical results in solving boundary value problems.

Because few boundary value problems have been solved for deformations with these discontinuities, there has been little basis for discussion of the consequences of the various stability criteria. The purpose of this paper is to examine some implications of the *Maxwell relation*, which is necessarily satisfied by deformations that are locally stable in the sense described above. The setting for this study is the anti-plane shear of a *trilinear* material, whose equilibrium is described by a very simple set of equations.

It will be shown that many reasonable boundary value problems for this material do not possess solutions which obey the Maxwell relation. However, the relation can be satisfied in the sense of a limit of an infinite sequence of increasingly chaotic deformations. Examples of such chaos are provided by the numerical simulations described in Chapter 7 of Part I of this work. This sequence corresponds to the minimizing sequence

for the potential energy functional, as discussed by Ball [2]. However, the properties of the sequence as derived in a variational setting are not fully understood, especially for multidimensional problems. In the present work, a purely mechanical approach to this sequence will be used rather than a variational approach.

The remainder of this thesis is organized as follows. Chapter 10 reviews the basic mechanics of anti-plane shear, two-phase deformations, and stability. Chapter 11 describes the trilinear material, which will be considered in much of the remainder of the paper. Chapter 12 discusses two-phase deformations that satisfy the Maxwell relation. Some properties of solutions that fail to satisfy the Maxwell relation are briefly discussed in Chapter 13. Chapter 14 hypothesizes mixed deformations, which represent the limiting case mentioned above. To make this idea precise, Chapter 15 derives general results for the constitutive properties of the limit of a sequence of elastic states. Chapter 16 shows that a mixed deformation is the limit of a sequence which satisfies the Maxwell relation in an asymptotic sense.

Chapter 10. Anti-plane shear

10.1 Preliminaries

Let a rectangular coordinate system (x_1, x_2, x_3) be given. Let B be a closed cylinder with generators parallel to the x_3-direction, and let R be the cross-section of B in the (x_1, x_2)-plane. An **anti-plane shear** deformation is a mapping of the form

$$y_1 = x_1, \quad y_2 = x_2, \quad y_3 = x_3 + u(x_1, x_2) \tag{10.1}$$

where (y_1, y_2, y_3) are the coordinates of the image of a material particle originally at (x_1, x_2, x_3), and u is a function on R called the **displacement field** or simply the **deformation**. The smoothness required of u will depend on the problem at hand. In various contexts it will be convenient to express u and related quantities as a function of either the position vector in the plane or the complex representation of it, and it is to be understood that $u(x_1, x_2)$, $u(\mathbf{x})$, and $u(x_1 + ix_2)$ all mean the same thing.

The field ∇u defined at all points in R where u is differentiable will be called the **displacement gradient field** or simply the **gradient field**. The scalar field k on this same subset of R defined by $k = |\nabla u|$ will be called the **amount of shear field** or simply the **shear field**.

Let $\mathbf{e}_i$ be the unit vector in the x_i-direction. At any point $\mathbf{x} \in R$ where the Cauchy stress tensor σ is defined (*i.e.*, wherever u is sufficiently smooth) let $\mathbf{T}(\mathbf{x})$ be the projection of $\sigma(\mathbf{x})\mathbf{e}_3$ into the (x_1, x_2)-plane. $\mathbf{T}$ will be called the **stress vector field**. Its components are $T_1 = \sigma_{13} = \sigma_{31}$ and $T_2 = \sigma_{23} = \sigma_{32}$. The scalar field T on R defined by $T = |\mathbf{T}|$ will be called the **shear stress field**.

A deformation u will be called a **single phase** deformation if $u \in C^2(R)$. It will be called a **multiphase** deformation if

(a) $u \in C(R)$, and

(b) There is a set (empty, finite, or infinite) of smooth curves Γ_i, $i = 1, 2, \ldots, N$ in R which partition R into open subregions R_i such that (1) the restriction of u to any

R_i is in $C^2(R_i)$, and (2) $\Gamma_1 \cup \Gamma_2 \cup \ldots \cup \Gamma_N$ is the set of all points in R at which ∇u is discontinuous.

Each curve Γ_i will be called a **shock**. Define $\Gamma = \Gamma_1 \cup \Gamma_2 \cup \ldots \cup \Gamma_N$. The regions R_i will be called **phases**.

A stress vector field will be called **equilibrated** if for every simple closed curve C in R,

$$\int_C \mathbf{T} \cdot \mathbf{n} ds = 0 \tag{10.2}$$

where $\mathbf{n}$ is the outward-directed unit vector normal to C and s denotes arc length. It will be assumed throughout this work that there are no body forces. Cauchy's theorem shows that if $\mathbf{T}$ is equilibrated, and if $\mathbf{x}$ is an interior point of R at which $\mathbf{T}$ is differentiable, then

$$\nabla \cdot \mathbf{T}(\mathbf{x}) = \mathbf{0} \tag{10.3}$$

or equivalently

$$\frac{\partial T_1}{\partial x_1}(\mathbf{x}) + \frac{\partial T_2}{\partial x_2}(\mathbf{x}) = 0 \tag{10.4}$$

This work will be concerned exclusively with homogeneous, isotropic, hyperelastic bodies whose constitutive relations in terms of the stress vector field may be written as

$$\mathbf{T}(\mathbf{x}) = \mathbf{h}(\nabla u(\mathbf{x})) = \begin{cases} \mathbf{0}, & k(\mathbf{x}) = \mathbf{0} \\ \tau(k(\mathbf{x}))\nabla u(\mathbf{x})/k(\mathbf{x}), & k(\mathbf{x}) \neq \mathbf{0} \end{cases} \tag{10.5}$$

where τ is a continuous and piecewise continuously differentiable nonnegative scalar-valued function on $[0, \infty)$ such that $\tau(0) = 0$. $\mathbf{h}$ will be called the **constitutive relation**, and τ will be called the **stress-strain relation**.

One special class of materials of this type consists of the *generalized neo-Hookean* materials. For these materials the strain energy density is a function of the trace of the Green strain tensor only. In anti-plane shear, this means that the strain energy density may be expressed as $w(k)$ where $w \in C^2([0, \infty))$. The stress-strain relation is computed from w by

$$\tau(k) = w'(k), \qquad k \geq 0. \tag{10.6}$$

The equilibrium equation (10.3) may be locally elliptic, parabolic, or hyperbolic depending on the material and the deformation. Knowles [3] shows that the type is established from the local slope of the stress-strain relation as follows:

$$\begin{aligned} \tau' > 0 &\iff \text{elliptic} \\ \tau' = 0 &\iff \text{parabolic} \\ \tau' < 0 &\iff \text{hyperbolic} \end{aligned} \tag{10.7}$$

Since $\mathbf{h}$ is a continuous function, the definition of a multiphase deformation requires that the following limits exist at a point $\mathbf{a}$ on a shock separating subregions R^+ and R^-:

$$\mathbf{T}^+(\mathbf{a}) = \lim_{\substack{\mathbf{x}\to\mathbf{a} \\ \mathbf{x}\in R^+}} \mathbf{T}(\mathbf{x}) \quad \text{and} \quad \mathbf{T}^-(\mathbf{a}) = \lim_{\substack{\mathbf{x}\to\mathbf{a} \\ \mathbf{x}\in R^-}} \mathbf{T}(\mathbf{x}) \tag{10.8}$$

If $\mathbf{T}$ is equilibrated, then (10.2) implies the **traction jump condition**,

$$\mathbf{T}^+(\mathbf{a})\cdot\mathbf{n} = \mathbf{T}^-(\mathbf{a})\cdot\mathbf{n} \tag{10.9}$$

where $\mathbf{n}$ is the unit vector normal to Γ at $\mathbf{a}$ directed into R^+.

If u is a multiphase deformation, and if (10.3) holds in the interiors of the phases while (10.9) holds on the shocks, then u is equilibrated.

Defining

$$u^+(\mathbf{a}) = \lim_{\substack{\mathbf{x}\to\mathbf{a} \\ \mathbf{x}\in R^+}} u(\mathbf{x}) \quad \text{and} \quad u^-(\mathbf{a}) = \lim_{\substack{\mathbf{x}\to\mathbf{a} \\ \mathbf{x}\in R^-}} u(\mathbf{x}) \tag{10.10}$$

and using the required continuity of u yields the **displacement jump condition**,

$$u^+(\mathbf{a}) = u^-(\mathbf{a}). \tag{10.11}$$

Suppose one defines the coordinate system so that the origin is at a point $\mathbf{b}$ on Γ, the x_1-axis is tangent to Γ at $\mathbf{b}$, and the positive x_2-axis extends into R^+ (see Figure 10.1). Since (10.11) must hold at any $\mathbf{a}$ on Γ, differentiation of it shows

$$\frac{\partial u^+}{\partial x_1}(\mathbf{b}) = \frac{\partial u^-}{\partial x_1}(\mathbf{b}). \tag{10.12}$$

Also (10.9) implies $T_2^+(\mathbf{b}) = T_2^-(\mathbf{b})$. The constitutive relation (10.5) shows that $\mathbf{h}$ is **direction preserving**, *i.e.*, that ∇u and $\mathbf{T}$ have the same directions. Then one can unambiguously define R^+ and R^- as the sides such that $k^+(\mathbf{b}) \geq k^-(\mathbf{b})$. Referring to Figure 10.1, it is clear that since $\nabla u^+(\mathbf{b})$ and $\nabla u^-(\mathbf{b})$ have same x_1-component, and since $\mathbf{T}^+(\mathbf{b})$ and $\mathbf{T}^-(\mathbf{b})$ have the same x_2-component, $T^+(\mathbf{b}) \leq T^-(\mathbf{b})$. The following result therefore holds, and may be proved rigorously:

PROPOSITION 10.1. Let u be an equilibrated multiphase deformation. Let $\mathbf{b}$ be a point on Γ separating subregions R^+ and R^-. Let $k^+(\mathbf{b})$ and $k^-(\mathbf{b})$ be the limiting values of k at $\mathbf{b}$, where $k^+(\mathbf{b}) \geq k^-(\mathbf{b})$. Then $T^+(\mathbf{b}) \leq T^-(\mathbf{b})$.

10.2 Stability and the Maxwell relation

Let $\mathbf{h}$ now be the constitutive relation of what will be called here a **nonmonotone** material, as shown in Figure 10.2:

$$\begin{aligned} \tau'(k) &>0, \quad 0 \leq k < K^- \\ \tau'(k) &<0, \quad K^- < k < K^+ \\ \tau'(k) &>0, \quad K^+ < k \end{aligned} \tag{10.13}$$

where K^+ and K^- are positive constants, $K^- < K^+$.

For at least two reasonable notions of stability, equilibrated deformations which contain some $\mathbf{x}$ such that $\tau'(k(\mathbf{x})) < 0$ are unstable. They are *infinitesimally* unstable in the sense of Pearson [4], meaning that their potential energy is reduced by some small perturbation. They also do not possess *strong ellipticity* [3], with the consequence that a small plane wave in the vicinity of $\mathbf{x}$ would grow unboundedly in time, assuming the same constitutive behavior in the dynamic case as in the equilibrium case. So, when attempting to solve boundary value problems, there is good reason to exclude the descending branch of the stress-strain relation. For the remainder of this paper it will be required that if $\mathbf{x}$ is any point at which a deformation u is differentiable, then $\tau'(k(\mathbf{x})) \geq 0$.

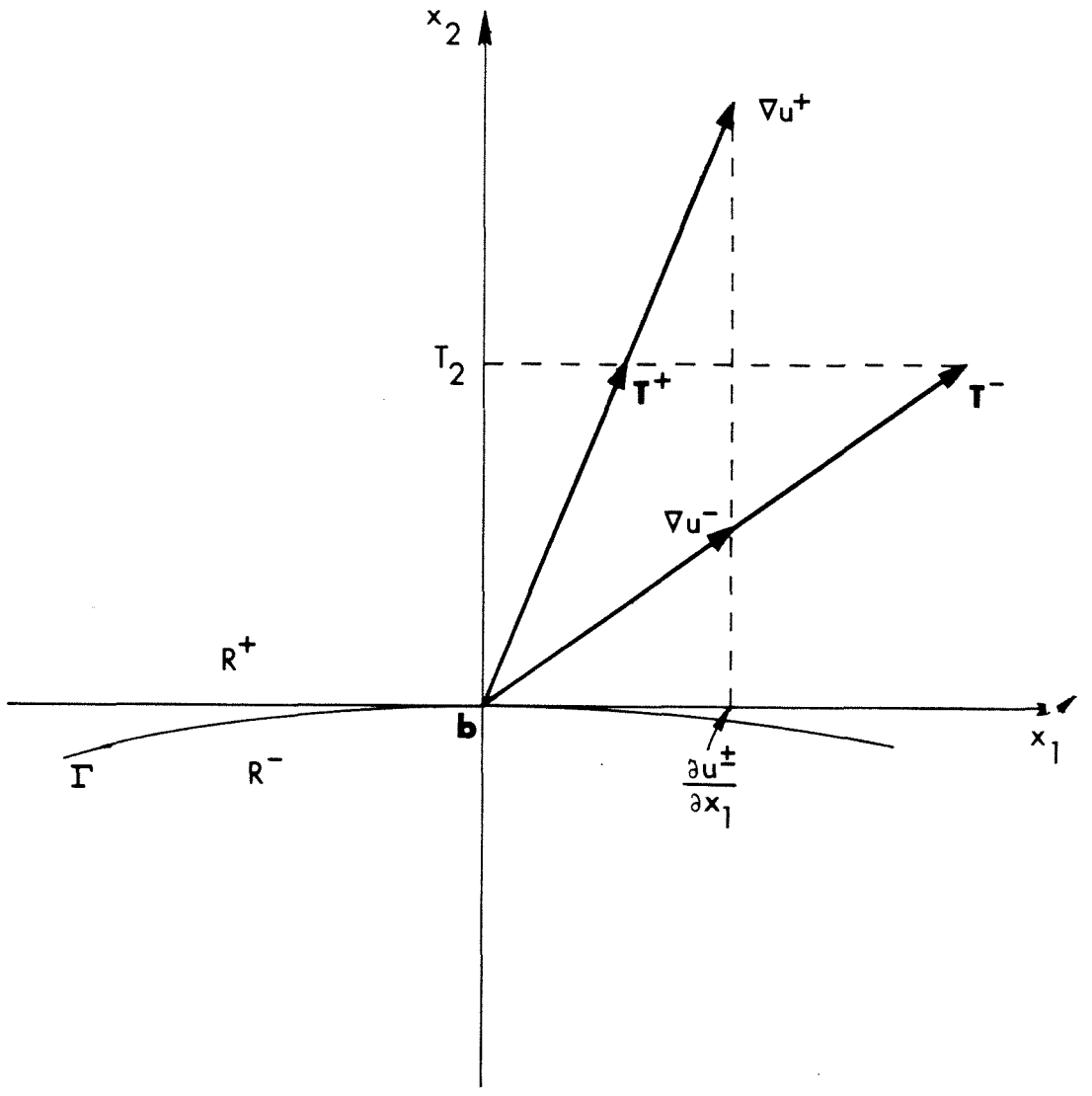

Figure 10.1. Vectors associated with limiting values on a shock.

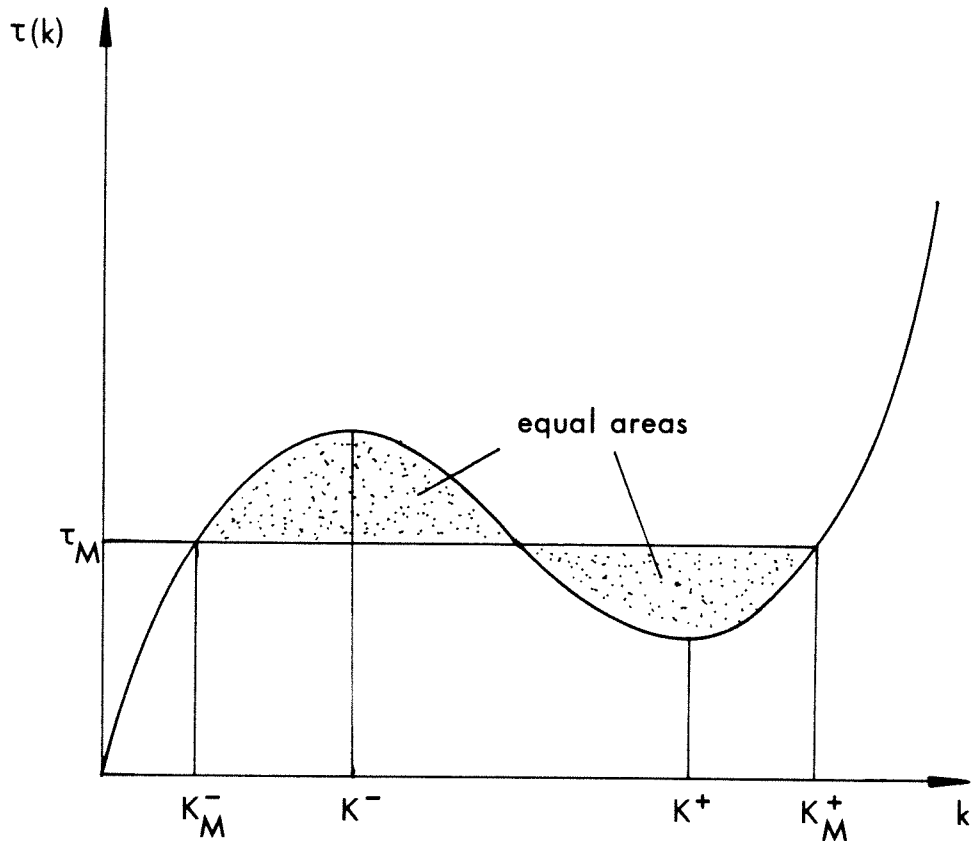

Figure 10.2. Stress-strain relation for a nonmonotone material.

Even after so excluding the descending branch, the stress-strain relation is not uniquely invertible. It is this lack of invertibility that gives rise to multiphase equilibrated deformations, since k can jump from one branch to the other across a shock while the traction on the shock remains continuous.

If u is a multiphase equilibrated deformation of a nonmonotone material, then Γ partitions R into **low-strain phase** R^- in which $k \leq K^-$ and a **high-strain phase** R^+ in which $k \geq K^+$. In this case the multiphase deformation will be called a **two-phase** deformation.

Ericksen [5] found that in simple bar problems, if points on both branches are present simultaneously in an equilibrated two-phase deformation that minimizes potential energy, then the stress in the bar is necessarily equal to τ_M, the **Maxwell stress** for the material. τ_M is the unique value such that there are two numbers K_M^- and K_M^+ with the properties

$$\tau_M = \tau(K_M^+) = \tau(K_M^-) \tag{10.14}$$

and

$$w(K_M^+) - w(K_M^-) = (K_M^+ - K_M^-)\tau_M. \tag{10.15}$$

The important role of the Maxwell stress has been explored extensively by other authors. Gurtin [6], generalizing work by James [7], has shown that at in an equilibrated deformation which is a *local minimizer* of potential energy, the **Maxwell relation** holds on the shocks:

$$w(k^+) - w(k^-) = (k^+ - k^-)\tau(k^\pm) \quad \text{on } \Gamma, \tag{10.16a}$$

or equivalently (in view of the jump conditions)

$$\mathbf{T}^+ = \mathbf{T}^- = \tau_M \mathbf{n} \quad \text{on } \Gamma \tag{10.16b}$$

where $\mathbf{n}$ is the unit vector normal to Γ directed into R^+. The term *local minimizer* means that the deformation minimizes potential energy with respect to variations that

have sufficiently small displacements. If u is a local minimizer of potential energy, it also follows that

$$k \leq K_M^- \text{ on } R^- \quad \text{and} \quad k \geq K_M^+ \text{ on } R^+ \tag{10.17a}$$

or equivalently

$$T \leq \tau_M \text{ on } R^- \quad \text{and} \quad T \geq \tau_M \text{ on } R^+. \tag{10.17b}$$

(10.17) follow from the localization theorem of Gurtin [6], and can also be proved by other means. The importance of the Maxwell relation motivates the following definition:

DEFINITION. Let u be an equilibrated two-phase deformation. u is **Maxwell-stable** or **M-stable** if (10.16) and (10.17) hold. u is **Maxwell-unstable** or **M-unstable** otherwise.

The main reason for introducing the notion of Maxwell-stability as an idea distinct from local stability is that we wish to study it in a mechanical setting rather than a variational setting. This will allow discussion of unbounded regions, which are problematic when minimization of potential energy is sought. Also, since the Maxwell relation is a necessary but not sufficient condition for local stability, the question of whether or not a deformation satisfies Maxwell-stability is more clear-cut than the question of local stability. (In particular, Maxwell-stability is unrelated to the boundary conditions for a problem.)

Let an equilibrated two-phase deformation u be Maxwell-stable. As consequences of (10.16) and the displacement jump condition (10.11) it follows

$$u = u_i = \text{constant} \quad \text{on } \Gamma_i, \quad i = 1, 2, \ldots, N, \tag{10.18}$$

and

$$\tau(k^{\pm}) = \tau(k^+) = \tau(k^-) = \tau_M \quad \text{on } \Gamma, \tag{10.19a}$$

or equivalently

$$k^+ = K_M^+ \quad \text{on } \Gamma, \qquad k^- = K_M^- \quad \text{on } \Gamma. \tag{10.19b}$$

Note that (10.18) and (10.19) together imply (10.16).

Equation (10.18) means that any shock Γ_i is a *normal shock*, *i.e.*, the vectors shown in Figure 10.1 are all normal to Γ_i.

Note that if a deformation is a local minimizer of potential energy, then it is Maxwell-stable. However, the converse of this statement is *not* true.

There is some experimental evidence that Maxwell-unstable deformations are of physical importance. James, for example, interprets the nature of shape-memory alloys in terms of Maxwell-unstable elastic behavior [8]. Yield phenomena such as Luders bands, which are frequently observed in certain metals, are generally explained in terms of plastic behavior that strongly resembles Maxwell-unstable behavior in the elastic material considered here [9]. Also, a numerical model of a boundary value problem involving phase changes typically predicts a Maxwell-unstable deformation as an approximation to some presumably locally stable exact solution.

Chapter 11. Trilinear material

The trilinear material represents a prototype of the nonmonotone material introduced in Chapter 10. Its constitutive relation is given by

$$\mathbf{h}_{\triangleleft}(\mathbf{v}) = \begin{cases} \mathbf{0}, & \mathbf{v} = \mathbf{0} \\ \tau_{\triangleleft}(|\mathbf{v}|)\mathbf{v}/|\mathbf{v}|, & \mathbf{v} \neq \mathbf{0} \end{cases} \tag{11.1}$$

where

$$\tau_{\triangleleft}(k) = \begin{cases} \mu^- k, & 0 \leq k \leq K^- \\ \mu^- K^- + (k - K^-)\frac{\mu^+ K^+ - \mu^- K^-}{K^+ - K^-}, & K^- \leq k \leq K^+ \\ \mu^+ k, & K+ \leq k \end{cases} \tag{11.2}$$

and where K^+, K^-, μ^+, and μ^- are positive constants such that $K^- < K^+$, $\mu^- > \mu^+$, and $\mu^- K^- > \mu^+ K^+$. (See Figure 11.1.) Note that the high-strain branch in (11.2) lies on a line directed through the origin.

A strain energy density for the trilinear material is given by

$$w_{\triangleleft}(k) = \begin{cases} \frac{\mu^- k^2}{2}, & 0 \leq k \leq K^- \\ \frac{\mu^- K^{-2}}{2} + (k - K^-)\left[\mu^- K^- + \frac{1}{2}(k - K^-)\frac{\mu^+ K^+ - \mu^- K^-}{K^+ - K^-}\right], & K^- \leq k \leq K^+ \\ \frac{\mu^- K^{-2}}{2} + \frac{K^+ - K^-}{2}(\mu^+ K^+ + \mu^- K^-) + \frac{\mu^+}{2}\left(k^2 - K^{+2}\right), & K^+ \leq k \end{cases} \tag{11.3}$$

The Maxwell stress is

$$\tau_M = \sqrt{\mu^+ \mu^- K^+ K^-} \tag{11.4}$$

and the associated shears are

$$K_M^- = \sqrt{\frac{\mu^+ K^+ K^-}{\mu^-}} \quad \text{and} \quad K_M^+ = \sqrt{\frac{\mu^- K^+ K^-}{\mu^+}} \tag{11.5}$$

Let Γ be a shock separating the phases R^+ and R^-. The equilibrium equation in terms of displacement takes a particularly simple form for the trilinear material. Setting $\mathbf{T}(\mathbf{x}) = \mathbf{h}_{\triangleleft}(\nabla u(\mathbf{x}))$ in (10.3) yields

$$\Delta u = 0 \text{ on } R^+ \quad \text{on} \quad \Delta u = 0 \text{ on } R^- \tag{11.6}$$

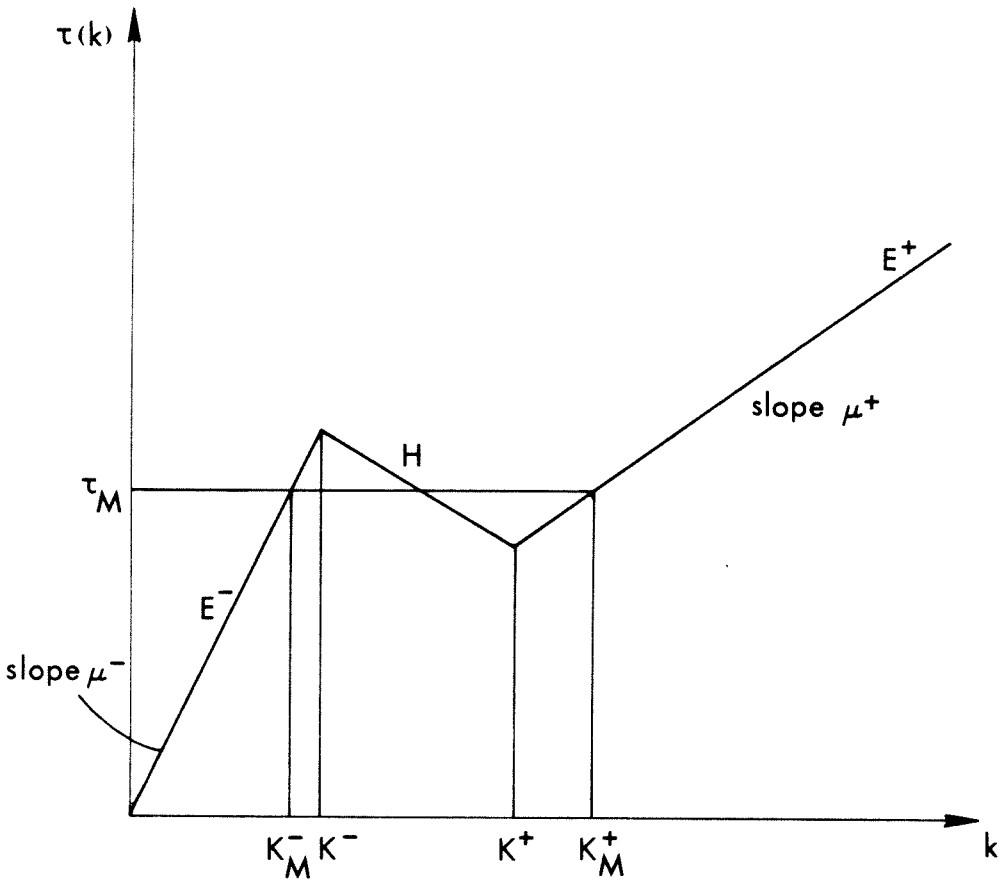

Figure 11.1. Stress-strain relation for the trilinear material.

where Δ is the Laplacian operator, $\Delta = \nabla \cdot \nabla$.

Letting $\partial u^+/\partial n$ and $\partial u^-/\partial n$ denote the limiting values of $\nabla u \cdot \mathbf{n}$ as Γ is approached, the traction jump condition for the trilinear material is

$$\mu^+ \frac{\partial u^+}{\partial n} = \mu^- \frac{\partial u^-}{\partial n} \quad \text{on } \Gamma. \tag{11.7}$$

If the deformation is M-stable as well as equilibrated, then the quantity in (11.7) also equals τ_M.

Chapter 12. M-stable deformations of the trilinear material

Suppose u is a two-phase deformation of a trilinear body occupying R and $\mathbf{T}$ is the associated stress vector field. Let R^- and R^+ be the low-strain and high-strain phases respectively. Let u^- and u^+ be the restrictions of u to these regions, and let $\mathbf{T}^-$ and $\mathbf{T}^+$ be the restrictions of $\mathbf{T}$. Let Γ be the shocks. As discussed in the previous chapters, u is equilibrated and M-stable if and only if (12.1)–(12.3) hold:

$$\Delta u^- = 0 \quad \text{on } R^-, \qquad \Delta u^+ = 0 \quad \text{on } R^+ \tag{12.1}$$

$$T^- \leq \tau_M \quad \text{on } R^-, \qquad T^+ \geq \tau_M \quad \text{on } R^+, \tag{12.2}$$

$$\mathbf{T}^- = \mathbf{T}^+ = \tau_M \mathbf{n} \quad \text{on } \Gamma \tag{12.3}$$

where $\mathbf{n}$ is the unit vector normal to Γ directed into R^+. Equation (12.3) holds if and only if (12.4) and (12.5) hold:

$$\mu^- \frac{\partial u^-}{\partial n} = \mu^+ \frac{\partial u^+}{\partial n} = \tau_M \quad \text{on } \Gamma, \tag{12.4}$$

$$u^- = u^+ = u_i = \text{constant} \quad \text{on } \Gamma, \quad i = 1, 2, \ldots, N. \tag{12.5}$$

The main result of this chapter will be that infinitely many M-stable two-phase deformations are possible, but they are solutions to only a very limited class of boundary value problems. The results of this chapter apply only to the trilinear material.

12.1 The most general M-stable deformation

It will be shown here that any M-stable two-phase deformation (the phrase "two-phase" will hereafter be omitted for brevity) is equivalent to a piecewise homogeneous deformation under a certain conformal mapping. This equivalence provides a recipe for constructing an infinite number of M-stable deformations.

Suppose that the deformation u defined above is M-stable. Let (X_1, X_2) be any fixed point in R. Because of its lack of smoothness, the displacement field u is awkward

to deal with directly. It is therefore convenient to define a new field ϕ which is essentially the same as the displacement field, but which will be shown to have more smoothness. Define this scalar field ϕ on R by the path-independent line integral

$$\phi(x_1,x_2) = \int_{(X_1,X_2)}^{(x_1,x_2)} \frac{\mu(\xi,\eta)}{\tau_M}\Big[\frac{\partial u}{\partial \xi}(\xi,\eta)d\xi + \frac{\partial u}{\partial \eta}(\xi,\eta)d\eta\Big], \qquad (x_1,x_2)\in R \qquad (12.6)$$

where μ is the scalar function on R defined by

$$\mu(x_1,x_2) = \begin{cases} \mu^+, & (x_1,x_2)\in R^+ \\ \mu^-, & (x_1,x_2)\in R - R^+. \end{cases} \qquad (12.7)$$

The path-independence of the above line integral follows from the fact that u is constant along the shocks. The inverse of the transformation in (12.6) is supplied by the path-independent integral

$$u(x_1,x_2) = u(X_1,X_2) + \int_{(X_1,X_2)}^{(x_1,x_2)} \frac{\tau_M}{\mu(\xi,\eta)}\Big[\frac{\partial \phi}{\partial \xi}(\xi,\eta)d\xi + \frac{\partial \phi}{\partial \eta}(\xi,\eta)d\eta\Big], \qquad (x_1,x_2)\in R. \qquad (12.8)$$

Observing that

$$\partial\phi/\partial x_1 = T_1/\tau_M, \qquad \partial\phi/\partial x_2 = T_2/\tau_M \qquad (12.9)$$

and using (12.3) shows that ϕ is continuously differentiable on the shocks. Thus ϕ is harmonic on all of R because u is harmonic on the individual phases. Since ϕ is harmonic on R, it follows that $\phi\in C^\infty(R)$.

Let ψ be a harmonic conjugate of ϕ on R, and let $\varsigma = \phi + i\psi$ be the associated analytic function of the complex variable $z = x_1 + ix_2$. Now consider the mapping that this function provides from the $z-$plane into the $\varsigma-$plane. Let $R_* = \varsigma(R)$. The requirement that u be constant on each shock Γ_i means that the image $\varsigma(\Gamma_i)$ is a vertical line (see Figure 12.1).

The mapping $\varsigma(z)$ is not necessarily one-to-one, since various parts of R could have images that overlap in the $\varsigma-$plane. However, the inverse mapping $z(\varsigma)$ may be rendered single-valued by regarding it as a function on a generalized region in which one specifies

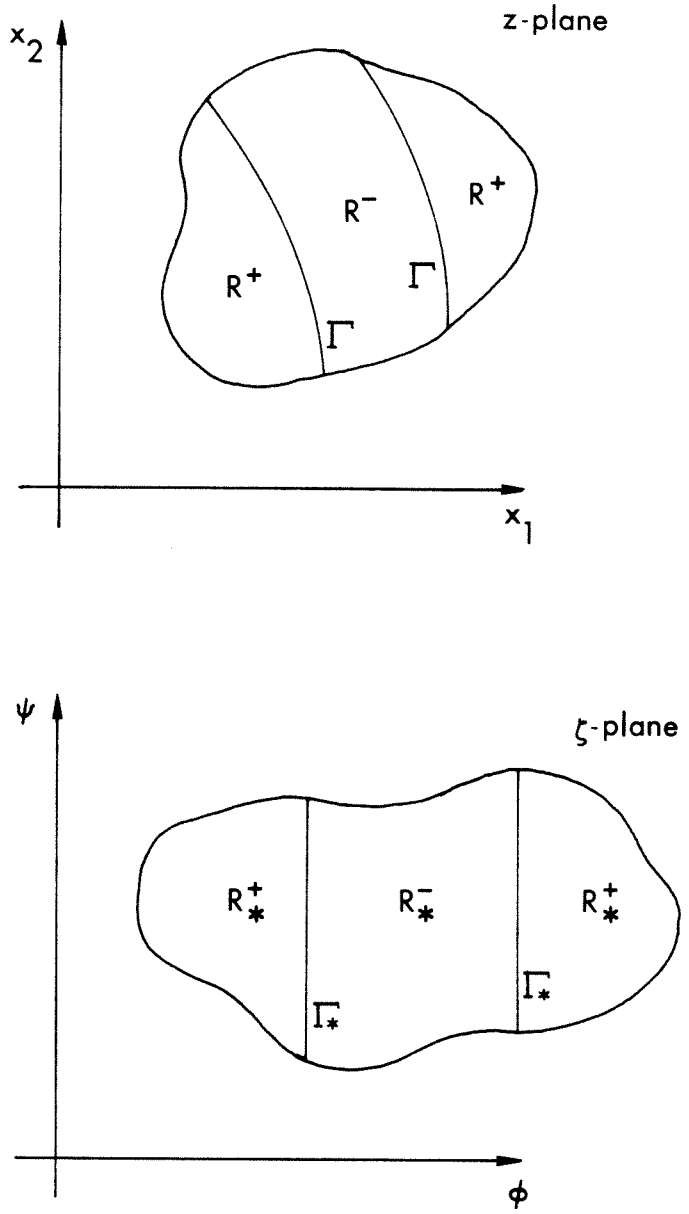

Figure 12.1. Deformation in z- and ζ-planes.

a particular Riemann sheet when evaluating the function at any point [10]. Keeping this possibility in mind, the issue of single-valuedness of the inverse mapping will not be discussed further.

The derivative of the inverse mapping, $dz/d\varsigma$, cannot have zeroes in R_* since such points would correspond to points at which the stress vector field is irregular, contrary to assumption. It can, however, have isolated singularities. Therefore the inverse mapping $z(\varsigma)$ is *conformal* at all points of R_* except for these singularities.

Suppose one treats ϕ and ψ like physical coordinates. By applying the inverse transformation in (12.8) to a field on R_* whose value equals ϕ at any point (ϕ, ψ), it may be seen that the displacement field u_* derived in this manner is the piecewise homogeneous deformation found by the following path-independent line integral:

$$u_*(\phi,\psi) = \int_{(\Phi,\Psi)}^{(\phi,\psi)} \frac{\tau_M}{\mu_*(\xi,\eta)} d\xi, \qquad (\phi,\psi) \in R_* \tag{12.10}$$

where

$$\mu_*\left(\phi(x_1,x_2)\right), \psi(x_1,x_2)) = \mu(x_1,x_2), \qquad (x_1,x_2) \in R$$

and (Φ, Ψ) is an arbitrary point in R_*.

Moreover, the analogues of (12.9) for the (ϕ, ψ) coordinates imply that the stress vector component fields associated with u_* are simply

$$T_{*\phi} = \tau_M, \qquad T_{*\psi} = 0 \quad \text{on } R_*. \tag{12.11}$$

So, by the M-stability criteria (12.2)–(12.3), u_* is an *M-stable* piecewise homogeneous deformation.

One other property of the inverse mapping $z(\varsigma)$ will be important. Since (12.9) shows that $T = \tau_M |d\varsigma/dz|$ at any regular point of the deformation, the M-stability requirements (12.2) and (12.3) are equivalent to

$$|d\varsigma/dz| \le 1 \quad \text{on } R^-, \quad |d\varsigma/dz| = 1 \quad \text{on } \Gamma, \quad 1 \le |d\varsigma/dz| < \infty \quad \text{on } R^+. \tag{12.12}$$

Let $R_*^- = \varsigma(R^-)$, $R_*^+ = \varsigma(R^+)$, $\Gamma_* = \varsigma(\Gamma)$. Then (12.12) implies

$$|dz/d\varsigma| \geq 1 \quad \text{on } R_*^-, \quad |dz/d\varsigma| = 1 \quad \text{on } \Gamma_*, \quad 1 \geq |dz/d\varsigma| > 0 \quad \text{on } R_*^+. \tag{12.13}$$

Thus the inverse mapping is *length-preserving* on Γ_*.

The above results are summarized in the following proposition:

PROPOSITION 12.1. Let u be an M-stable deformation on a region R. Then there is a generalized region R_*, a piecewise homogeneous deformation u_* on R_*, and a one-to-one mapping z on R_* such that

(a) z is conformal on R_* except possibly at isolated singularities,

(b) z satisfies (12.13),

(c) $R = z(R_*)$,

(d) $u(z(\varsigma)) = u_*(\varsigma), \quad \varsigma \in R_*$.

The following converse to the above proposition also holds:

PROPOSITION 12.2. If u_* is any M-stable piecewise homogeneous deformation of a generalized region R_*, and z is a one-to-one mapping on R_* satisfying (a) and (b) of Proposition 12.1, then the deformation u on R defined by (c) and (d) of Proposition 12.1 is an M-stable deformation.

Proposition 12.2 may be verified by reversing the arguments that led to the properties of $z(\varsigma)$ above.

One can now write down the most general M-stable deformation. Let u_* and R_* be as stated in the propositions. (12.13) and the properties of the exponential function imply that without loss of generality the mapping $z(\varsigma)$ may be written

$$z(\varsigma) = \int_{\varsigma_0}^{\varsigma} e^{if(\sigma)} d\sigma, \qquad \varsigma \in R_* \tag{12.14}$$

where ς_0 is an arbitrary fixed point in R_*, f is an analytic function on R_* (except for isolated singularities) such that

$$\text{Im } f \leq 0 \quad \text{on } R_*^-, \quad \text{Im } f = 0 \quad \text{on } \Gamma_*, \quad \text{Im } f \geq 0 \quad \text{on } R_*^+, \tag{12.15}$$

and such that the resulting z is one-to-one. Then the deformation supplied by applying (c) and (d) of Proposition 12.1 tp (12.14) is an M-stable deformation. Moreover, the propositions show that *any* M-stable deformation may be generated in this manner.

EXAMPLE 12.1. Let

$$R_*^+ = \{\phi + i\psi | \phi \leq 0,\ |\psi| \leq \pi\},$$

$$R_*^- = \{\phi + i\psi | \phi \geq 0,\ |\psi| \leq \pi\},$$

$$\Gamma_* = \{i\psi | |\psi| \leq \pi\},$$

$$f(\varsigma) = \varsigma/i.$$

(see Figure 12.2). Then (12.14) leads to

$$z(\varsigma) = e^{\phi + i\psi} + z_0$$

where $z_0 = x_{01} + ix_{02}$ is an arbitrary point. Thus Γ is the unit circle centered at z_0, R^+ is the punctured interior of this circle, and R^- is the exterior of this circle. A simple calculation yields $\phi = \ln|z - z_0|$. Applying the inverse transformation (12.8) then shows

$$u(x_1, x_2) = \begin{cases} (\tau_M \ln r)/\mu^+ + u_0, & 0 < r \leq 1 \\ (\tau_M \ln r)/\mu^- + u_0, & 1 \leq r \end{cases}$$

where $r = \sqrt{(x_1 - x_{01})^2 + (x_2 - x_{02})^2}$ and u_0 is an arbitrary real constant. This deformation corresponds to a concentrated load of magnitude $2\pi\tau_M$ applied into the plane at point (x_{01}, x_{02}).

The following example demonstrates why R_* may be a *generalized* region and illustrates a mapping z which contains a singularity.

EXAMPLE 12.2. Let r_* and θ_* be polar coordinates in the ς−plane. Let $R_* \equiv R_*^-$ be the circle of radius 1/9 centered at the origin, together with its interior. (12.10) shows that $u_*(\phi, \psi) = \tau_M \phi/\mu^-$. Let

$$z(\varsigma) = \varsigma^{1/2} = \sqrt{r_*} e^{i\theta_*/2}, \quad 0 \leq \theta_* < 4\pi,\ 0 \leq r_* \leq 1/9.$$

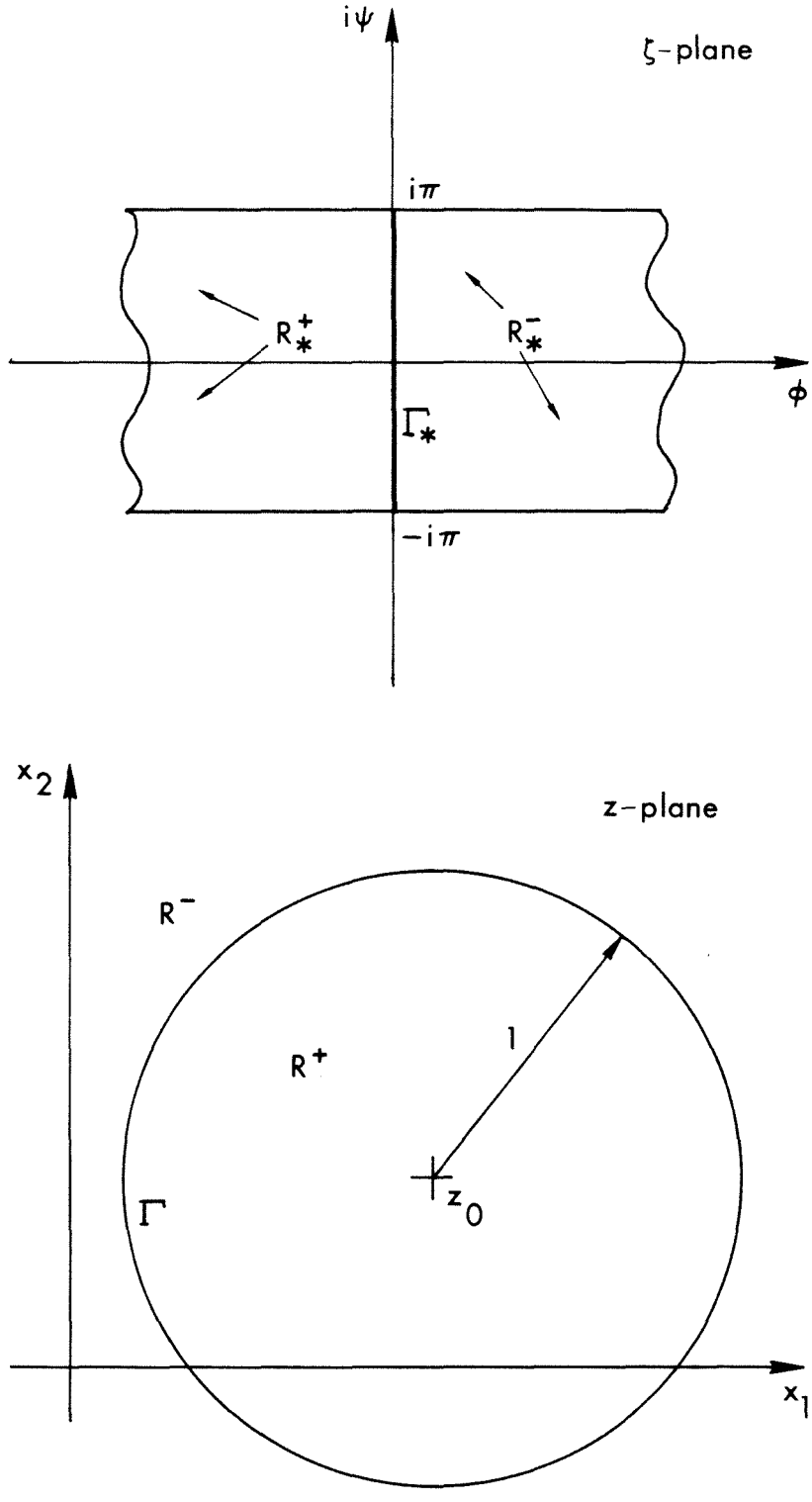

Figure 12.2. Deformation in Example 12.1 in ς- and z-planes.

There are two Riemann surfaces in R_* which are accessed by the interval $0 \leq \theta_* < 4\pi$. Calculation gives the following deformation in the $z-$plane:

$$u(x_1, x_2) = \frac{\tau_M}{\mu^-}(x_1^2 - x_2^2).$$

Also $|dz/d\zeta| = 1/(2\sqrt{r_*}) \geq 3/2$, so the first of (12.13) is satisfied. Note that $dz/d\zeta$ has a singularity at the origin which corresponds to a point at which $|\nabla u| = 0$ in the $z-$plane.

A consequence of Proposition 12.1 is that in an M-stable deformation shocks cannot intersect. This follows from an asymptotic analysis of the mapping $z(\zeta)$ in the vicinity of such an intersection. Near an intersection, $z \sim \zeta^\alpha$, with α a real constant, $0 < \alpha < 1$. This is clearly inconsistent with the requirement that z be length-preserving on the shocks.

Similarly, shocks cannot have endpoints in the interior of an M-stable deformation.

12.2 Traction boundary value problem

The above discussion showed that any M-stable deformation of the trilinear material is obtainable by a conformal mapping of an M-stable piecewise homogeneous deformation. This suggests that M-stable deformations are of a special nature, and it is not to be expected that an arbitrary boundary value problem will have this kind of deformation as a solution. It will now be shown that for a given traction boundary value problem one can detect whether or not an M-stable solution exists. Those problems for which such a solution does exist will turn out to be a very limited class.

First the role of ϕ as a stress potential will be examined, and it will be shown that a traction boundary value problem has a unique stress field for all M-stable solutions (if any exist).

DEFINITION. A **traction boundary value problem** consists of a region R, whose boundary will be called ∂R, and a given traction field $S \in C^1(\partial R)$ such that $\int_{\partial R} S ds = 0$. A **solution** to such a problem is an equilibrated, multiphase deformation u with

associated stress vector field $\mathbf{T}$ such that $\mathbf{T} \cdot \mathbf{n} = S$ on ∂R where $\mathbf{n}$ is the outward-directed unit vector normal to ∂R.

Equations (12.9) show that the field ϕ defined in (12.6) may be used as a stress potential in an M-stable deformation. Thus the problem of finding the stress vector field associated with an M-stable solution to a traction boundary value problem is equivalent to the following Neumann problem:

$$\Delta\phi = 0 \quad \text{on } R, \quad \partial\phi/\partial n = S/\tau_M \quad \text{on } \partial R. \tag{12.16}$$

We will restrict our attention to those traction boundary value problems whose associated Neumann problems (12.16) have solutions. It is well-known that such solutions are unique except for an arbitrary additive constant. This immediately proves the following result:

PROPOSITION 12.3. Let u and u' be M-stable solutions to a traction boundary value problem, and let their respective stress vector fields be $\mathbf{T}$ and $\mathbf{T}'$. Then $\mathbf{T} = \mathbf{T}'$.

Another consequence of the role of ϕ as a stress potential is that $\mathbf{T} \in C^\infty(R)$. This follows because, as has been shown above, $\phi \in C^\infty(R)$.

Having established a uniqueness result for M-stable solutions of a traction boundary value problem, let us turn to the question of *existence* of such solutions. Let such a problem be given. Suppose temporarily that an M-stable solution u exists. If the stress vector component fields associated with u are not identically equal to constants, the implicit function theorem assures that the condition $|\nabla\phi| = 1$ defines a set of curves, which will be called Γ_i, $i = 1, 2, \ldots, N$. (This set may be empty, finite, or infinite.)

It will now be shown that these curves are shocks, *i.e.*, they are the boundaries between different phases. To prove this, it is sufficient to show that a point P in the interior of R which lies on any Γ_i is not an extremum point of the scalar field $|\nabla\phi|$. Recall that $|\nabla\phi| = |d\varsigma/dz|$. Applying the maximum modulus theorem to the analytic

function $d\zeta/dz$ shows that P cannot be a maximum. Applying it to $(d\zeta/dz)^{-1}$ shows that P cannot be a minimum. So P is not an extremum of $|\nabla\phi|$, and therefore the Γ_i are shocks. Also, (12.2) shows that the Γ_i represent the *totality* of all shocks.

Recall also that as a consequence of M-stability u is constant on any shock. Therefore ϕ is constant on any shock. Thus a *necessary* condition for a traction boundary value problem to have an M-stable solution is that ϕ be constant on all curves such that $|\nabla\phi| = 1$. With a view toward showing that this is also a *sufficient* condition, note that a ϕ field which satisfies the Neumann problem (12.16) always exists regardless of whether an M-stable deformation which generates this ϕ field exists.

No longer assuming that an M-stable solution exists, let ϕ be a solution to the Neumann problem. Suppose that ϕ is constant on all curves such that $|\nabla\phi| = 1$, and call these curves Γ_i, $i = 1, 2, \ldots, N$. In this case the integral in the inverse transformation (12.8) is path-independent provided (12.7) is replaced by

$$\mu(x_1, x_2) = \begin{cases} \mu^+, & |\nabla\phi(x_1, x_2)| > 1 \\ \mu^-, & |\nabla\phi(x_1, x_2)| \leq 1 \end{cases} \qquad (x_1, x_2) \in R. \tag{12.17}$$

Let u be the field defined in this manner.

Evaluation of the partial derivatives of u using (12.8) shows that (12.1) is satisfied at all regular points of R. The same argument used above to show that the Γ_i are shocks applies again here, with the consequence that (12.2) is satisfied. (12.3) is satisfied because ϕ is constant on the shocks and because $|\nabla\phi| = 1$ there. Thus u is an M-stable deformation. Also, u satisfies the traction boundary conditions because it was derived from a stress potential field which satisfies them. The following result has been proven:

PROPOSITION 12.4. Let a traction boundary value problem be given, and let ϕ be a solution to the associated Neumann problem (12.16). Then a necessary and sufficient condition for the boundary value problem to have an M-stable solution is that $\phi =$ constant on all curves such that $|\nabla\phi| = 1$.

The following example shows that not all traction boundary value problems have

M-stable solutions.

EXAMPLE 12.3. Let R be the unit circle together with its interior. Let a traction field on ∂R be given by $S(\theta) = 2\tau_M \sin 2\theta$, $0 \leq \theta < 2\pi$. The stress potential field which solves the Neumann problem (12.16) in this case is $\phi(x_1, x_2) = 2x_1x_2$. The curve along which $|\nabla\phi| = 1$ is the circle $r = 1/2$. But ϕ is constant only on the family of hyperbolas $x_2 = \phi/2x_1$. So the condition of Proposition 12.4 is not satisfied, and therefore there is no M-stable deformation which is a solution to this problem. Figure 12.3 shows a numerical solution to this problem. Only the wedge $0 \leq \theta \leq \pi/4$ is modeled. Each phase of the solution is shown in the figure as a different shade. Note the chaotic pattern of the phases near the x_1-axis, suggesting that this chaos may be a consequence of the nonexistence of an M-stable solution to the problem. (This is indeed the case, as will be shown later.)

Experience with problems of physical interest has shown that the class of traction boundary value problems which have M-stable solutions is very limited (although Proposition 12.2 shows that it is infinite). However, subsequent sections of this paper will show that if one generalizes the idea of a deformation to include fields with an infinitely fine mixture of the phases, then M-stability may be satisfied in general in spite of this result.

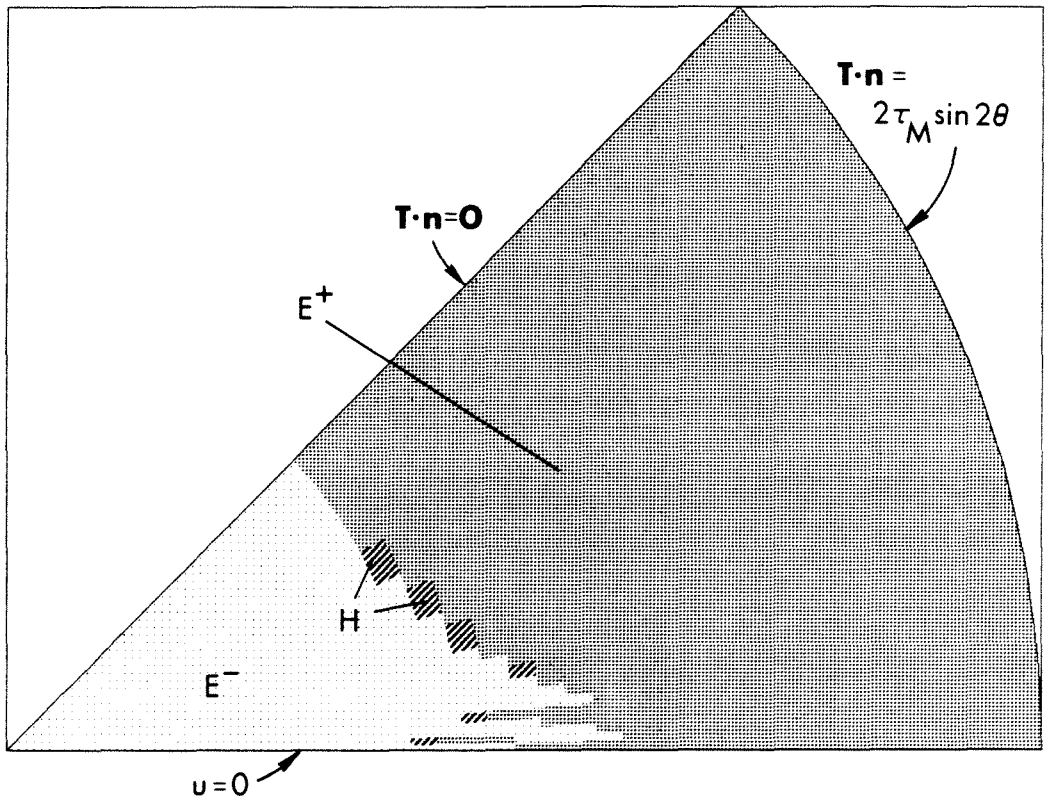

Figure 12.3. Numerical solution of Example 12.3.

Chapter 13. M-unstable deformations of the trilinear material

The previous section showed that M-stable deformations exist only as solutions to a special class of boundary value problems. The present chapter is concerned with the wider class of deformations which are M-unstable.

M-unstable deformations are amenable to conformal mapping techniques similar to those described in the previous section. However, these will not be examined here, since this paper is mainly concerned with M-stable deformations. M-unstable solutions will be discussed merely as a transition to *mixed* M-stable solutions, which will be dealt with in subsequent sections. The property of interest in this transition is the ability of shocks to intersect in M-unstable deformations.

As shown in the previous section, shocks never intersect in an M-stable deformation, a consequence of the fact that they are level curves of displacement. But shocks need not be level curves of displacement in an M-unstable deformation, so there is a possibility that shocks could intersect. It will be shown here that an asymptotic solution near such an intersection does exist in the M-unstable case. It will also be shown that such an intersection is necessarily in the shape of a cusp.

Let two shocks Γ and Γ' intersect at a point P, as shown in Figure 13.1. Assume that the phases R^- and R^+ occupy the regions to the left and the right of the shocks resepectively. For simplicity, assume that the x_1-axis is a line of anti-symmetry for the displacement field u, so that $u = 0$ there. Define a polar coordinate system centered at P by $x_1 = r\cos\theta$, $x_2 = r\sin\theta$, $r \geq 0$, $-\pi < \theta \leq \pi$. Let u^- and u^+ be the restrictions of u to R^- and R^+ respectively, and define fields k^- and k^+ on these phases by $k^- = |\nabla u^-|$ and $k^+ = |\nabla u^+|$.

The deformation u is an M-unstable equilibrated asymptotic solution to this problem if and only if (13.1)–(13.4) hold:

$$\Delta u^- = 0 \quad \text{on } R^-, \qquad \Delta u^+ = 0 \quad \text{on } R^+, \tag{13.1}$$

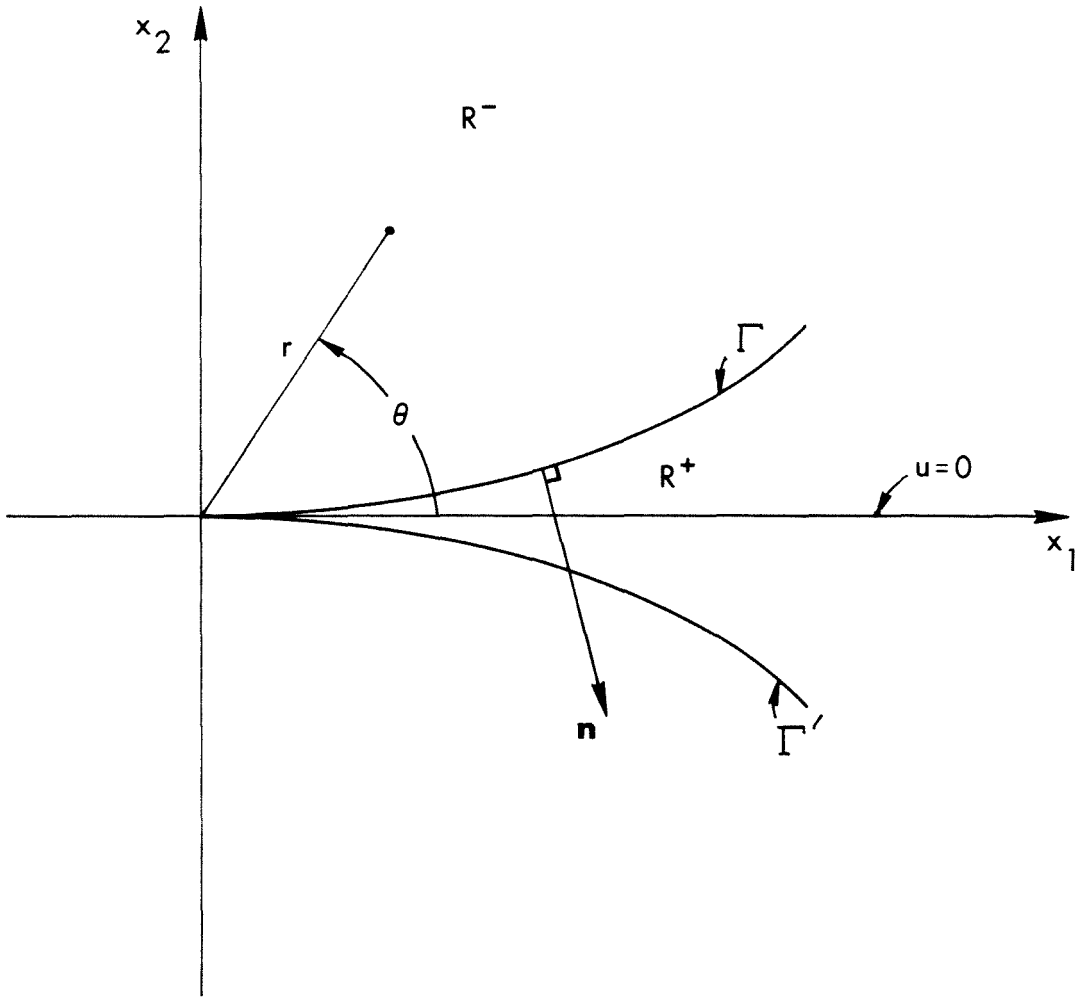

Figure 13.1. Intersection between two shocks.

$$\mu^- \frac{\partial u^-}{\partial n} \sim \mu^+ \frac{\partial u^+}{\partial n} \quad \text{on } \Gamma, \tag{13.2}$$

$$u^- \sim u^+ \quad \text{on } \Gamma, \tag{13.3}$$

$$k^- \leq K^- \quad \text{on } R^-, \quad k^+ \geq K^+ \quad \text{on } R^+. \tag{13.4}$$

The symbol $\sim$ above is defined as follows: if $f(r)$ and $g(r)$ are two functions such that $f = g + o(|f| + |g|)$ as $r \to 0$, then f and g are said to be *asymptotically equal*, and we write $f \sim g$.

Let Γ near P be parametrized by $\Gamma : \theta = \varphi(r)$ on some interval containing 0.

As an initial attempt at finding an asymptotic solution, let us try to construct a lowest-order approximation of the form $u^+ = r^m v^+(\theta)$, $u^- = r^m v^-(\theta)$ where m is a constant and v^+ and v^- are functions. Laplace's equation (13.1) requires that $v^\pm$ be linear combinations of $\cos m\theta$ and $\sin m\theta$. It follows that $m = 1$ since (13.4) implies that $k^\pm = O(1)$ as $r \to 0$. The boundary conditions implied by the symmetries in the problem then dictate that

$$u^+(r,\theta) \sim Ar \sin\theta, \quad 0 \leq \theta \leq \varphi(r), \quad \text{as } r \to 0, \tag{13.5a}$$

$$u^-(r,\theta) \sim Br \sin\theta, \quad \varphi(r) \leq \theta \leq \pi, \quad \text{as } r \to 0, \tag{13.5b}$$

where A and B are nonzero constants. Note that $A \neq B$ by (13.4). To relate the constants, (13.3) implies

$$Ar \sin\varphi(r) = Br \sin\varphi(r). \tag{13.6}$$

So either $\varphi \equiv 0$ or $\varphi \equiv \pi$. Thus the lowest-order solution is unsatisfactory, since it has either one phase or the other collapsed onto the x_1-axis. It does, however, correctly suggest that one look for a cusp in a higher-order solution.

A higher-order solution is supplied by

$$u^+ \sim Ar \sin\theta + ar^\nu \sin\nu\theta, \quad 0 \leq \theta \leq \varphi(r), \quad \text{as } r \to 0, \tag{13.7a}$$

$$u^- \sim Br \sin\theta + br^\nu \sin\nu(\pi - \theta), \quad \varphi(r) \leq \theta \leq \pi, \quad \text{as } r \to 0, \tag{13.7b}$$

where ν, a, b, A, and B are constants, $\nu > 1$. Once again $A \neq B$, and a and b cannot both vanish. Applying (13.3) and expanding the sine terms in (13.7) for small φ yields

$$Ar\varphi + ar^{\nu}\nu\varphi = Br\varphi + br^{\nu}\left[\sin\nu\pi - (\cos\nu\pi)\nu\varphi\right], \quad \varphi = \varphi(r) \tag{13.8}$$

This shows immediately that ν cannot be an integer, for if $\sin\nu\pi = 0$ it would follow that $A = B$ by equating the lower-order terms. Now assume that $\phi \sim Cr^{\gamma}$ for some constants C and γ. Using this in (13.8), comparing the lower-order and higher-order terms separately, and solving for φ gives

$$\varphi(r) \sim Cr^{\nu-1}, \qquad C = \frac{b}{A-B}\sin\nu\pi, \qquad a = -b\cos\nu\pi. \tag{13.9}$$

The asymptotic traction jump condition (13.2) may be applied by computing the normal derivatives of displacement along the shock as $\partial u^{\pm}/\partial n = \nabla u^{\pm} \cdot \mathbf{n}$. The asymptotic expression for $\mathbf{n}$ is

$$\mathbf{n} \sim \mathbf{e}_r C(\nu-1)r^{\nu-1} - \mathbf{e}_\theta, \tag{13.10}$$

where $\mathbf{e}_r$ and $\mathbf{e}_\theta$ are the unit vectors in the polar coordinate system. The gradient fields along Γ obey

$$\nabla u^{+} \sim \mathbf{e}_r ACr^{\nu-1} + \mathbf{e}_\theta(A + \nu a r^{\nu-1}), \tag{13.11a}$$

$$\nabla u^{-} \sim \mathbf{e}_r(BC + \nu b\sin\nu\pi)r^{\nu-1} + \mathbf{e}_\theta(B - \nu b(\cos\nu\pi)r^{\nu-1}). \tag{13.11b}$$

Using (13.10) and (13.11) the requirement (13.2) becomes

$$\mu^{+}\left[-A - \nu a r^{\nu-1}\right] \sim \mu^{-}\left[-B + \nu b(\cos\nu\pi)r^{\nu-1}\right]. \tag{13.12}$$

Comparing the lower-order and higher-order terms in (13.12) separately shows

$$\mu^{+}A = \mu^{-}B, \qquad \mu^{+}a = \mu^{-}b\cos\nu\pi. \tag{13.13}$$

Now comparing the second of (13.13) with the third of (13.9) shows that

$$a = 0 \quad \text{and} \quad \nu = i + 1/2, \quad i = 0, \pm1, \pm2, \ldots. \tag{13.14}$$

But $\nu > 1$ by assumption, and the only value of interest is the smallest value that is consistent with the above analysis. Hence $\nu = 3/2$.

Summarizing, the asymptotic higher-order solution is as follows:

$$u^+(r,\theta) \sim Ar\sin\theta, \tag{13.15a}$$

$$u^-(r,\theta) \sim \frac{\mu^+}{\mu^-}Ar\sin\theta + br^{3/2}\sin\frac{3}{2}(\pi-\theta), \tag{13.15b}$$

$$\Gamma:\ \theta = \varphi(r) \sim \frac{-br^{1/2}}{(1-\mu^+/\mu^-)A}. \tag{13.15c}$$

The constant A is arbitrary except that by (13.4), $K^+ \le A \le \mu^- K^-/\mu^+$. The constant b must be nonpositive in order that $\varphi(r)$ be nonnegative on Γ, but b is otherwise arbitrary. There is an analogous solution for the case of R^- inside the cusp and R^+ outside of it.

It is of interest to find the choice of constants that leads to an asymptotic solution which is as close as possible to an M-stable deformation. This choice is $A = \tau_M/\mu^+$, since this choice makes the lower-order terms in (13.15a,b) correspond to an M-stable homogeneous deformation.

It is also worth emphasizing that the asymptotic solution near an intersection between shocks has both bounded displacement fields and bounded stress fields as the intersection is approached.

Although no exact solution for an M-unstable deformation with intersecting shocks is known, the numerical solution of Example 12.3 above demonstrates a number of cusps.

Chapter 14. Mixed deformations of a nonmonotone material

It was shown in Chapter 12 that only certain special boundary value problems have M-stable solutions for the trilinear material. The present chapter proposes the idea of *mixed* deformations, in which the two phases are so finely interspersed that their constitutive properties are in effect those of a mixture. This situation is similar to that of a gas-liquid mixture in fluid mechanics, in which the gross properties of the mixture are of more interest in practical problems than those of the individual phases.

The following discussion begins with the constitutive law for mixed deformations, hypothesizing that they exist, based on a generalization of behavior in a one-dimensional bar problem. Then solutions to the equilibrium equation in anti-plane shear for a material with this constitutive law are examined. Finally, the properties of interfaces between mixed regions and single-phase regions will be considered.

14.1 Constitutive behavior

The prototype for mixed M-stable deformations is the bar problem investigated by Ericksen [5]. Ericksen considered the elastostatic solutions of a bar composed of a hyperelastic solid similar to the nonmonotone material being considered here (see Figure 14.1a). When subjected to displacement boundary conditions at the ends, M-stable solutions produce loads at the ends as shown in Figure 14.1b. In the region of the load-stretch curve corresponding to two-phase deformations, the load is constant and equal to the Maxwell stress. Ericksen derives this result from the Weierstrass condition of variational calculus. The distribution of the phases within the bar is indeterminable by a static analysis and is totally arbitrary. Thus one may assume a very large number of alternating layers of the two phases.

Since such a mixture can exist in bars, it is reasonable to conjecture that they can exist in multidimensional problems as well, provided they are possible kinematically. The question of kinematics will be discussed in Chapter 16, and for the time being it

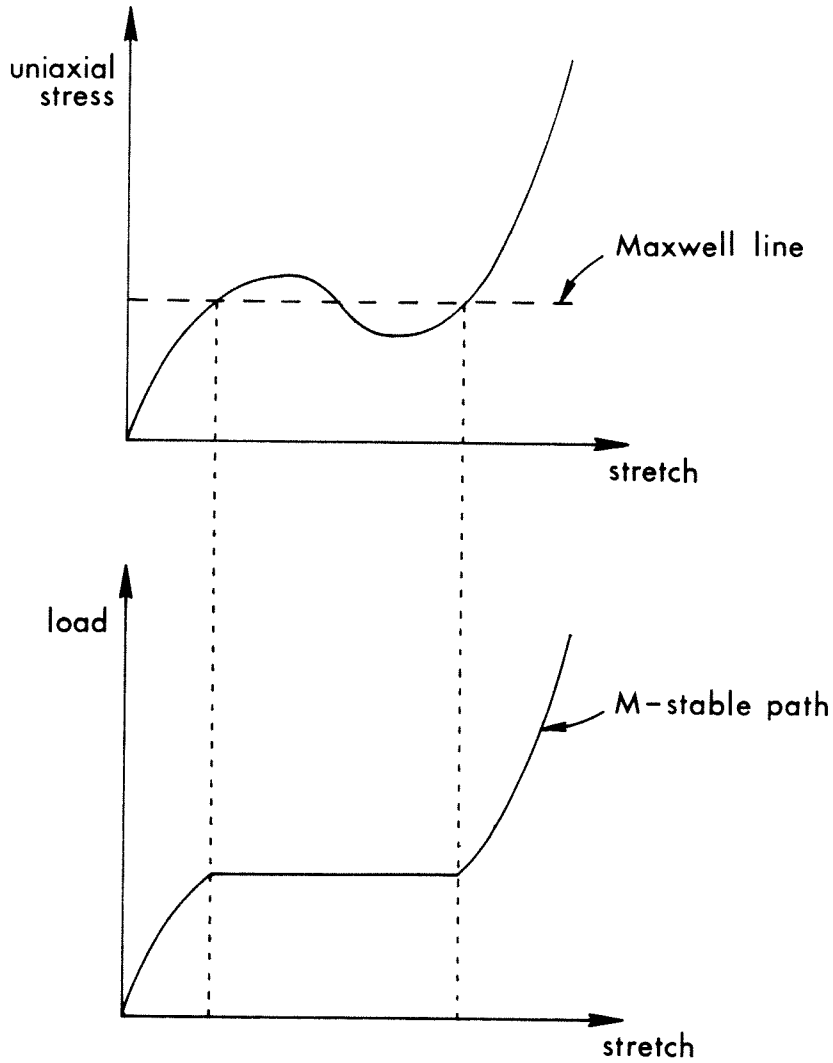

Figure 14.1. (a) Stress-strain relation for material considered in bar problem by Ericksen. (b) Load-stretch relation for hard-device bar problem.

will be necessary to examine the constitutive properties of such mixtures without any assurance that they exist.

Let u be an anti-plane shear deformation on R of a body composed of a nonmonotone material with stress-strain relation τ. Applying the analogy with the bar problem, suppose that a similar mixture is present in some neighborhood of a point $\mathbf{x}$ in R. Assume that a very large number of layers of the two phases oriented parallel to the level curves of displacement is present in this neighborhood. Then by localizing the load-stretch relation of the bar problem, the following stress-strain relation $\tilde{\tau}$ is obtained (see Figure 14.2):

$$\tilde{\tau}(k) = \begin{cases} \tau(k), & 0 \le k \le K_M^-, \\ \tau_M, & K_M^- \le k \le K_M^+, \\ \tau(k), & K_M^+ \le k \end{cases} \tag{14.1}$$

where τ_M is the Maxwell stress. The material whose stress-strain relation is given by (14.1) will be called the **mixed material** associated with τ. A subregion $\tilde{R}$ of R in which $K_M^- \le k \le K_M^+$ will be called a **mixed region**, and the restriction of u to $\tilde{R}$ will be called a **mixed deformation**.

14.2 Solution of the equilibrium equation

Let u be a mixed deformation. It is easily shown that the equilibrium equation (10.3) specializes to

$$\frac{\partial}{\partial x_1}\cos\theta(x_1,x_2) + \frac{\partial}{\partial x_2}\sin\theta(x_1,x_2) = 0, \quad (x_1,x_2) \in \tilde{R} \tag{14.2}$$

where θ is a field on $\tilde{R}$ defined by

$$\cos\theta = \frac{1}{k}\frac{\partial u}{\partial x_1}, \quad \sin\theta = \frac{1}{k}\frac{\partial u}{\partial x_2}, \quad -\pi < \theta \le \pi \quad \text{on } \tilde{R} \tag{14.3}$$

The following gives the most general solution to the equilibrium equation on $\tilde{R}$.

PROPOSITION 14.1. Let $\tilde{R}$ be an open region, and let $u \in C^2(\tilde{R})$ be a scalar field whose gradient does not vanish at any point in $\tilde{R}$. Let θ be defined by (14.3). Define

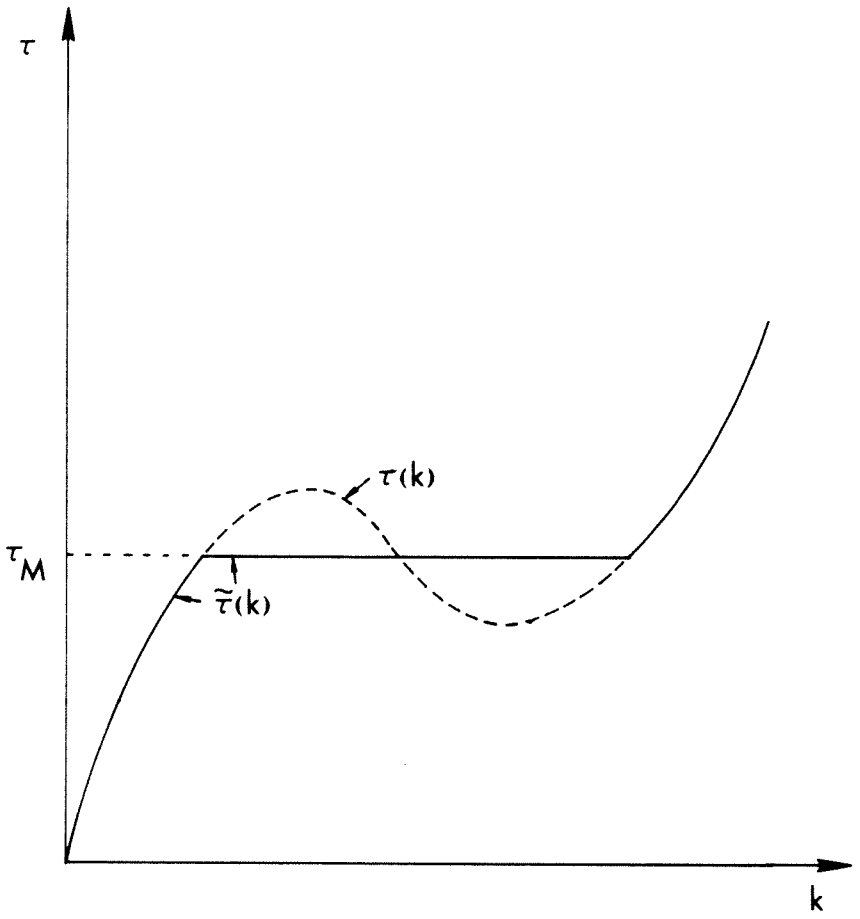

Figure 14.2. Stress-strain relation $\tilde{\tau}$ for mixed material in anti-plane shear.

a set of numbers G by $G = \{u(\mathbf{x}) | \mathbf{x} \in \tilde{R}\}$. For any $u_0 \in G$, let Γ_{u_0} be the curve in $\tilde{R}$ along which $u = u_0$. Let s denote arc length along any Γ_{u_0} measured from an arbitrary location on the curve. Then the deformation u is a solution of the equilibrium equation (14.2) if and only if

$$\frac{d\theta}{ds} = 0 \quad \text{on } \Gamma_{u_0}, \text{ for all } u_0 \in G. \tag{14.4}$$

The proof of the proposition will merely be sketched here since the details are straightforward. It is possible to define a smoothly invertible mapping $(x_1, x_2) \rightarrow (u, s)$ in some neighborhood N of an arbitrary point $\mathbf{p}$ in the interior of $\tilde{R}$. The Jacobian determinant field for this mapping is given by

$$\Delta = \frac{\partial s}{\partial x_1}\frac{\partial u}{\partial x_2} - \frac{\partial s}{\partial x_2}\frac{\partial u}{\partial x_1} \tag{14.5}$$

in N. Therefore $\Delta \neq 0$ in N. Let N_* be the image of N under this mapping. Call the inverse mapping $x_1 = x_1(s,u)$, $x_2 = x_2(s,u)$. Define a function Θ by $\Theta(s,u) = \theta(x_1(s,u), x_2(s,u))$. Applying the chain rule for partial differentiation to (14.2) shows that u is a solution of (14.2) in N if and only if

$$-\sin\theta\left(\frac{\partial\Theta}{\partial s}\frac{\partial s}{\partial x_1} + \frac{\partial\Theta}{\partial u}\frac{\partial u}{\partial x_1}\right) + \cos\theta\left(\frac{\partial\Theta}{\partial s}\frac{\partial s}{\partial x_2} + \frac{\partial\Theta}{\partial u}\frac{\partial u}{\partial x_2}\right) = 0 \quad \text{on } N \tag{14.6}$$

Suppose (14.4) holds in N. Then $\partial\Theta/\partial s = 0$. This together with (14.3) implies (14.6).

Conversely, suppose (14.6) holds. Then (14.3) and (14.6) imply

$$-\frac{1}{k}\frac{\partial u}{\partial x_2}\left(\frac{\partial\Theta}{\partial s}\frac{\partial s}{\partial x_1} + \frac{\partial\Theta}{\partial u}\frac{\partial u}{\partial x_1}\right) + \frac{1}{k}\frac{\partial u}{\partial x_1}\left(\frac{\partial\Theta}{\partial s}\frac{\partial s}{\partial x_2} + \frac{\partial\Theta}{\partial u}\frac{\partial u}{\partial x_2}\right) = 0 \quad \text{on } N \tag{14.7}$$

which upon rearrangement yields

$$\frac{\partial\Theta}{\partial s}\left(\frac{\partial s}{\partial x_1}\frac{\partial u}{\partial x_2} - \frac{\partial s}{\partial x_2}\frac{\partial u}{\partial x_1}\right) = 0 \quad \text{on } N. \tag{14.8}$$

The quantity in parentheses is Δ, which is nonzero in N, so $\partial\Theta/\partial s = 0$ on N. Hence (14.4) holds./

Another way of stating the conclusion of Proposition 14.1 is as follows: u is a solution of the equilibrium equation (14.2) if and only if all curves of constant u in $\tilde{R}$ are straight lines. It is worth mentioning that the proposition also gives the most general solution for a perfectly plastic material in anti-plane shear, and this solution was used by Hult and McClintock [11].

14.3 Interface with single-phase regions

It will now be shown that the interface between a single-phase region and a mixed region consists of regular points, and it is therefore not a shock.

Let u be a deformation on R of a body composed of a nonmonotonic material. Assume that u is partitioned by a curve Γ into a low-strain single-phase region R^- and a mixed region $\tilde{R}$. Call the restrictions of u to these subregions u^- and $\tilde{u}$ respectively. Let the shear fields be k^- and $\tilde{k}$, so that $k^- \leq K_M^-$ on R^- and $K_M^- \leq \tilde{k} \leq K_M^+$ on R^+. Let the stress vector fields be $\mathbf{T}^-$ and $\tilde{\mathbf{T}}$. The constitutive relation (14.1) implies that $\tilde{T} \equiv \tau_M$.

Application of Proposition 10.1 shows that $T^- \geq \tau_M$ on Γ. But the constitutive law (14.1) shows that $\tilde{\tau}(k)$ is a non-decreasing function. Therefore, since $k^- \leq \tilde{k}$, it follows that $T^- \leq \tau_M$ on Γ. So it must be that

$$T^- = \tau_M \quad \text{on } \Gamma. \tag{14.9}$$

Let $\mathbf{x}$ be a point on Γ, and let $\mathbf{n}$ and $\mathbf{s}$ be normal and tangential unit vectors on Γ oriented as shown in Figure 14.3. Let θ^- and $\tilde{\theta}$ be angles in $(-\pi, \pi]$ such that

$$\nabla u^-(\mathbf{x}) = k^- \left(\mathbf{n}\cos\theta^- + \mathbf{s}\sin\theta^-\right), \quad \nabla\tilde{u}(\mathbf{x}) = \tilde{k}\left(\mathbf{n}\cos\tilde{\theta} + \mathbf{s}\sin\tilde{\theta}\right) \tag{14.10}$$

The jump conditions (which must hold on Γ whether or not it is a shock) require

$$k^-\sin\theta^- = \tilde{k}\sin\tilde{\theta}, \qquad T^-\cos\theta^- = \tau_M\cos\tilde{\theta}. \tag{14.11}$$

These together with (14.9) imply

$$\theta^- = \tilde{\theta}, \qquad k^- = \tilde{k}. \tag{14.12}$$

So $\nabla u^- = \nabla \tilde{u}$ on Γ, and therefore the deformation is continuously differentiable on Γ. Thus Γ is not a shock.

Similar considerations hold for the case of an interface between a mixed region and a high-strain single-phase region.

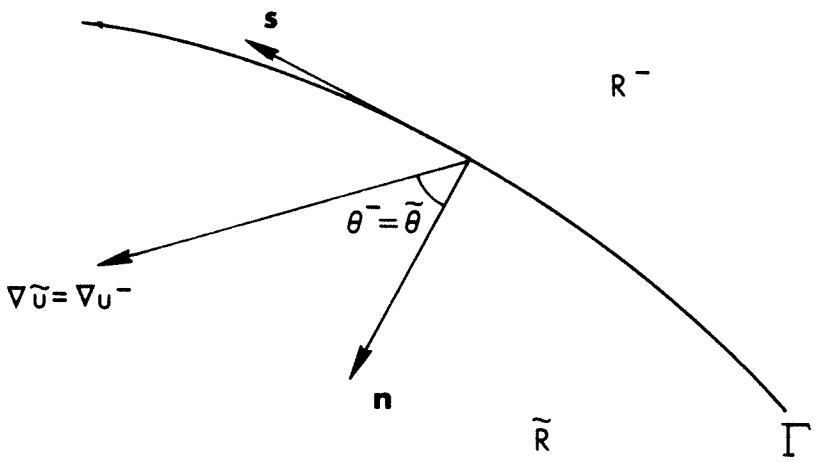

Figure 14.3. Interface between a single-phase region and a mixed region.

Chapter 15. Sequences of states of a nonmonotone material

It will be shown in Chapter 16 that a mixed deformation is obtainable as the limit of a sequence of two-phase deformations. To make this idea precise, it is first necessary to establish some properties of such sequences. The results of Chapters 15 and 16 apply to nonmonotone materials in general and are not restricted to the trilinear material.

15.1 Definitions

In discussing a sequence of functions, it is awkward if each term in the sequence is not defined on the same set. Because the displacement gradient vector field and stress vector field are not defined on the shocks in a two-phase deformation, these fields will be extended to the shocks in the following arbitrary manner. For any field that is continuous in the phases R^+ and R^-, values on Γ will be taken to be the limiting values from the high-strain phase R^+. This extension will be assumed for the remainder of this paper.

DEFINITION. A **state** S is an ordered pair of fields $[u, \mathbf{h}(\nabla u)]$ on R in which u is a single-phase or a two-phase deformation and $\mathbf{h}$ is a constitutive relation for a possibly nonmonotone material.

DEFINITION. Let $Q = \{S_n\} = \{[u_n, \mathbf{h}(\nabla u_n)]\}$, $n = 1, 2, \ldots$, be a sequence of states. Then $\mathbf{h}$ is called the **underlying** constitutive relation of the sequence. Let $S = [u, \mathbf{T}]$ be an ordered pair of fields on R, with u a continuous scalar field and $\mathbf{T}$ a continuous vector field. Q **converges** to S if the sequence $\{u_n\}$ converges uniformly to u and the sequence $\{\mathbf{h}(\nabla u_n)\}$ converges uniformly to $\mathbf{T}$. In this case S is called the **limit** of Q, and we write $Q \to S$.

Note that a limit of a sequence of states need not be a state. In this discussion the following will be assumed:

(A1) $\mathbf{h}$ is direction preserving, *i.e.*, there is a nonnegative continuous scalar function τ on $[0,\infty)$ such that $\mathbf{h}(\mathbf{v}) = \tau(|\mathbf{v}|)\mathbf{v}/|\mathbf{v}|$ for all $\mathbf{v} \neq \mathbf{0}$ and $\tau(0) = 0$.

(A2) The sequence $\{\nabla u_n\}$ and the field ∇u associated with the limit S are uniformly bounded by some number κ.

(A3) There are positive numbers M_1 and M_2 such that $M_1 < \tau(k)/k < M_2$ for all $0 < k \leq \kappa$.

(A4) $\lim_{k\to 0} \tau(k)/k$ exists and is equal to some positive number μ, where $M_1 < \mu < M_2$.

DEFINITION. A convergent sequence of states $Q \to S = [u, \mathbf{T}]$ has an **equilibrated limit** if $\mathbf{T}$ is continuous and is equilibrated.

DEFINITION. Let z be a continuous and piecewise continuously differentiable scalar field on R. The **gradient range** $G\{z\}$ associated with z is defined by $G\{z\} = \{\nabla z(\mathbf{x}) | \mathbf{x} \in R\}$.

DEFINITION. A convergent sequence of states $Q \to S = [u, \mathbf{T}]$ has an **elastic limit** if there is a vector-valued function $\mathbf{h}_Q$ defined on $G\{u\}$ such that $\mathbf{T} = \mathbf{h}_Q(\nabla u)$ on R. In this case $\mathbf{h}_Q$ is called the **limiting constitutive relation** of Q.

Of special interest are those elastic limits whose limiting constitutive relations are independent of the details of the sequences which converge to them, motivating the following definition.

DEFINITION. Let $Q \to S = [u, \mathbf{T}]$ be a convergent sequence of states with an elastic limit. Let Ω be a set of sequences of states, and let Ω contain Q. Suppose that every convergent sequence $Q' \in \Omega$ such that $u \equiv u'$ also has the property $\mathbf{T} \equiv \mathbf{T}'$, where $[u', \mathbf{T}']$ is the limit of Q'. Then S is **autonomous** with respect to Ω.

Even if a sequence has an elastic limit, the limiting constitutive relation need not be the same as the underlying constitutive relation. This is demonstrated in the following example.

EXAMPLE 15.1. Consider the rectangle $R = \{(x_1, x_2) | 0 \leq x_1 \leq 2\pi,\ 0 \leq x_2 \leq 1\}$. Let R be occupied by a homogeneous body composed of the trilinear material. Define a square wave function ω on $(-\infty, \infty)$ by $\omega(t) = \text{sgn } \sin t$, $-\infty < t < \infty$. Define a sequence of anti-plane shear deformations by

$$u_n(x_1, x_2) = \int_0^{x_1} \left\{ \frac{K_M^+ + K_M^-}{2} + \frac{K_M^+ - K_M^-}{2} \omega(nt) \right\} dt, \quad (x_1, x_2) \in R, \quad n = 1, 2, \ldots \tag{15.1}$$

(See Figure 15.1.) Each u_n is a piecewise homogeneous deformation composed of vertical strips with amount of shear alternately K_M^+ and K_M^-. The total number of strips in each deformation is $2n$. The stress vectors for each term are given by $\mathbf{h}(\nabla u_n) = \tau_M \mathbf{e}_1$, since either of the two values for amount of shear correspond to the Maxwell stress. It is easily shown that the sequence of states $Q = \{[u_n, \mathbf{h}(\nabla u_n)]\}$ converges to $S = [u, \mathbf{T}]$ where $u(x_1, x_2) = (K_M^+ + K_M^-)x_1/2$, $\mathbf{T}(x_1, x_2) = \tau_M \mathbf{e}_1$, $(x_1, x_2) \in R$. So Q has an equilibrated elastic limit, and the domain of $\mathbf{h}_Q$ consists of the single vector $\bar{k}\mathbf{e}_1$, where $\bar{k} = (K_M^+ + K_M^-)/2$. Note that $\mathbf{h}_Q(\bar{k}\mathbf{e}_1) \neq \mathbf{h}(\bar{k}\mathbf{e}_1)$. It is easy to find other sequences of states which have equilibrated elastic limits and converge to some limit $[u, \mathbf{T}']$ where $\mathbf{T}' \neq \mathbf{T}$, demonstrating that the limit S is not autonomous with respect to the set of all sequences. (However, it will be shown later that this limit is autonomous with respect to an important class of sequences, the asymptotically M-stable sequences.)

Note that in the Example 15.1 the sequence $\{\nabla u_n\}$ diverges. Subsequent sections will show that the convergence properties of this sequence are crucial in determining the constitutive properties of the limit.

15.2 General convergence properties

This section discusses convergence properties of $\{\nabla u_n\}$ and related fields. Example 15.1 showed that $\{\nabla u_n\}$ does not necessarily converge even if the sequence of states converges. Nevertheless, this sequence of gradients has many interesting properties. The following proposition shows that even if it does not converge, the associated sequence

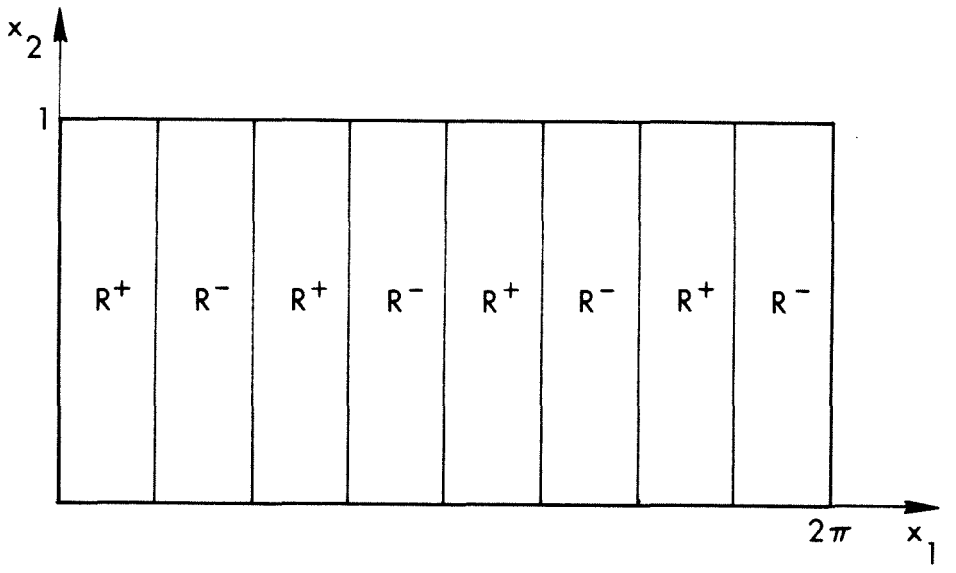

n = 4 term

Figure 15.1. A term in the sequence of states considered in Example 15.1.

of *area-averages* does in any subregion.

PROPOSITION 15.1. Let $Q = \{[u_n, \mathbf{h}(\nabla u_n)]\}$ be a sequence of states converging to a limit $S = [u, \mathbf{T}]$. Let $\mathbf{x}$ be a point in R, and let D be a neighborhood in R centered at $\mathbf{x}$. Then

$$\left\{ \int_D \nabla u_n dA \right\} \rightarrow \int_D \nabla u \, dA. \tag{15.2}$$

PROOF. Let ∂D denote the boundary of D. Each deformation in the sequence has sufficient smoothness to apply Green's theorem:

$$\int_{\partial D} u_n dx_1 = -\int_D \frac{\partial u_n}{\partial x_2} dA, \quad \int_{\partial D} u_n dx_2 = \int_D \frac{\partial u_n}{\partial x_1} dA. \tag{15.3}$$

The first of these upon subtracting a similar equation for u leads to

$$\int_{\partial D} (u_n - u) dx_1 = \int_D \left(\frac{\partial u_n}{\partial x_2} - \frac{\partial u}{\partial x_2} \right) dA. \tag{15.4}$$

Since $\{u_n\} \rightarrow u$ uniformly, the sequence of line integrals defined by the left-hand side of (15.4) converges to zero. This fact combined with the analogue of (15.4) derived from the second of (15.3) implies $\{\int_D (\nabla u_n - \nabla u) dA\} \rightarrow 0$ which proves the result./

COROLLARY. Under the assumptions of the above proposition, let D_r be the neighborhood in R of radius r centered at $\mathbf{x}$. Then

$$\lim_{\substack{r \rightarrow 0 \\ n \rightarrow \infty}} \frac{1}{\pi r^2} \int_{D_r} (\nabla u_n - \nabla u) dA = 0. \tag{15.5}$$

The next three propositions establish certain properties of the sequences of direction vectors associated with sequences of states. They show that the sequence of unit vectors in the direction of $\nabla u_n(\mathbf{x})$ converges, provided $\nabla u(\mathbf{x}) \neq \mathbf{0}$. In each term of the sequence, ∇u_n and $\mathbf{h}(\nabla u_n)$ have the same direction, so the limit of the sequence is the direction of $\mathbf{T}$. Further, it will be shown that this limiting direction is the same as the direction of ∇u. Thus $\mathbf{T}$ and ∇u have the same direction. So in a sense all convergent sequences of states have elastic limits to the extent that the *directions* of $\mathbf{T}$ and ∇u must coincide.

Define a function $\mathbf{d}$ on the set of all vectors by

$$\mathbf{d}(\mathbf{v}) = \begin{cases} \mathbf{v}/|\mathbf{v}|, & \text{if } \mathbf{v} \neq \mathbf{0}; \\ \mathbf{0}, & \text{if } \mathbf{v} = \mathbf{0}. \end{cases} \tag{15.6}$$

Call $\mathbf{d}(\mathbf{v})$ the **direction** of $\mathbf{v}$. The following very plausible result may be proved using the elementary properties of uniformly convergent sequences.

PROPOSITION 15.2. Let $\{\mathbf{v}_n\}$ be a sequence of vector-valued functions on a set V converging uniformly to a function $\mathbf{v}$. Then

(a) $\{|\mathbf{v}_n|\} \to |\mathbf{v}|$ uniformly on V;

(b) $\{\mathbf{d}(\mathbf{v}_n(\mathbf{x}))\} \to \mathbf{d}(\mathbf{v}(\mathbf{x}))$ pointwise at any $\mathbf{x} \in V$ such that $\mathbf{v}(\mathbf{x}) \neq \mathbf{0}$;

(c) $\{\mathbf{d}(\mathbf{v}_n)\} \to \mathbf{d}(\mathbf{v})$ uniformly on any compact subset of V in which $\mathbf{v}$ does not vanish at any point.

For any deformation u on R define the fields k and $\mathbf{s}$ on R by $k = |\nabla u|$ and $\mathbf{s} = \mathbf{d}(\nabla u)$. For any stress vector field $\mathbf{T}$ on R define the fields T and $\mathbf{t}$ on R by $T = |\mathbf{T}|$, and $\mathbf{t} = \mathbf{d}(\mathbf{T})$. Thus $\nabla u = k\mathbf{s}$ and $\mathbf{T} = T\mathbf{t}$. The next result follows from assumption A1 above and from (b) and (c) of Proposition 15.2.

PROPOSITION 15.3. Let $Q = \{[u_n, \mathbf{h}(\nabla u_n)]\}$ be a sequence of states converging to a limit $S = [u, \mathbf{T}]$. Then

(a) $\mathbf{s}_n = \mathbf{t}_n$, $n = 1, 2, \ldots$;

(b) $\{\mathbf{t}_n(\mathbf{x})\} \to \mathbf{t}(\mathbf{x})$ and $\{\mathbf{s}_n(\mathbf{x})\} \to \mathbf{t}(\mathbf{x})$ pointwise at any $\mathbf{x}$ such that $\mathbf{T}(\mathbf{x}) \neq \mathbf{0}$;

(c) $\{\mathbf{t}_n\} \to \mathbf{t}$ and $\{\mathbf{s}_n\} \to \mathbf{t}$ uniformly on any compact subset in which $\mathbf{T}$ does not vanish at any point.

The next result shows that the sequence of area-averages of shear may converge regardless of whether the sequence of gradient vector fields converges. The proposition is proved using the corollary to Proposition 15.1, the uniform convergence of $\{\mathbf{T}_n\}$, and the direction-preserving property of $\mathbf{h}$ (assumption A1).

PROPOSITION 15.4. Let $Q = \{[u_n, \mathbf{h}(\nabla u_n)]\}$ be a sequence of states converging to a limit $S = [u, \mathbf{T}]$. Let $\mathbf{a}$ be a point in R at which ∇u is continuous. For any $r > 0$, let D_r be defined as the neighborhood in R of radius r centered at $\mathbf{a}$. Then:

(a) $\mathbf{s}(\mathbf{a}) = \mathbf{t}(\mathbf{a})$.

(b)

$$\lim_{\substack{r \to 0 \\ n \to \infty}} \frac{1}{\pi r^2} \int_{D_r} (k_n - k) dA = 0. \tag{15.7}$$

15.3 Pure limits and constitutive invertibility

Example 15.1 above suggests that a failure of the limiting constitutive relation, if one exists, to coincide with the underlying constitutive relation may be related to a failure of the sequence of gradient vectors to converge. This is indeed the case, as will be shown in this section. The primary result will be that invertibility of the underlying constitutive relation implies that the limiting constitutive relation exists and coincides with it.

DEFINITION. Let $Q = \{[u_n, \mathbf{h}(\nabla u_n)]\}$ be a sequence of states converging to a limit $S = [u, \mathbf{T}]$. Let $\mathbf{x}$ be a point in R. If the sequence $\{\nabla u_n(\mathbf{x})\}$ converges to $\nabla u(\mathbf{x})$ then S is **pure** at $\mathbf{x}$. Otherwise it is **mixed** at $\mathbf{x}$.

PROPOSITION 15.5. Let $Q = \{S_n\} = \{[u_n, \mathbf{h}(\nabla u_n)]\}$ be a sequence of states converging to a limit $S = [u, \mathbf{T}]$. Let S be pure at some point $\mathbf{x}$ in R at which ∇u is continuous. Then $\mathbf{T}(\mathbf{x}) = \mathbf{h}(\nabla u(\mathbf{x}))$.

PROOF. Let $\mathbf{x}$ be as stated, and choose any $\epsilon > 0$. Since $\mathbf{h}$ is continuous, there is a $\delta > 0$ such that $|\mathbf{h}(\mathbf{v}) - \mathbf{h}(\nabla u(\mathbf{x}))| < \epsilon$ whenever $|\mathbf{v} - \nabla u(\mathbf{x})| < \delta$. Since the sequence $\{\nabla u_n(\mathbf{x})\}$ converges to $\nabla u(\mathbf{x})$, $|\nabla u_n(\mathbf{x}) - \nabla u(\mathbf{x})| < \delta$ for n sufficiently large. Thus, for n sufficiently large, $|\mathbf{h}(\nabla u_n(\mathbf{x})) - \mathbf{h}(\nabla u(\mathbf{x}))| < \epsilon$. This proves $\{\mathbf{h}(\nabla u_n(\mathbf{x}))\} \to \mathbf{h}(\nabla u(\mathbf{x}))$. But by the definition of convergence of a sequence of states, $\{\mathbf{h}(\nabla u_n(\mathbf{x}))\} \to \mathbf{T}(\mathbf{x})$. So by the uniqueness of limits, $\mathbf{T}(\mathbf{x}) = \mathbf{h}(\nabla u(\mathbf{x}))$./

The next two propositions concern sufficient conditions for a limit to be pure. These results involve underlying constitutive relations that are continuously invertible at points in the limit. The significance of these results is that under certain conditions the limit is necessarily elastic and autonomous with respect to all sequences, and $\mathbf{h}_Q = \mathbf{h}$.

DEFINITION. Let $\mathbf{h}$ be any constitutive relation. Suppose there is a domain of vectors H_T such that there is a uniformly continuous vector-valued mapping $\mathbf{h}^{-1}$ on H_T with the property $\mathbf{h}(\mathbf{h}^{-1}(\mathbf{v})) = \mathbf{v}$ for all $\mathbf{v} \in H_T$. Let $H_G = \mathbf{h}^{-1}(H)$. Then $\mathbf{h}$ is **invertible** on H_G. H_G is the **gradient domain of invertibility** of $\mathbf{h}$, and H_T is the **stress domain of invertibility** of $\mathbf{h}$. $\mathbf{h}^{-1}$ is called the **inverse** of $\mathbf{h}$.

It is easily shown that if $\mathbf{h}$ has a gradient domain of invertibility H_G, then $\mathbf{h}^{-1}(\mathbf{h}(\mathbf{v}))$ $= \mathbf{v}$ for all $\mathbf{v} \in H_G$. Since $\mathbf{h}$ is direction-preserving (see assumption A1) τ has an inverse mapping τ^{-1} defined on the set $|H_T|$ in the obvious way. Since H_T is an open connected set by assumption, so is H_G. Therefore in general one can write $|H_T| = (T_1, T_2)$ and $|H_G| = (k_1, k_2)$ for some constants T_1, T_2, k_1, and k_2. The only exception is the special case $T_1 = k_1 = 0$, for which it is possible that $|H_T| = [0, T_2)$ and $|H_G| = [0, k_2)$. Note also that by assumption A1, τ is monotonically strictly increasing on $|H_G|$.

PROPOSITION 15.6. Let $Q = \{S_n\} = \{[u_n, \mathbf{h}(\nabla u_n)]\}$ be a sequence of states converging to a limit $S = [u, \mathbf{T}]$. Suppose $\mathbf{h}$ has a stress domain of invertibility H_T. Suppose further that there is a point $\mathbf{a}$ in R such that ∇u is continuous at $\mathbf{a}$ and $\mathbf{T}(\mathbf{a}) \in H_T$. Then S is pure at $\mathbf{a}$.

PROOF. Let ϵ be any positive number. Since $\mathbf{h}^{-1}$ is uniformly continuous on H_T, there is a $\delta_1 > 0$ such that $|\mathbf{h}^{-1}(\mathbf{v}) - \mathbf{h}^{-1}(\mathbf{T}(\mathbf{a}))| < \epsilon$ whenever $|\mathbf{v} - \mathbf{T}(\mathbf{a})| < \delta_1$ and $\mathbf{v} \in H_T$. $\mathbf{T}(\mathbf{a})$ is an interior point of H_T, since H_T is a domain. Therefore there is a neighborhood of $\mathbf{T}(\mathbf{a})$ contained entirely within H_T. Call the radius of this neighborhood δ_2. The sequence $\{\mathbf{h}(\nabla u_n)\}$ converges to T uniformly on R, by the definition of a convergent sequence of states. Then there is a positive number N such

that $n > N$ implies $|\mathbf{h}(\nabla u_n(\mathbf{a})) - \mathbf{T}(\mathbf{a})| < \min\{\delta_1, \delta_2\}$. So for $n > N$, $\mathbf{h}(\nabla u_n(\mathbf{a})) \in H_T$ and $\left|\mathbf{h}^{-1}\left(\mathbf{h}(\nabla u_n(\mathbf{a}))\right) - \mathbf{h}^{-1}\left(\mathbf{T}(\mathbf{a})\right)\right| < \epsilon$ which implies $\left|\nabla u_n(\mathbf{a}) - \mathbf{h}^{-1}\left(\mathbf{T}(\mathbf{a})\right)\right| < \epsilon$. This proves that $\{\nabla u_n(\mathbf{a})\} \to \mathbf{h}^{-1}(\mathbf{T}(\mathbf{a}))$.

It remains to prove that $\{\nabla u_n(\mathbf{a})\} \to \nabla u(\mathbf{a})$. To do this, first note that since $\mathbf{T}(\mathbf{a})$ is an interior point of H_T, the above argument is valid for all points in any closed neighborhood D_r with radius r centered at $\mathbf{a}$ provided $r < \delta_2$. Therefore $\{\nabla u_n\} \to \mathbf{h}^{-1}(\mathbf{T})$ on D_r. Moreover, the convergence is uniform, since $\mathbf{h}^{-1}$ is uniformly continuous and since the sequence $\mathbf{h}(\nabla u_n)$ converges uniformly on R. It follows that

$$\lim_{\substack{r\to 0 \\ n\to\infty}} \frac{1}{\pi r^2}\int_{D_r} (\mathbf{h}^{-1}(\mathbf{T}) - \nabla u_n)dA = 0. \tag{15.8}$$

The termwise sum of any two convergent sequences is convergent. Then, using (15.8) and the corollary to Proposition 15.1,

$$\begin{aligned}\lim_{\substack{r\to 0 \\ n\to\infty}} \frac{1}{\pi r^2}\int_{D_r} (\mathbf{h}^{-1}(\mathbf{T}) - \nabla u)dA = \\ \lim_{\substack{r\to 0 \\ n\to\infty}} \frac{1}{\pi r^2}\int_{D_r} (\mathbf{h}^{-1}(\mathbf{T}) - \nabla u_n)dA + \lim_{\substack{r\to 0 \\ n\to\infty}} \frac{1}{\pi r^2}\int_{D_r} (\nabla u_n - \nabla u)dA = 0.\end{aligned} \tag{15.9}$$

This result together with the continuity of $\mathbf{h}^{-1}(\mathbf{T})$ and ∇u at $\mathbf{a}$ proves that $\mathbf{h}^{-1}(\mathbf{T}(\mathbf{a})) = \nabla u(\mathbf{a})$. It was already shown that $\{\nabla u_n(\mathbf{a})\} \to \mathbf{h}^{-1}(\mathbf{T}(\mathbf{a}))$. So, by the uniqueness of limits, $\{\nabla u_n(\mathbf{a})\} \to \nabla u(\mathbf{a})$./

The following lemma may be readily proved using the definition of uniform convergence.

LEMMA. Let $\{f_n\}$ be a sequence of real-valued functions on some region D each of which is bounded on D. Suppose the sequence converges uniformly to a function f. Then

$$\left\{\sup_D f_n\right\} \to \sup_D f \quad \text{and} \quad \left\{\inf_D f_n\right\} \to \inf_D f.$$

The following result is similar to Proposition 15.6, but its premise is that $\nabla u(\mathbf{x}) \in H_G$ rather than $\mathbf{T}(\mathbf{x}) \in H_T$.

PROPOSITION 15.7. Let $Q = \{S_n\} = \{[u_n, \mathbf{h}(\nabla u_n)]\}$ be a sequence of states converging to a limit $S = [u, \mathbf{T}]$, with underlying constitutive relation $\mathbf{h}$. Suppose $\mathbf{h}$ has a gradient domain of invertibility H_G. Suppose further that there is a point $\mathbf{a}$ in R such that ∇u is continuous at $\mathbf{a}$ and $\nabla u(\mathbf{a}) \in H_G$. Then S is pure at $\mathbf{a}$.

PROOF. By Proposition 15.6 it is sufficient to show that $\mathbf{T}(\mathbf{a}) \in H_T$, *i.e.*, that $T(\mathbf{a}) \in |H_T|$. This proof will show that every neighborhood of $\mathbf{a}$ contains points with T values in $|H_T|$, and that this is inconsistent with the assumption that $T(\mathbf{a})$ is not contained in $|H_T|$.

Let the subscript a denote evaluation of a quantity at $\mathbf{a}$. Assume that T_a is not contained in $|H_T|$. Recall that the domains of invertibility may be expressed as $|H_G| = (k_1, k_2)$, $|H_T| = (T_1, T_2)$. (The lower endpoints of the intervals may be closed if $k_1 = T_1 = 0$, but this possibility will be temporarily ignored.) Then $k_1 < k_a < k_2$, but either $T_a \leq T_1$ or $T_a \geq T_2$. First assume the former. Recall that τ is monotonically strictly increasing on $|H_G|$. Let $w = (\tau(k_a) - T_1)/3$. So w is a positive number. Let $\epsilon = k_a - \tau^{-1}(\tau(k_a) - w)$. Since $\mathbf{T}$ is continuous at $\mathbf{a}$, there is a positive number r such that $|T - T_a| < w$ on D_r, where D_r is the neighborhood in R of radius r centered at $\mathbf{a}$. Hence

$$\sup_{D_r} T \leq w + T_a \leq w + T_1 = \frac{\tau(k_a) + T_1}{2} - \frac{\tau(k_a) - T_1}{6} \tag{15.10}$$

Proposition 15.4 ensures that there is a positive number N such that $n > N$ implies

$$\frac{1}{\pi r^2} \left| \int_{D_r} (k_n - k_a) dA \right| < \epsilon. \tag{15.11}$$

If $k_n - k_a < -\epsilon$ *everywhere* in D_r, then (15.11) could not be satisfied. So for any $n > N$ there is *some* $\mathbf{x} \in D_r$ such that $k_n(\mathbf{x}) \geq k_a - \epsilon = \tau^{-1}(\tau(k_a) - w)$, which implies $T_n(\mathbf{x}) \geq \tau(k_a) - w$ since τ is increasing. Hence

$$\sup_{D_r} T_n \geq \tau(k_a) - w = \frac{\tau(k_a) + T_1}{2} + \frac{\tau(k_a) - T_1}{6}. \tag{15.12}$$

So (15.10) and (15.11) imply

$$\sup_{D_r} T_n - \sup_{D_r} T \geq \frac{\tau(k_a) - T_1}{6}. \tag{15.13}$$

Since the right hand side of (15.13) is positive and independent of n, the preceding lemma is contradicted. The case of $T_a \geq T_2$ similarly leads to a contradiction. Thus $T_1 < T_a < T_2$, so $T_a \in |H_T|$.

In the case $|H_G| = [0, k_2)$, $|H_T| = [0, T_2)$, the fact that each T_n is nonnegative and the preceding lemma show that T_a cannot possibly be negative. There is no change needed to the proof that $T_a < T_2$./

The key results of this section are summarized as follows:

PROPOSITION 15.8. Let $Q = \{S_n\} = \{[u_n, \mathbf{h}(\nabla u_n)]\}$ be a sequence of states converging to a limit $S = [u, \mathbf{T}]$. Suppose H_T and H_G are stress and gradient domains of invertibility of $\mathbf{h}$, respectively, with inverse $\mathbf{h}^{-1}$. Suppose that there is a subregion R_1 of R on which ∇u is continuous, and that $\nabla u(R_1) \subset H_G$ or $\mathbf{T}(R_1) \subset H_T$. Then:

(a) S is pure on R_1.

(b) S is elastic and autonomous on R_1 with respect to the set of all sequences of states.

(c) $\mathbf{h}_Q$ is the restriction of $\mathbf{h}$ to $\nabla u(R_1)$.

Part (c) shows that pure limits do not exhibit any surprising constitutive behavior. However, the properties of pure limits will enable the constitutive properties of mixed limits to be derived, as shown in the next section.

Chapter 16. Mixed limits in a nonmonotone material

The previous two chapters established general results about convergent sequences of states in a nonmonotone material and the constitutive properties of their limits. It was shown that any such limit has $\mathbf{T}$ and ∇u vector fields that are parallel. If these fields assume only values for which $\mathbf{h}$ is invertible, then the limit is necessarily pure and elastic, with the limiting constitutive relation a restriction of $\mathbf{h}$ to the gradient range of the limit. The first objective of this section is to define a sense in which a limit may be regarded as M-stable. Then it will be shown that any limit which is M-stable in this sense is essentially a mixed deformation.

16.1 Asymptotically M-stable limits

DEFINITION. Let $\mathbf{h}$ be the constitutive relation of a nonmonotone material, and let K_M^- and K_M^+ be the shears associated with the Maxwell stress (see Chapter 11). Let $Q = \{S_n\} = \{[u_n, \mathbf{h}(\nabla u_n)]\}$ be a sequence of states converging to a limit $S = [u, \mathbf{T}]$. Q is **asymptotically M-stable** if for any $\epsilon > 0$ there is a number N such that $n > N$ implies

$$\left\{k(\mathbf{x}) \mid K_M^- + \epsilon \leq k(\mathbf{x}) \leq K_M^+ - \epsilon,\ \mathbf{x} \in R\right\} = \emptyset. \tag{16.1}$$

The above definition means that in an asymptotically M-stable sequence, for n sufficiently large, the admissible k_n values become restricted to the intervals $[0, K_M^-]$ and $[K_M^+, \infty)$.

PROPOSITION 16.1. Let $Q = \{S_n\} = \{[u_n, \mathbf{h}(\nabla u_n)]\}$ be an asymptotically M-stable sequence of states converging to a limit $S = [u, \mathbf{T}]$. Suppose there are curves collectively called Γ in R which partition R into open subregions R_S and $\tilde{R}$, and that ∇u is continuous on $R_S \cup \tilde{R}$. Suppose further that for any $\mathbf{x} \in R_S$, $k(\mathbf{x}) < K_M^-$ or $k(\mathbf{x}) > K_M^+$, and that for any $\mathbf{x}$ in $\tilde{R}$, $K_M^- \leq k(\mathbf{x}) \leq K_M^+$. Then:

(a) S is pure on R_S.

(b) S is elastic and autonomous on $R_S \cup \tilde{R}$ with respect to the set of all asymptotically M-stable sequences.

(c) $\mathbf{h}_Q$ is a restriction of $\tilde{\mathbf{h}}$, the constitutive relation for mixed deformations, to $G\{u\}$.

PROOF. Let $\mathbf{a}$ be a point in R_S. Then $k(\mathbf{a}) < K_M^-$ or $k(\mathbf{a}) > K_M^+$. First assume the latter. Let $\delta = (k(\mathbf{a}) - K_M^+)/2$, $k_1 = k(\mathbf{a}) - \delta$, and $k_2 = k(\mathbf{a}) + \delta$. Since Q is asymptotically M-stable, there is a number N such that $n > N$ implies that if $k_1 < k_n(\mathbf{x}) < k_2$ for some $\mathbf{x}$ in R, then $k_n(\mathbf{x})$ is the *only* number k such that $\tau(k) = \tau(k_n(\mathbf{x}))$. Therefore τ is effectively invertible on (k_1, k_2) for terms in the sequence beyond N. If the proof of Proposition 15.7 is modified so that r is chosen to be sufficiently small that $|k - k(\mathbf{a})| < \delta$ on D_r and $n > N$, then the conclusion holds in the present case. So S is pure on R_S and $\mathbf{T} = \mathbf{h}(\nabla u)$ on R_S.

Now choose $\mathbf{a}$ in $\tilde{R}$. Suppose $T(\mathbf{a}) \neq \tau_M$. Then $T(\mathbf{a})$ is in an effective stress domain of invertibility of $\mathbf{h}$ similar to the above situation for gradients. Therefore by Proposition 15.6, S is pure at $\mathbf{a}$, contradicting the assumption that S is mixed at $\mathbf{a}$. Hence $T(\mathbf{a}) = \tau_M$, and so $T = \tau_M$ on $\tilde{R}$.

It has been shown that $\mathbf{T} = \tilde{\mathbf{h}}(\nabla u)$ on $\tilde{R} \cup R_S$. Therefore S is elastic there and $\mathbf{h}_Q$ is a restriction of $\tilde{\mathbf{h}}$ to $G\{u\}$, the gradient range of u. Because of the arbitrariness of Q, S is also autonomous with respect to the set of all asymptotically M-stable sequences./

16.2 Sequence convergent to a mixed deformation

A converse of Proposition 16.1 will now be established. The following shows how to construct, given any mixed deformation, an asymptotically M-stable sequence of states whose limit is that deformation.

Suppose u is an equilibrated mixed deformation, partitioned into single-phase and mixed regions R^+, R^-, and $\tilde{R}$ by a set of curves collectively called Γ. Let $\Gamma^- = \tilde{R} \cap R^-$ and $\Gamma^+ = \tilde{R} \cap R^+$. For the sake of simplicity, assume that $\tilde{R}$ is a connected convex region in the interior of R. Let $u_{\max} = \max_\Gamma u$ and $u_{\min} = \min_\Gamma u$.

Let $\mathbf{T}$ be the stress vector field associated with u, so that $\mathbf{T} = \tilde{\mathbf{h}}(\nabla u)$ on R, where $\tilde{\mathbf{h}}$ is the constitutive relation of the mixed material defined earlier. The monotonocity of u on Γ^+ and Γ^- as a function of arc length follows from the fact that u is equilibrated on R. Therefore one can define vector-valued functions $\mathbf{P}^+$ and $\mathbf{P}^-$ on $[u_{\min}, u_{\max}]$ as follows. For any $U \in [u_{\min}, u_{\max}]$, let $\mathbf{P}^+(U)$ be the unique point on Γ^+ such that $u(\mathbf{P}^+(U)) = U$, and let $\mathbf{P}^-(U)$ be the unique point on Γ^- such that $u(\mathbf{P}^-(U)) = U$. Note that $\mathbf{P}^+$ and $\mathbf{P}^-$ are continuous functions since u is a continuous function.

For any integer $n > 2$ define a set of $n+1$ equally spaced numbers $U_{n,i} \in [u_{\min}, u_{\max}]$ by $U_{n,i} = u_{\min} + (i/n)(u_{\max} - u_{\min})$, $i = 0, 1, 2, \ldots, n$. Now construct a network of line segments connecting the $\mathbf{P}^+(U_{n,i})$ and the $\mathbf{P}^-(U_{n,i})$ as shown in Figure 16.1. For fixed n, consider the piecewise homogeneous deformation u_n on $\tilde{R}$ which takes on the u-values of the vertices in each triangular subregion. This deformation is clearly continuous along the line segments.

Define a sequence of states on $\tilde{R}$ by $Q = \{[u_n, \mathbf{h}(\nabla u_n)]\}$. The convergence of this sequence to $S = [u, \tilde{\mathbf{h}}(\nabla u)]$ is easily established using the fact that for large n, the line segments become oriented along the level curves of displacement for mixed solutions (Proposition 14.1). The asymptotic M-stability of the sequence follows from the special properties of intersections between single-phase and mixed regions (Section 14.3), which require that $k = K_M^-$ on Γ^- and $k = K_M^+$ on Γ^+. Thus for increasing n the shears in the triangular subregions approach the values K_M^- and K_M^+ alternately.

The above argument is easily extended to the case of nonconvex $\tilde{R}$ and cases in which $\tilde{R}$ intersects the boundary of R. The following result has therefore been established.

PROPOSITION 16.2. Let u be an equilibrated mixed deformation on R. Then there is an asymptotically M-stable sequence of states $Q = \{[u_n, \mathbf{h}(\nabla u_n)]\}$ converging to a limit $S = [u, \tilde{\mathbf{h}}(\nabla u)]$.

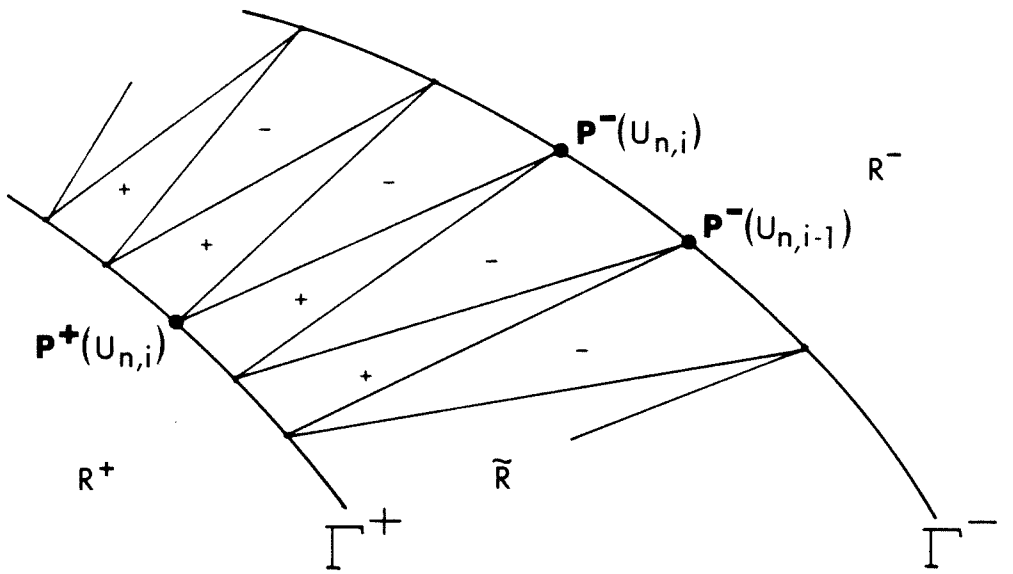

Figure 16.1. A term in an asymptotically M-stable sequence of states converging to a mixed deformation.

16.3 Example: screw dislocation in the trilinear material

This example illustrates the convergence of an asymptotically M-stable sequence of states to a mixed deformation.

Let R be the entire plane, occupied by a body composed of the trilinear material. Suppose one seeks an equilibrated deformation equation on $r > 0$ and $0 \leq \theta \leq 2\pi$ subject to the following conditions:

$$u(r,0) = 0, \quad u(r,2\pi) = b, \quad r > 0, \tag{16.2}$$

and

$$u(r,\theta) \sim b\theta/2\pi \quad \text{as } r \to \infty, \quad 0 \leq \theta \leq 2\pi \tag{16.3}$$

where b is a constant. Define the field u_L on R by

$$u_L(r,\theta) = b\theta/2\pi, \quad r > 0, \quad 0 \leq \theta \leq 2\pi. \tag{16.4}$$

Direct evaluation of the stress vector field $\mathbf{h}_{\triangleleft}(\nabla u_L)$ and substitution into the equilibrium equation shows that this is a solution to the nonlinear boundary value problem. However, it is an M-unstable solution, since $k_L(r,\theta) = b/2\pi r$ and therefore

$$K^- < k_L(r,\theta) < K^+ \quad \text{for } \frac{b}{2\pi K^+} < r < \frac{b}{2\pi K^-}. \tag{16.5}$$

So u_L is not an acceptable solution.

Now suppose one looks for solutions containing shocks in the hope of finding an M-stable two-phase solution. Because of the unboundedness of k expected near the origin and the vanishing k values expected as $r \to \infty$, it is safe to assume that any shocks will be confined to some annular region. Because of the evident symmetry that the problem exhibits with respect to θ, one possibility for a solution might contain a single smooth shock having endpoints on $\theta = 0$ and $\theta = 2\pi$ in this annulus. But along such a shock u would necessarily vary from 0 to b, in contradiction of the M-stability requirement that u be constant along shocks.

Terms in a sequence constructed as prescribed by the remarks preceding Proposition 16.1 form a network of shocks in the shape of a star (see Figure 16.2). Call the term in this sequence with n vertices on the star u_n. By raising n, the total path length of shocks is raised. Therefore the tangential derivative of displacement along any shock is progressively reduced as n is raised. Each u_n field resembles spiral staircase in the annulus $\tilde{R}$, whose inner and outer radii are given in (16.5).

By taking the limit of this sequence as $n \to \infty$, an equilibrated limit of an asymptotically M-stable sequence is obtained. Call this limit u. Surprisingly, it happens that $u \equiv u_L$. But the limit of the sequence of stress vector fields, $\{\mathbf{h}_{\triangleleft}(\nabla u_n)\}$, is different from $\mathbf{h}_{\triangleleft}(\nabla u_L)$. The limiting constitutive relation is that of mixed deformations, $\tilde{\mathbf{h}}$. The limiting stress vector field is

$$\mathbf{T}(r,\theta) = \begin{cases} \mu^+ b\mathbf{e}_\theta/2\pi r, & 0 < r < b/2\pi K_M^+ \\ \tau_M \mathbf{e}_\theta, & b/2\pi K_M^+ \le r \le b/2\pi K_M^- \\ \mu^- b\mathbf{e}_\theta/2\pi r, & b/2\pi K_M^- < r. \end{cases} \tag{16.6}$$

Substitution of this field into the equilibrium equation shows that u is equilibrated.

In this context the utility of the analysis presented in this section is evident. It frees us from any obligation to examine the details of whatever sequence converges to the mixed limit, since it proved that the limit is independent of those details.

It is of interest to see what a numerical model predicts as a solution to this boundary value problem. The solution found using the APE program [12] is shown in Figure 16.3. APE uses a dynamic relaxation algorithm, so it predicts only dynamically stable solutions. Note the strong resemblance between the numerical solution and the M-unstable terms in the sequence discussed above.

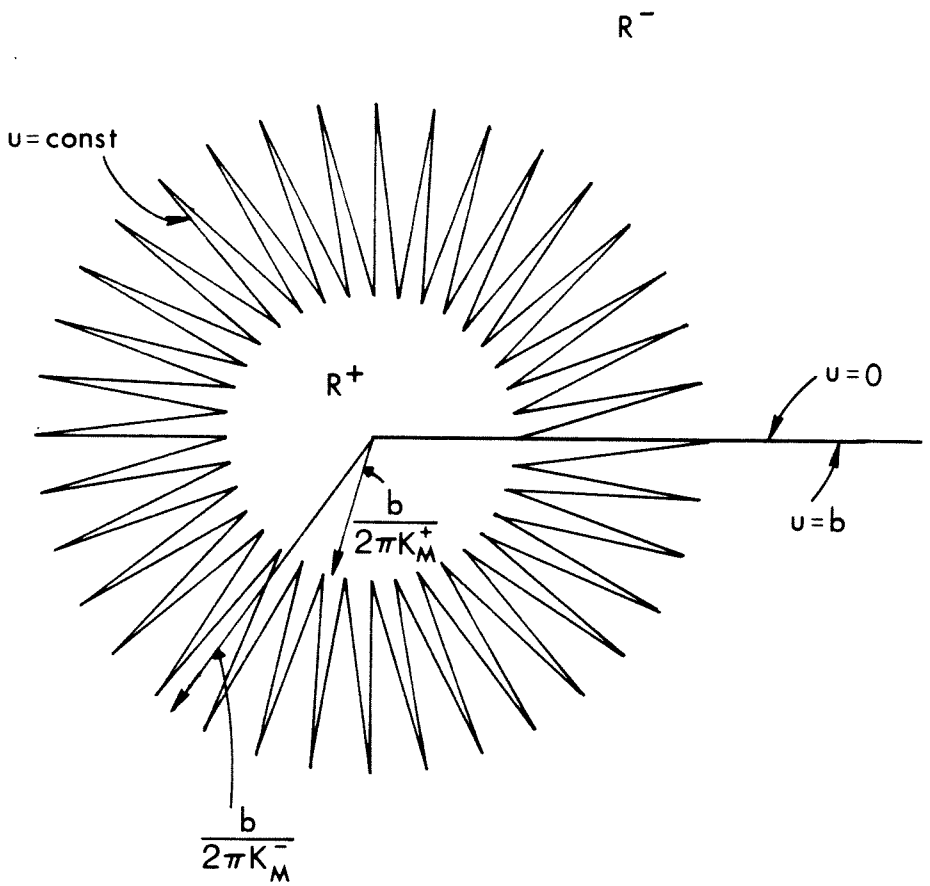

Figure 16.2. A term in an asymptotically stable M-sequence of states converging to a mixed solution of the screw dislocation problem.

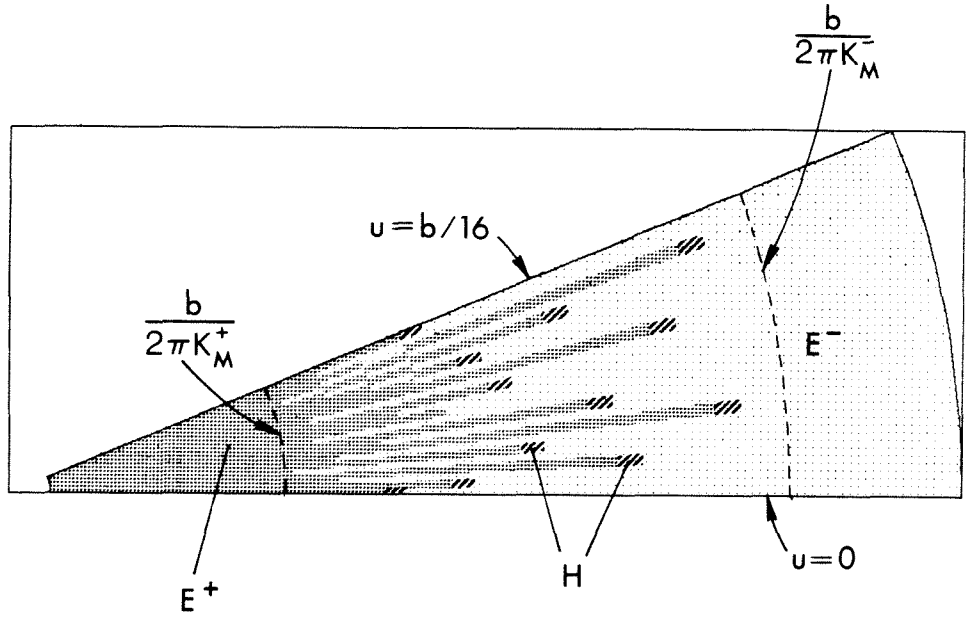

Figure 16.3. Numerical solution of screw dislocation problem in the trilinear material. Shading represents phases: E^-= low-strain elliptic, H=hyperbolic, E^+=high-strain elliptic.

Chapter 17. Conclusions

This work has shown that in general M-stability can be achieved only approximately in the anti-plane shear of a nonmonotone elastic material. For the trilinear material, an arbitrary M-stable deformation can be generated by a conformal mapping from a piecewise homogeneous deformation. For a given traction boundary value problem with this material, Proposition 12.4 provides a test for whether or not there is an M-stable two-phase solution. If there is no such solution, M-stability may be achieved in the sense of a limit of a sequence of increasingly chaotic deformations. The limit of this sequence for a given boundary value problem is found by computing the solution for a mixed material.

There is experimental evidence of chaos in the growth of crystals in liquids [13] and in other cases. However, in attempting to relate the present results to physical problems, the question arises of how to interpret the infinite complexity of the deformations required to satisfy M-stability. It is possible that there is some phenomenon in solids analogous to surface tension in fluids which limits the ultimate complexity of a solution. The modification of the underlying constitutive relation in solids to include a dependence of the strain energy density on second derivatives of displacement has been proposed as such a phenomenon [14]. An alternate approach would be to relax the requirement of local stability, which implies M-stability, in favor of some concept such as weak stability. The cusps discussed in Chapter 13 are weakly stable but not locally stable.

It appears probable that the results discussed here for anti-plane shear can be generalized to plane or three-dimensional deformations. A possible stumbling block in such an extension is the issue of constitutive invertibility, which plays an important role in deriving the properties of mixed deformations, but which is quite subtle outside the context of anti-plane shear. It seems likely that some limited notion of constitutive invertibility making use of kinematical considerations along shocks would be sufficient.

References for Part II

[1] R. D. James, "Finite deformation by mechanical twinning," *Archive for Rational Mechanics and Analysis* **77** (1981) 143–176

[2] J. M. Ball, "Material instabilities and the calculus of variations," in *Phase Transitions and Material Instabilities in Solids*, M. E. Gurtin, ed., New York, Academic Press (1984) 1–19

[3] J. K. Knowles, "The finite anti-plane shear field near the tip of a crack for a class of incompressible elastic solids," *International Journal of Fracture* **13** (1977) 611–639

[4] C. E. Pearson, "General theory of elastic stability," *Quarterly of Applied Mathematics* **14** (1956) 133–144

[5] J. L. Ericksen, "Equilibrium of bars," *Journal of Elasticity* **5** (1975) 191–201

[6] M. E. Gurtin, "Two-phase deformations of elastic solids," *Archive for Rational Mechanics and Analysis* **83** (1983) 1–29 (?)

[7] R. D. James, "Co-existent phases in the one-dimensional theory of elastic bars," *Archive for Rational Mechanics and Analysis* **72** (1979) 99–140

[8] R. D. James, "A relation between the jump in temperature across a propagating phase boundary and the stability of solid phases," *Journal of Elasticity* **13** (1983) 357–378

[9] F. A. McClintock and Ali S. Argon, *Mechanical Behavior of Materials*, Reading, Mass., Addison-Wesley (1966) 186

[10] A. I. Markushevich, *The Theory of Analytic Functions: a Brief Course*, Moscow, Mir Publishers (1983) 336

[11] J. A. H. Hult and F. A. McClintock, "Elastic-plastic stress and strain distribution around sharp notches under repeated shear," *Proceedings of the Ninth International Congress of Applied Mechanics, Brussels, Belgium* **8** (1956) 51–58

[12] S. A. Silling, "CHIMP – a computer program for finite elastostatics," to appear.

[13] J. S. Langer and H. Muller-Krumbhaar, "Theory of dendritic growth – I. Elements of a stability analysis," *Acta Metallurgica* **26** (1978) 1681-1687

[14] M. E. Gurtin, "The gradient theory of phase transitions on a finite interval," in *Phase Transitions and Material Instabilities in Solids*, M. E. Gurtin, ed., New York, Academic Press (1984) 99–112